Title

Further Studies in the Liquid-Drop Theory of Nuclear Fission

Author

Nix, James Rayford

Publication Date

1968-07-01

UCRL-17958

ey. 2

University of California

Ernest O. Lawrence Radiation Laboratory

FURTHER STUDIES IN THE LIQUID-DROP THEORY OF NUCLEAR FISSION

James Rayford Nix

July 1, 1968

DISCLAIMER

Submitted to Nuclear Physics

UCRL-17958
Preprint

UNIVERSITY OF CALIFORNIA

Lawrence Radiation Laboratory
Berkeley, California

AEC Contract No. W-7405-eng-48

FURTHER STUDIES IN THE LIQUID-DROP THEORY OF NUCLEAR FISSION

James Rayford Nix

July 1, 1968

FURTHER STUDIES IN THE LIQUID-DROP THEORY OF NUCLEAR FISSION

James Rayford Nix†

Lawrence Radiation Laboratory
University of California
Berkeley, California

July 1, 1968

Abstract

We study the properties of the division of an idealized nucleus, using a simplified version of the liquid-drop model. The shape of the nuclear surface is specified by means of a parameterization that has six degrees of freedom, defined in terms of three smoothly joined portions of quadratic surfaces of revolution (e.g. two spheroids connected by a hyperboloidal neck). The system's Hamiltonian is treated in an approximation in which the potential energy is considered to be a sum of surface and Coulomb energies. The kinetic energy is calculated according to the method of Werner and Wheeler, which approximates the internal hydrodynamical flow by the flow of circular layers of fluid; this type of flow corresponds approximately to the irrotational flow of a nonviscous incompressible fluid. On the basis of this model we calculate probability distributions for the masses and kinetic energies of the fragments at infinity. For nuclei throughout the periodic table the calculated distributions are compared with experimental distributions, as functions of the internal excitation energy of the compound nuclei undergoing fission. The comparisons indicate that this simplified version of the nonviscous irrotational liquid-drop model is not capable of accounting for the properties of the division of heavy nuclei at low excitation energies (e.g. for the observed mass asymmetry). However, it does reproduce approximately experimental fission-fragment mass and energy distributions for the fission of heavy nuclei at high excitation energies (energies above about 40 MeV) and medium nuclei at all excitation energies. In all cases the experimental kinetic energies and widths are larger than the calculated ones (for

nonviscous irrotational flow), and this, along with other evidence, suggests that in the fission process the flow of nuclear matter is either rotational or viscous.

---

†Present address: Group T-9, Los Alamos Scientific Laboratory, Los Alamos, New Mexico

CONTENTS

1. Introduction

In a recent simplified treatment[1]) of the liquid-drop theory of nuclear fission, a certain approximation was employed to calculate the properties of the fission of nuclei lighter than about radium. This approximation consisted of parameterizing the shape of the nuclear surface in terms of two overlapping or separated quadratic surfaces of revolution (spheroids). For light and medium nuclei[†] the resulting saddle-point shapes are fair approximations to the true dumbbell-like liquid-drop saddle-point shapes[2]). The two-spheroid saddle-point shapes consist of two tangent collinear spheroids and therefore coincide with possible scission shapes. It was therefore possible to disregard the dynamical descent of the fissioning nucleus from its saddle point to scission, and this made it fairly easy to work out in a consistent way the predictions of the model. This was done by applying standard static, dynamical and statistical methods to the Hamiltonian for the system. For medium nuclei experimental distributions in the masses and kinetic energies of the fragments at infinity were available for comparison, and certain, but not all, of the properties of these distributions were reproduced by the calculations without the use of adjustable parameters.

Because of the outcome of this study, it was decided to perform similar calculations with a more realistic parameterization of the nuclear shape, so that more could be learned about the predictions of the liquid-drop model for the fission of heavy nuclei. For heavy nuclei the saddle point is <u>not</u> close to the scission point, and consequently it is necessary to calculate the dynamical descent from saddle to scission. The properties of the fission process that we predict are mass and energy distributions of the fragments at infinity. We especially want to establish whether the most probable mass division of an idealized nonviscous irrotational liquid drop is a division into two equal parts or into two unequal parts. The incomplete dynamical calculations of Hill[3,4]) and Hill and Wheeler[5]) left the impression that the

---

[†]We refer to nuclei lighter than about silver as light, to those between about silver and radium as medium, and to those heavier than about radium as heavy.

observed mass asymmetry in the fission of heavy nuclei at low excitation energies is possibly associated with a classical hydrodynamical effect during the descent from the saddle point to scission. Also, from a consideration of statics alone, Businaro and Gallone[6,7]) and Nossoff[8]) concluded that there is possibly a loss of stability against asymmetry between the saddle point and scission. However, as emphasized by Wilets[9,10]), it is impossible to determine whether or not motion beyond the saddle point is stable against asymmetry unless dynamics is also considered (since the shape of the potential-energy surface is not invariant under a change of deformation coordinates). We hope that our dynamical calculations will shed light on this question of the most probable mass division of an idealized nonviscous irrotational liquid drop. We are also interested in the most probable division of the total energy released in the process between the translational kinetic energies of the centers of mass of the fragments at infinity and their vibrational energies. In addition to the most probable values, we also calculate the widths of the fission-fragment mass and energy distributions.

Although of crucial importance in a general theory of the fission process, the dynamics of nuclear division has received only fragmentary attention. Indeed fission dynamics has been considered by a number of authors[1,3-6,11-27]), but in each case only certain limited aspects were studied. For a few special cases the equations of motion for a dividing drop were integrated numerically by Kelson[19]) and by Lawrence[22]). Kelson calculated the kinetic energy by use of the Werner-Wheeler approximation[1,12]),† which is the method that we use for most of our studies here, whereas Lawrence used an exact method (for irrotational flow).‡ Both these studies were restricted to shapes with reflection symmetry, and consequently the most probable mass division was outside their scope. Also, not enough

---

†As we discuss in appendix 6.4.2, one of the terms [eq. (26) of ref. [19])] appearing in Kelson's expression for the kinetic energy is incorrect.

‡However, the small number of terms (two) retained by Lawrence in the expansion of the velocity potential leads to serious numerical inaccuracies, particularly for shapes close to scission.

cases were considered to establish a relationship between initial conditions and final results. Methods for calculating the kinetic energy of the drop have been given in refs. [20,21]) for the case of irrotational flow, and in refs. [23-25]) for realistic single-particle motion, but the solution of the equations of motion was not considered.

The normal modes of oscillation of the system about its saddle-point shape have been studied in ref. [20]) for an idealized drop, and by Hasse[26]) for a system whose potential energy contains curvature and shell energies in addition to the surface and Coulomb energies of the liquid-drop model. For a system whose potential energy contains four such terms, Hasse[27]) is now calculating the properties of the dynamical descent from the vicinity of the saddle point to slightly beyond the scission point. He parameterizes the shape of the drop in terms of the three deformation coordinates of ref. [21]), and since one of these describes asymmetrical shapes, it is possible for him to discuss in an approximate way the question of mass asymmetry, as well as the division of energy between the translational kinetic energies and vibrational energies of the fragments.

The general procedure that we use for calculating mass and energy distributions is analogous to that employed in ref. [1]) and consists of the following steps: (1) The potential energy, which is the sum of the surface energy and the Coulomb energy, is calculated as a function of the deformation coordinates, and the saddle point is located and its properties studied. (2) The kinetic energy is calculated as a function of the coordinates and their time derivatives. (3) The frequencies and eigendisplacements of the normal modes of oscillation of the system about its saddle-point shape are determined. (4) The transition-state method is used to calculate the probability for finding the system in a given state of motion as it passes through the vicinity of the saddle point. (5) The solution of Hamilton's equations of motion tells us the motion of the system from the vicinity of the saddle point onward, for a given set of initial conditions near the saddle point. This final step converts the probability distributions for the states of motion near the saddle point into the desired probability distributions for the observable characteristics of the fission fragments at infinity, namely their masses and energies.

For computational simplicity it is desirable to take into account explicitly as few degrees of freedom as possible. A general discussion of

the degrees of freedom relevant to the fission process is given in ref. [1]). Because we are interested here in the kinetic and vibrational energies and masses of the fragments, we restrict our attention to those degrees of freedom connected with the fragments' separation, eccentricities and relative masses. We consider a total of six such degrees of freedom, and specify the shape of the nuclear surface in terms of three smoothly joined portions of quadratic surfaces of revolution (e.g. two spheroids connected by a hyperboloidal neck)[1,19]). Of the six degrees of freedom associated with such a parameterization, three describe symmetrical deformations, and the remaining three describe asymmetrical deformations. We will wait until later to define precisely our choice of generalized coordinates, but physically the three symmetrical degrees of freedom represent (1) the distance between the centers of the two halves of the drop, (2) the eccentricities of the two halves and (3) the radius of the drop's neck. The three asymmetrical degrees of freedom represent (1) the position of the drop's center of mass, (2) the amount of matter in one half of the drop relative to the other and (3) the position of the drop's neck relative to its center of mass.

By restricting our consideration to these six degrees of freedom, we of course exclude the possibility of discussing certain important aspects of the fission process. For example, because we do not consider the degrees of freedom specifying the angular orientations of the fragments and the orientation of the system as a whole, we are unable to discuss the angular momenta of the fragments and their angular distributions. Our specialization to axially symmetrical shapes excludes the possibility of discussing gamma-like vibrations and the bending or "wriggling" of the system. Also, because our parameterization permits only binary division, we are unable to discuss division into more than two bodies.

Our point of view—and reason for performing this study—is the following: We want to calculate the properties of the division of liquid drops whose charge, surface tension, mass and size correspond to those of nuclei, and to compare the results of these calculations with what is observed experimentally in the fission of real nuclei. Then from the comparisons we hope to learn unambiguously to what extent an idealized nonviscous irrotational liquid-drop model is capable of representing the essential characteristics of fission. This we feel we can do because there are no adjust-

able parameters in the problem—the values of all the relevant constants that enter the theory are taken directly from analyses of nuclear masses, etc., rather than being adjusted arbitrarily to the fission data themselves.

The general conclusion reached from the comparisons is that the non-viscous irrotational liquid-drop model yields an approximate description of mass and energy distributions for the fission of medium nuclei at all excitation energies and heavy nuclei at high excitation energies, but that, within the limitation of a parameterization that permits only binary division, it does not reproduce the observed properties of the fission of heavy nuclei at low excitation energies (e.g. mass asymmetry).

2. Hamiltonian

We are concerned in this section with the Hamiltonian for the system—with defining the generalized deformation coordinates, and with calculating the potential and kinetic energies. In preparation for this discussion we first review our system of natural liquid-drop units[1]), which is based on the radius, surface energy and mass of the spherical drop. In converting from these natural units to conventional units, we use for the constants of the semi-empirical mass formula the second set of Myers and Swiatecki[28]).

The radius R_0 of the spherical drop is related to A, the number of nucleons in the compound nucleus, by

$$R_0 = r_0 A^{1/3} \quad , \tag{1a}$$

with

$$r_0 = 1.2249 \text{ fm} \quad .$$

The surface energy $E_s^{(0)}$ of the spherical drop is given by

$$E_s^{(0)} = a_s \left\{ 1 - \kappa [(N-Z)/A]^2 \right\} A^{2/3} \quad , \tag{1b}$$

with

$$a_s = 17.9439 \text{ MeV} \quad ,$$

$$\kappa = 1.7826 \quad ;$$

this expression includes a term for the dependence of the surface energy on the difference N - Z between neutron and proton numbers. The mass M_0 of the original drop, to an accuracy within one part per thousand, is given by

$$M_0 = m_0 A \quad , \tag{1c}$$

with

$$m_0 = 1.660 \times 10^{-24} \text{ g} = 931 \text{ MeV}/c^2 \qquad \text{[ref. 29)]};$$

the symbol c denotes the speed of light.

In terms of the above three fundamental units, the natural unit of time is given by

$$T_0 = [M_0/E_s^{(0)}]^{\frac{1}{2}} R_0 = 2.943 \times 10^{-23} \left\{ 1 - 1.7826[(N-Z)/A]^2 \right\}^{-\frac{1}{2}} A^{\frac{1}{2}} \text{ sec} \quad .$$

The unit of frequency is then

$$\Omega_0 = 1/T_0 = 3.398 \times 10^{22} \left\{ 1 - 1.7826[(N-Z)/A]^2 \right\}^{\frac{1}{2}} A^{-\frac{1}{2}} \text{ sec}^{-1} \quad , \tag{2a}$$

which becomes, upon multiplying by Planck's constant divided by 2π,

$$\hbar\Omega_0 = 22.36 \left\{ 1 - 1.7826[(N-Z)/A]^2 \right\}^{\frac{1}{2}} A^{-\frac{1}{2}} \text{ MeV} \quad . \tag{2b}$$

We next introduce the dimensionless fissility parameter x, which is defined by the equation

$$x = E_c^{(0)}/[2E_s^{(0)}] \quad . \tag{3a}$$

The quantity $E_c^{(0)}$ is given by

$$E_c^{(0)} = 3 Z^2 e^2/(5R_0) = a_c Z^2/A^{1/3} \quad ,$$

where e is the electronic charge and

$$a_c = 0.7053 \text{ MeV} \qquad [\text{ref. } 28)].$$

Although the semi-empirical mass formula of Myers and Swiatecki[28,30] takes into account the dependence of the Coulomb energy on the surface diffuseness of the charge distribution, $E_c^{(0)}$ represents physically what the Coulomb energy would be for an equivalent sharp drop[30]. A second convenient form for x is obtained by substituting for $E_c^{(0)}$ and $E_s^{(0)}$ in eq. (3a), and is

$$x = \frac{Z^2/A}{50.88\left\{1 - 1.7826[(N-Z)/A]^2\right\}} \quad . \tag{3b}$$

The advantage of using these natural liquid-drop units is that in terms of them the results of our calculations are functions of the single parameter x rather than functions of two parameters (e.g. Z and A).

2.1. DEFORMATION COORDINATES

We do not consider effects that arise from the deviation of the system from axial symmetry, and therefore specialize from the outset to shapes that are axially symmetrical. The conventional method for representing such shapes is to expand the drop's radius vector in a series of Legendre polynomials. Although this method is satisfactory for nearly spherical shapes, it has the disadvantages that (1) a large number of terms are required to represent adequately the more deformed shapes of interest in fission[2]), (2) it is impossible to describe in a continuous way the transition from a single body to separated fragments and (3) it is impossible to describe shapes with more than one neck.

A search was made for a better way to describe the shape of the nuclear surface, and the method that we decided upon overcomes the first two of these disadvantages but still suffers from the third. The parameterization specifies the nuclear shape in terms of three smoothly joined portions of quadratic surfaces of revolution (e.g. two spheroids connected by a hyperboloidal neck). An example of a shape described in this way is shown in fig. 1. Because three numbers are required for the specification of each

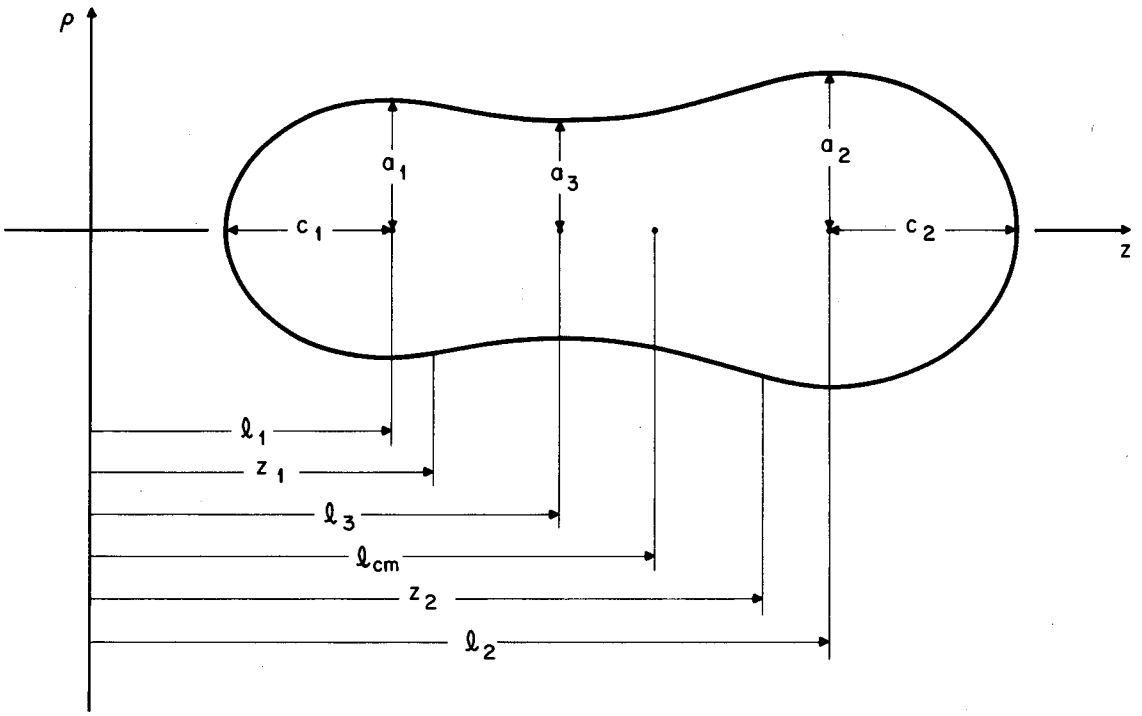

Fig. 1. An illustration of a shape described by three smoothly joined portions of quadratic surfaces of revolution. Each surface is specified by the position ℓ_i of its center, its transverse semiaxis a_i and its semisymmetry axis c_i (the quantity c_3 is imaginary for this shape and hence not shown). The middle hyperboloid of revolution joins smoothly with the two end spheroids at z_1 and z_2. The location ℓ_{cm} of the center of mass of the drop is also shown.

quadratic surface of revolution (e.g. its major and minor axes and the position of its center), nine numbers are required to specify a general shape made up of three such collinear surfaces of revolution. We denote the left-hand surface by the subscript 1, the right-hand one by 2, and the middle one by 3. In terms of a cylindrical coordinate system (see again fig. 1), the equation for the drop's surface can then be written explicitly as

$$\rho^2 = \begin{cases} a_1^2 - (a_1^2/c_1^2)(z-\ell_1)^2 & , \quad \ell_1 - c_1 \le z \le z_1 \\ a_2^2 - (a_2^2/c_2^2)(z-\ell_2)^2 & , \quad z_2 \le z \le \ell_2 + c_2 \\ a_3^2 - (a_3^2/c_3^2)(z-\ell_3)^2 & , \quad z_1 \le z \le z_2 \quad , \end{cases} \tag{4}$$

where z_1 and z_2 are the values of z at the intersections of the middle surface with, respectively, the left-hand and right-hand surfaces.

The constancy of the volume of the drop (arising from our assumption of incompressibility) eliminates one of the nine degrees of freedom, and the requirement that the middle surface join smoothly with each of the two end surfaces eliminates two more degrees of freedom. This introduces three relationships among the nine numbers and reduces to six the number of deformation coordinates required to specify our system. In principle the number of degrees of freedom could be reduced further to five by solving for and eliminating the position of the drop's center of mass. However, it turns out in practice to be advantageous to retain this coordinate, which is then eliminated implicitly when the equations of motion are solved.

Of these six degrees of freedom, three represent symmetrical deformations of the system, and the remaining three represent asymmetrical deformations. The deformation coordinates are defined in terms of appropriate ratios of the geometrical parameters that specify the three quadratic surfaces of revolution. To permit a natural division of the coordinates into those describing symmetrical deformations and those describing asymmetrical ones, we define an auxiliary unit of distance u by the equation

$$u = \left[\tfrac{1}{2}\left(a_1^2 + a_2^2\right)\right]^{\frac{1}{2}} \quad . \tag{5}$$

For a symmetrical shape the unit of distance is thus the transverse semi-axis of either end spheroid. The three symmetrical coordinates are then defined by

$$\sigma_1 = (\ell_2 - \ell_1)/u \quad , \tag{6a}$$

$$\sigma_2 = a_3^2/c_3^2 \quad , \tag{6b}$$

$$\sigma_3 = \tfrac{1}{2}\left[\left(a_1^2/c_1^2\right) + \left(a_2^2/c_2^2\right)\right] \quad , \tag{6c}$$

and the three asymmetrical coordinates by

$$\alpha_1 = \tfrac{1}{2}(\ell_1 + \ell_2)/u \quad , \tag{6d}$$

$$\alpha_2 = (a_1^2 - a_2^2)/u^2 \quad , \tag{6e}$$

$$\alpha_3 = (a_1^2/c_1^2) - (a_2^2/c_2^2) \quad . \tag{6f}$$

In practice the actual shape of the system is found in terms of these six coordinates by inverting eqs. (5) and (6) and the equations expressing volume conservation and the smooth connections of the middle surface with the two end surfaces. This inversion is carried out explicitly in appendix 6.1, but for qualitative purposes it suffices to know that the nine numbers ℓ_i, a_i^2 and a_i^2/c_i^2 ($i = 1, 2, 3$), which uniquely define the shape and linear position of the drop, are explicit functions of σ_1, σ_2, σ_3, α_1, α_2 and α_3. (It also proves necessary to be able to calculate the first partial derivatives of these numbers with respect to the generalized deformation coordinates, and formulas for such derivatives are given in appendix 6.2.)

This parameterization is capable of representing in a continuous way the sequence of shapes from the original sphere, through the saddle and scission shapes, to the two fragments at infinity. In going through these shapes the two end quadratic surfaces of revolution are always spheroids, but the middle quadratic surface of revolution is originally a spheroid, then becomes a hyperboloid of revolution of one sheet, and at the scission point becomes a hyperboloid of revolution of two sheets. These transitions

are illustrated in fig. 2, where we show some of the possible shapes that the middle quadratic surface of revolution can assume for certain values of a_3^2 and a_3^2/c_3^2. It is seen that since a_3^2 and a_3^2/c_3^2 can be either positive or negative (although the quadrant in which a_3^2 is negative and a_3^2/c_3^2 is positive is unphysical), the semiaxes a_3 and c_3 can assume imaginary values, which is one of our reasons for working in terms of a_3^2 and a_3^2/c_3^2 rather than a_3 and c_3.

It should be emphasized from the outset that, in addition to its restriction to axial symmetry, the present parameterization is deficient in two important respects. First of all, it is not as satisfactory for discussing small deviations of the drop from a spherical shape as an expansion of the drop's radius vector in spherical harmonics, or as satisfactory for discussing small deviations from a spheroidal shape as an expansion about a spheroid. Some comments are made in appendix 6.1 on the restrictions on this parameterization for shapes close to a sphere or a spheroid. However, this limitation is not serious here because the large deformations of primary interest in fission are far removed from a sphere or a spheroid.

The second deficiency of the parameterization is its inability to describe shapes with more than one neck or to describe division into more than two bodies. In the early stages of this work we planned not to require that the surfaces join smoothly; this would have permitted a rough description of a drop with two necks and a division into three bodies. However, a discontinuity of this type in the surface of the drop introduces difficulties in treating the time evolution of the system,† and the idea of permitting the surfaces to join with discontinuous slopes was abandoned. It must be borne in mind, then, that all the conclusions reached in this work are subject to the limitation of a parameterization that permits the formation of

---

†The difficulties arise because the amount of mass displaced in changing the point of intersection of two surfaces goes to zero as the slopes of the two joining surfaces become equal. If the resulting singular inertia matrix is transformed into a nonsingular one through a change of coordinates, a cusp at the point of tangency is introduced simultaneously into the potential energy.

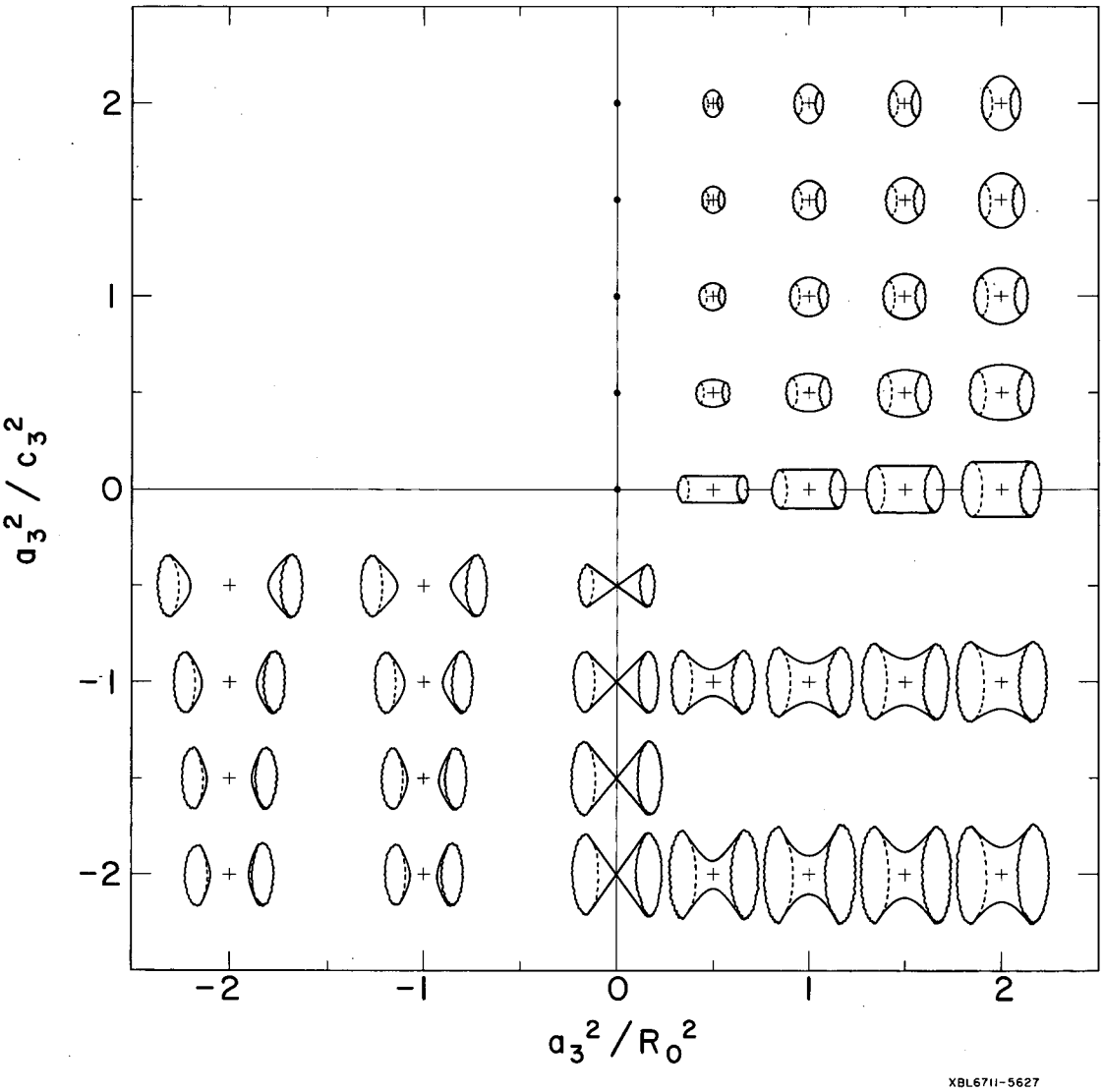

Fig. 2. Illustrations of the shape of the middle quadratic surface of revolution for selected values of a_3^2 and a_3^2/c_3^2. A thin reference mark (+) placed at the appropriate value of a_3^2 and a_3^2/c_3^2 locates the center of each shape (except for those with $a_3^2 = 0$). The complete surface of the system consists of such a shape plus a portion of a spheroid smoothly joined at each end. The left-hand and right-hand portions of the middle surface are in general not of the same length.

a single neck and division into only two bodies.

Finally we would like to point out that although the above parameterization is used here in a study of the liquid-drop model it is much more general and can be used for any study involving deformed axially symmetrical shapes. The calculation of the energies and wave functions of single particles in a potential well whose geometrical shape is described in this way is a particular example of importance in nuclear physics [see for example ref. [31]), where a somewhat related parameterization is suggested]. Also, if it is desired to describe deformed nonaxially symmetrical shapes (i.e. gamma deformations), the present parameterization could be generalized in a straightforward way by replacing the three quadratic surfaces of revolution by general quadratic surfaces (e.g. two ellipsoids connected by a hyperboloid). This generalization would be particularly useful for discussing the properties of the equilibrium shapes of a rotating charged or gravitating drop [see for example ref. [32]) for a discussion of this problem].

2.2. POTENTIAL ENERGY

In the simple version of the liquid-drop model that we are using the potential energy of the system is the sum of the surface energy, which tends to keep the drop spherical, and the Coulomb energy, which tends to deform it. As discussed in ref. [30]) the first-order correction to the Coulomb energy that results from the surface diffuseness of the charge distribution is strictly independent of deformation, and consequently it is sufficient to consider the Coulomb energy of an equivalent sharp distribution when discussing the deformation properties of the system. We should also be reminded at this point that the surface energy E_s includes an asymmetry term to account for the difference between the neutron and proton numbers.

The potential energy $\mathcal{V}$ of a deformed drop relative to the spherical drop is then

$$\begin{aligned} \mathcal{V} &= E_s - E_s^{(0)} + E_c - E_c^{(0)} \\ &= (B_s - 1)\, E_s^{(0)} + (B_c - 1)\, E_c^{(0)} \\ &= [(B_s - 1) + 2 \times (B_c - 1)]\, E_s^{(0)} \quad . \end{aligned} \tag{7}$$

We have used the definition (3a) of the fissility parameter x in going from the second to the third line. The function B_s is the total surface energy of the drop in units of the surface energy $E_s^{(0)}$ of the spherical drop, and B_c is the Coulomb energy of the drop (for a sharp charge distribution) in units of the corresponding Coulomb energy $E_c^{(0)}$ of the spherical drop. The two functions B_s and B_c depend only upon the six generalized deformation coordinates that specify the shape of the drop.

In addition to the surface and Coulomb energies, we must be able to calculate the generalized forces acting on the drop, i.e. (the negative of) the first partial derivatives of the energies with respect to the deformation coordinates. Because the drop's surface is made up of portions of quadratic surfaces of revolution, the surface energy and its derivatives are expressible in terms of elementary transcendental functions, whereas the Coulomb energy and its derivatives require for their evaluation two-fold numerical integrations. Formulas are given in appendix 6.3.1 for the surface energy and its derivatives, and in appendix 6.3.2 for the Coulomb energy and its derivatives.

The locations and properties of the saddle points that occur in the multidimensional potential-energy surface play a central role in fission theory. For a given value of the fissility parameter x the location of the saddle point is determined by solving (using a standard iterative method) the set of six nonlinear equations obtained by equating to zero the expressions for the six generalized forces. For the family of <u>symmetrical</u> saddle-point shapes the energies, shapes, and maximum and minimum radii of the shapes corresponding to our parameterization have already been shown in figs. 8-11 of ref. [1]). Comparisons are made there between the results calculated with the parameterization in terms of three quadratic surfaces of revolution and the results calculated by Cohen and Swiatecki[2]) and by Strutinskiĭ <u>et al</u>.[33]). The comparisons indicate that the present parameterization is remarkably accurate in representing the static properties of the symmetrical saddle-point shapes. For $x < 0.51$ the three-quadratic-surface parameterization is in fact more accurate than expanding the drop's radius vector in terms of a series of 18 Legendre polynomials[2]). This conclusion is based upon the principle that the more adequate parameterization yields a lower potential energy at the saddle point. For $x > 0.51$ the use of 18 Legendre polynomials is slightly better than the use of three quadratic

surfaces, but the potential energy calculated with the former parameterization is never less than that calculated with the latter by more than $0.00066\ E_s^{(0)} \approx 0.4$ MeV, which occurs at $x = 0.67$. In this connection it should be mentioned that Lawrence's parameterization[22,34], defined in terms of an expansion of ρ^2 in powers of z (with sufficient terms retained to make two symmetrical deformation coordinates), is also remarkably accurate for $x \gtrsim 0.7$ but deteriorates rapidly for smaller values of x.

The work reported in ref. [1] on the three-quadratic-surface parameterization was limited to symmetrical shapes, whereas the subsequent work has included in addition asymmetrical shapes. We have tested the symmetrical saddle-point shapes for stability against asymmetry, and have found them to be stable (apart from neutral stability against a shift of the center of mass) from $x = 1$ down to x_{BG}, the critical Businaro-Gallone point[35], whose value we determine as 0.396. This confirms the calculations of ref. [2], where x_{BG} was determined as 0.39_4 to within an accuracy of a few units in the third decimal place. Strutinskiĭ[36] has claimed that a loss of stability against asymmetry also occurs at $x \approx 0.8$, and the question of whether or not this is true was raised in ref. [37]. Both the present results and those of ref. [2] indicate that no loss of stability occurs at $x \approx 0.8$ and therefore suggest that Strutinskiĭ's conclusion is incorrect. For $x < x_{BG}$ the symmetrical saddle-point shapes are unstable with respect to mass asymmetry as well as with respect to the symmetrical distortion leading to fission[2,35,38], and consequently do not physically represent shapes at barrier tops[38].

We have also calculated the static properties of the asymmetrical saddle-point shapes for values of x from x_{BG} up to 0.80, and the results agree approximately with those of Strutinskiĭ[39]. These asymmetrical saddle-point shapes have energies that are higher than the symmetrical saddle-point shapes (for corresponding values of x), and are unstable with respect to two degrees of freedom (in addition to a center-of-mass shift). They therefore also do not represent shapes at barrier tops. For $x > 0.80$ we were unable to obtain solutions for the asymmetrical saddle points [as was also Strutinskiĭ[39])]. The fate of this family of asymmetrical equilibrium shapes for larger values of x is unknown but is of great interest in connection with general properties of families of equilibrium configurations [see for example ref. [32])].

We summarize in a set of four figures the static properties of the saddle-point shapes calculated with the three-quadratic-surface parameterization. In each figure we use solid lines for symmetrical shapes and dashed lines for asymmetrical shapes. The total potential energy of the saddle-point shape relative to the sphere is shown in fig. 3, and the individual surface and Coulomb energies B_s and B_c are shown in fig. 4. Figure 5 contains the values of the six generalized coordinates corresponding to the saddle-point shapes, and fig. 6 the maximum and minimum radii of the saddle-point shapes.

We also present in table 1 some of the static properties of the symmetrical saddle-point shapes at intervals of 0.02 in x over the range from x = 1.00 down to 0.06. The properties tabulated divide naturally into three groups. The first group includes the total potential energy $\mathcal{V}$ and the relative surface and Coulomb energies B_s and B_c. As discussed earlier the values of ref. [2]) for these three quantities should be slightly more accurate than our values for $x \geq 0.52$ [however, the results of ref. [2]) are slightly inaccurate for values of x close to 1], whereas our values are preferred for $x \leq 0.50$. The second group contains the values of the three symmetrical deformation coordinates σ_1, σ_2 and σ_3 (the three asymmetrical coordinates α_1, α_2 and α_3 are zero). The final group of tabulated quantities contains the geometrical parameters of the quadratic surfaces of revolution. In this connection see again fig. 1, and recall that since the shapes are symmetrical $u = a_1 = a_2$, $c_1 = c_2$, $\ell_1 = -\ell_2$, and $z_1 = -z_2$. For $x \leq 0.78$ the quantity c_3 is imaginary, and the symbol i is used to denote the square root of -1.

2.3. KINETIC ENERGY

We consider now the calculation of the kinetic energy of the system, which depends not only upon the shape of the drop and its time rate of change, but also upon the nature of the hydrodynamical flow of the fluid inside the drop. To arrive at a formula for the kinetic energy in terms of the generalized coordinates and their time derivatives, we must therefore specify the curl (rotation or vorticity) in the system. As a tractable limiting case for which it is important to know the consequences we consider the case of irrotational hydrodynamical flow.

Is the assumption of irrotational flow a logical one for a study of the dynamics of the fission process? It is already known that nuclear flow is not irrotational for two types of deformations of interest in fission: (1) small oscillations about ground-state equilibrium shapes[†] and (2) the penetration of the fission barrier in spontaneous fission.[‡] However, in fission one is also interested in the large deformations encountered beyond the position where the spontaneously fissioning nuclei emerge through the barrier, and in some cases in fairly high excitation energies. For these situations there is no direct experimental information concerning the type of flow. We therefore work out the consequences for irrotational flow, and hope to deduce whether or not the flow is in fact irrotational by comparing our calculations with experimental results. (The comparisons suggest that in the fission process the flow of nuclear matter is either rotational or viscous; see sect. 5.)

[†] See for example refs. [40,41]), where it is shown that quadrupole vibrational inertial parameters of even nuclei about spherical ground-state equilibrium shapes are several times as large as the values corresponding to irrotational flow.

[‡] Analyses of experimental spontaneous-fission half lives and fission-barrier heights for nuclei in the actinide region suggest that several times as much mass is displaced in penetrating the fission barrier as would correspond to irrotational flow[20,42]).

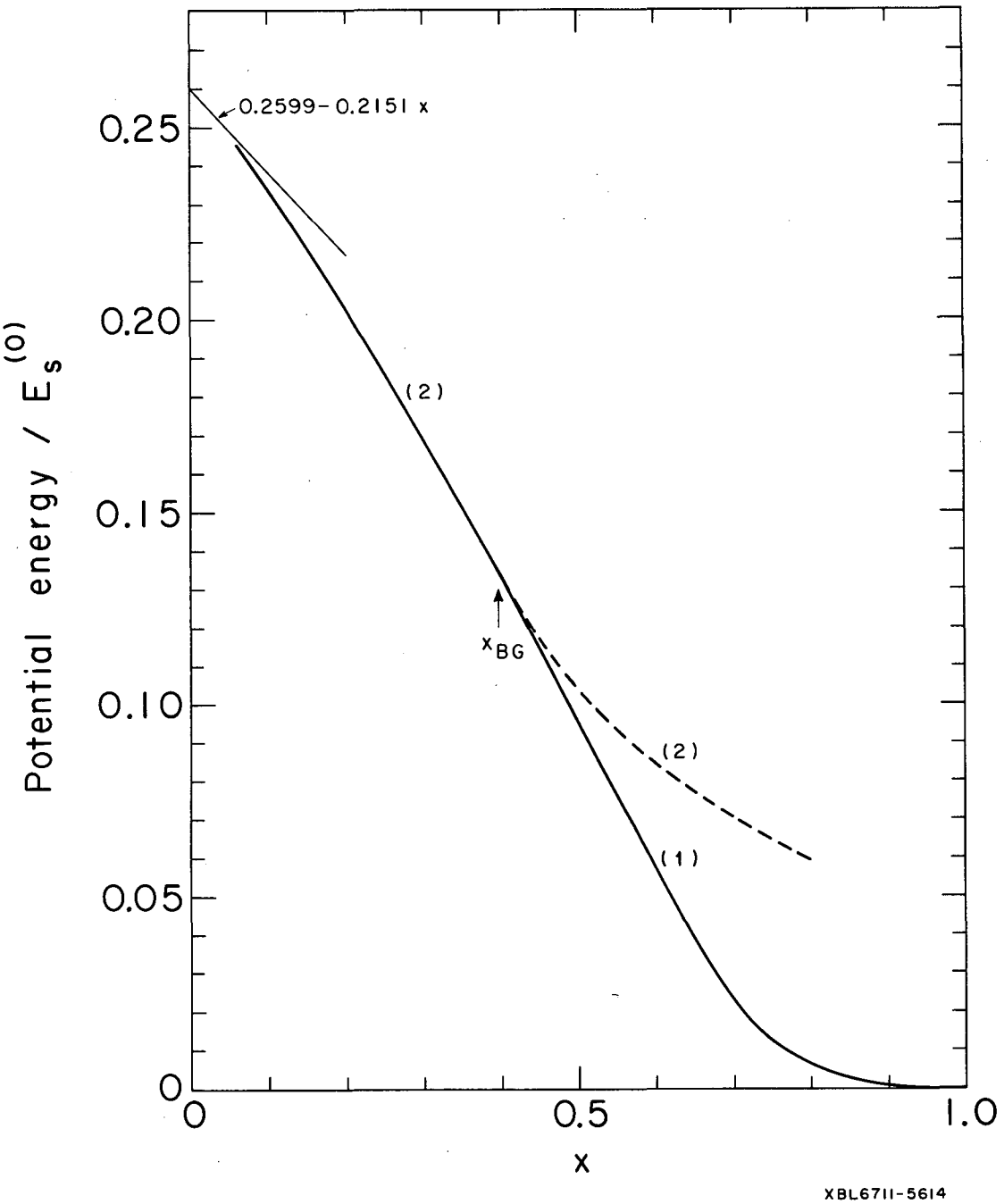

Fig. 3. The potential energies of saddle-point shapes as functions of the fissility parameter x. The energy of the symmetrical saddle-point shape is given by the solid curve, and of the asymmetrical saddle-point shape by the dashed curve. The critical Businaro-Gallone point is indicated by the arrow, and the degrees of instability by the numbers in parentheses. The thin straight line shows the known limiting form of the potential energy for small values of x.

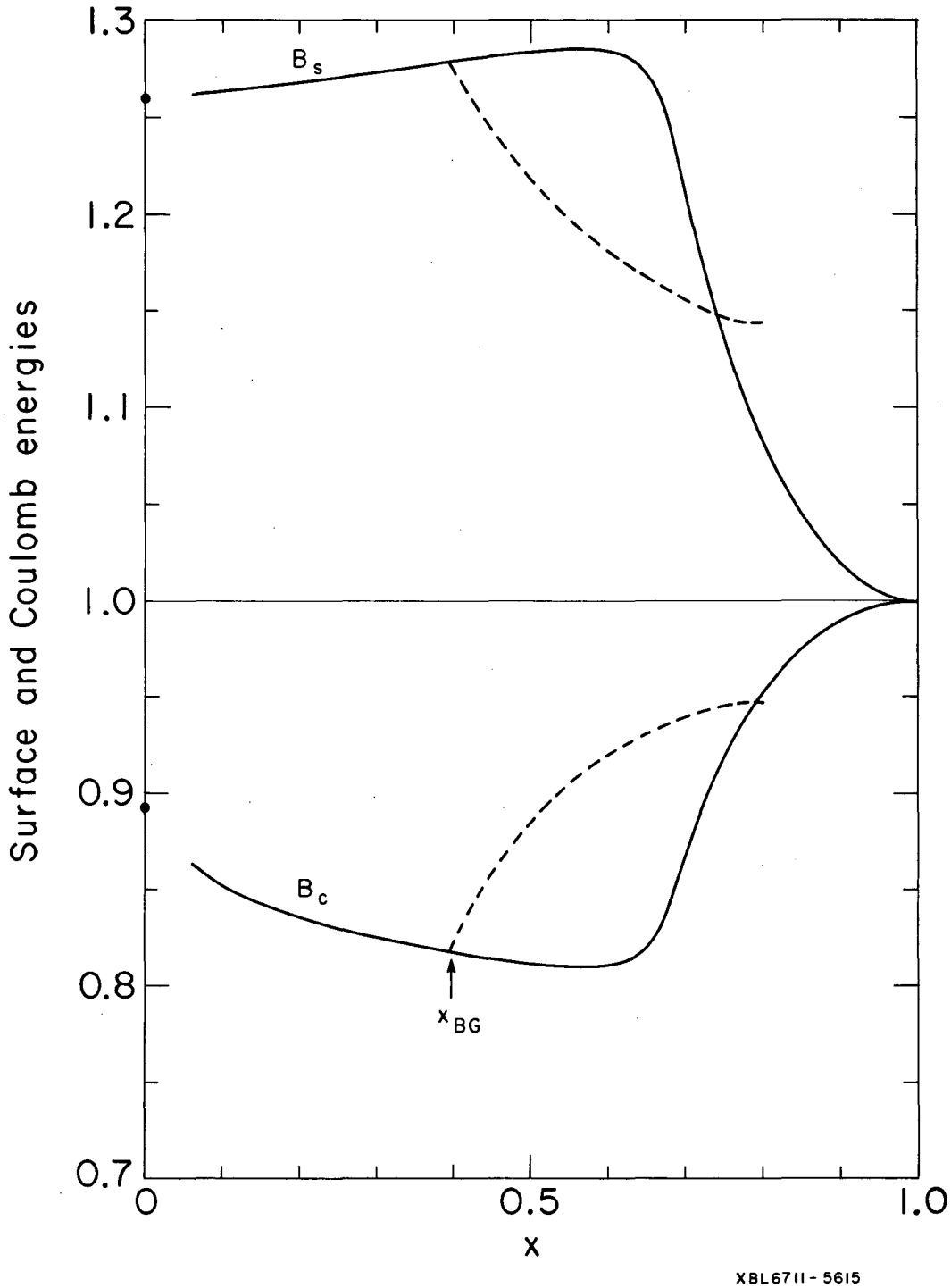

Fig. 4. The surface energies B_s and Coulomb energies B_c of saddle-point shapes as functions of the fissility parameter x. The results for the symmetrical saddle-point shapes are given by the solid curves, and the results for the asymmetrical saddle-point shapes by the dashed curves. The critical Businaro-Gallone point is indicated by the arrow, and the known values of B_s and B_c for x = 0 by solid points.

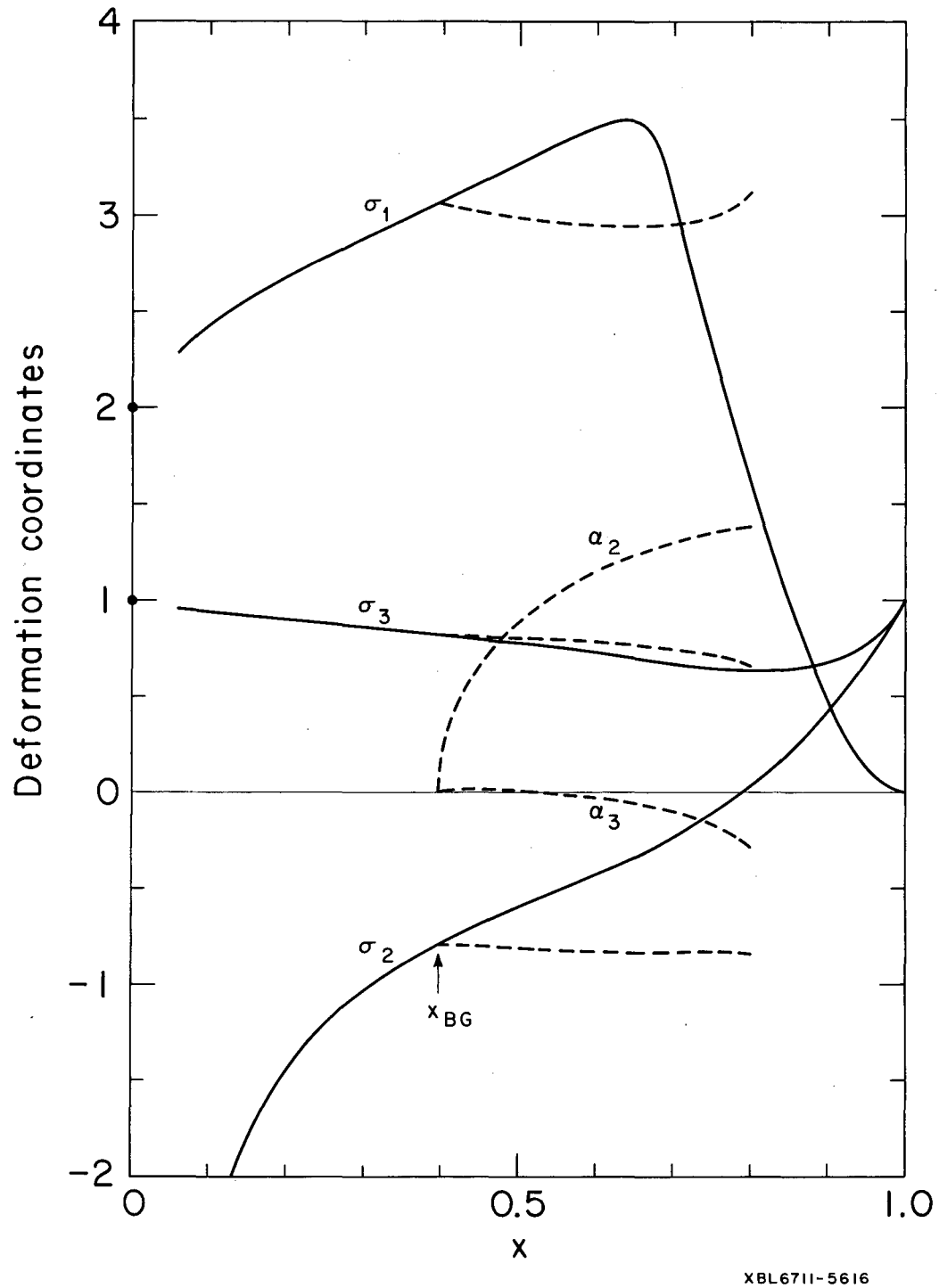

Fig. 5. The generalized deformation coordinates for saddle-point shapes as functions of the fissility parameter x. The results for the symmetrical saddle-point shapes are given by the solid curves, and the results for the asymmetrical saddle-point shapes by the dashed curves (asymmetrical saddle-point shapes of course exist corresponding to a change in sign of all the asymmetrical coordinates). The critical Businaro-Gallone point is indicated by the arrow, and the known values of σ_1 and σ_3 for x = 0 by solid points.

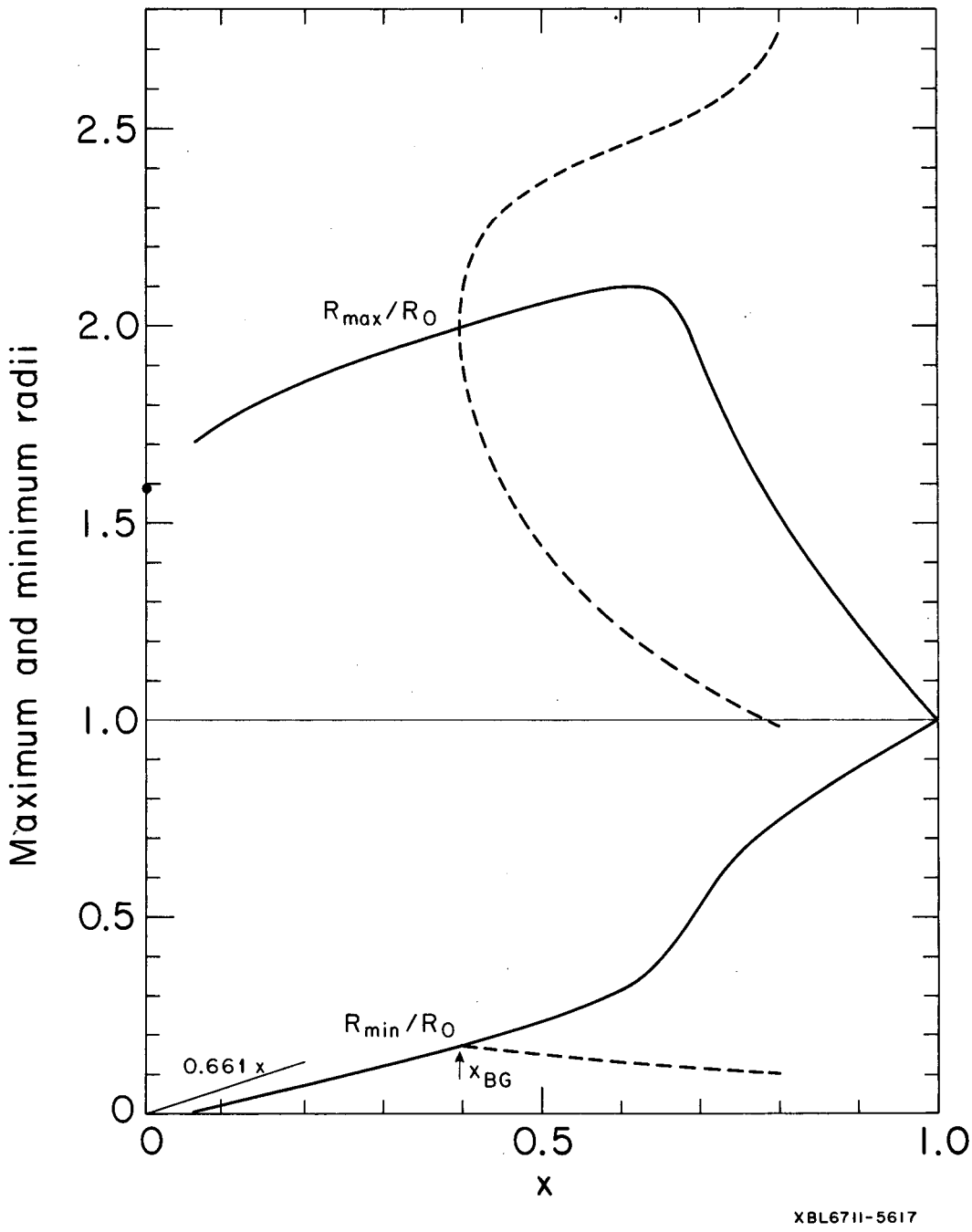

Fig. 6. The maximum and minimum radii of saddle-point shapes as functions of the fissility parameter x. The results for the symmetrical saddle-point shapes are given by the solid curves, and the results for the asymmetrical saddle-point shapes by the dashed curves. [For an asymmetrical shape the minimum radius is defined as the minimum radius of the neck, and the two maximum radii as the distances from the center of the neck (at its minimum radius) to the two ends of the drop.] The critical Businaro-Gallone point is indicated by the arrow, the known value of R_{max}/R_0 for x = 0 by the solid point, and the known limiting form of R_{min}/R_0 for small values of x by the thin straight line.

Table 1

Properties of saddle-point shapes as functions of the fissility parameter x

x	$\mathcal{V}/E_s^{(0)}$	B_s	B_c	σ_1	σ_2	σ_3	a_2/R_0	c_2/R_0	ℓ_2/R_0	z_2/R_0	a_3/R_0	c_3/R_0
1.00	0.00000	1.00000	1.00000	0.00000	1.00000	1.00000	1.00000	1.00000	0.00000	———	1.00000	1.00000
0.98	0.00001	1.00086	0.99957	0.02080	0.86581	0.88344	0.97444	1.03673	0.01013	0.50775	0.97672	1.04969
0.96	0.00005	1.00338	0.99827	0.08271	0.74226	0.80297	0.94554	1.05519	0.03910	0.51721	0.95344	1.10667
0.94	0.00016	1.00750	0.99609	0.18301	0.62855	0.74714	0.91503	1.05861	0.08373	0.52752	0.93008	1.17314
0.92	0.00037	1.01319	0.99303	0.31754	0.52373	0.70833	0.88437	1.05078	0.14041	0.53878	0.90649	1.25259
0.90	0.00073	1.02044	0.98905	0.48165	0.42699	0.68149	0.85464	1.03527	0.20582	0.55113	0.88252	1.35057
0.88	0.00126	1.02927	0.98409	0.67086	0.33758	0.66321	0.82661	1.01503	0.27727	0.56472	0.85799	1.47671
0.86	0.00201	1.03974	0.97807	0.88123	0.25485	0.65117	0.80077	0.99234	0.35283	0.57971	0.83268	1.64946
0.84	0.00303	1.05195	0.97088	1.10951	0.17822	0.64380	0.77739	0.96886	0.43126	0.59635	0.80633	1.90999
0.82	0.00436	1.06604	0.96239	1.35320	0.10719	0.64001	0.75661	0.94576	0.51192	0.61491	0.77859	2.37806
0.80	0.00606	1.08224	0.95238	1.61051	0.04130	0.63909	0.73852	0.92381	0.59470	0.63578	0.74902	3.68580
0.78	0.00819	1.10085	0.94060	1.88041	-0.01992	0.64062	0.72319	0.90355	0.67995	0.65945	0.71699	5.08066i
0.76	0.01084	1.12229	0.92667	2.16255	-0.07690	0.64439	0.71073	0.88538	0.76849	0.68655	0.68158	2.45779i
0.74	0.01409	1.14717	0.91008	2.45703	-0.13022	0.65046	0.70138	0.86965	0.86166	0.71793	0.64139	1.77740i
0.72	0.01808	1.17623	0.89017	2.76301	-0.18062	0.65918	0.69566	0.85683	0.96106	0.75436	0.59414	1.39798i
0.70	0.02293	1.20963	0.86664	3.07051	-0.22927	0.67122	0.69462	0.84783	1.06641	0.79490	0.53679	1.12105i
0.68	0.02876	1.24296	0.84250	3.32933	-0.27689	0.68643	0.69927	0.84400	1.16404	0.82946	0.47078	0.89467i
0.66	0.03542	1.26532	0.82584	3.46149	-0.32092	0.70144	0.70716	0.84436	1.22392	0.83972	0.41261	0.72835i
0.64	0.04258	1.27619	0.81749	3.49386	-0.35990	0.71404	0.71447	0.84552	1.24813	0.82986	0.37108	0.61855i
0.62	0.04997	1.28126	0.81347	3.48360	-0.39557	0.72499	0.72052	0.84621	1.25499	0.81197	0.34067	0.54165i
0.60	0.05747	1.28362	0.81155	3.45625	-0.42946	0.73502	0.72561	0.84635	1.25394	0.79148	0.31666	0.48320i
0.58	0.06503	1.28458	0.81073	3.42163	-0.46248	0.74451	0.73002	0.84605	1.24893	0.77038	0.29657	0.43609i
0.56	0.07260	1.28477	0.81056	3.38390	-0.49512	0.75363	0.73393	0.84543	1.24178	0.74942	0.27910	0.39664i
0.54	0.08017	1.28450	0.81081	3.34481	-0.52785	0.76249	0.73748	0.84456	1.23336	0.72882	0.26341	0.36256i

Table 1 (continued)

x	$\nu/E_s^{(0)}$	B_s	B_c	σ_1	σ_2	σ_3	a_2/R_0	c_2/R_0	ℓ_2/R_0	z_2/R_0	a_3/R_0	c_3/R_0
0.52	0.08773	1.28394	0.81133	3.30534	-0.56094	0.77116	0.74072	0.84350	1.22417	0.70868	0.24906	0.33255i
0.50	0.09526	1.28320	0.81206	3.26592	-0.59463	0.77965	0.74373	0.84230	1.21448	0.68899	0.23573	0.30570i
0.48	0.10276	1.28235	0.81293	3.22676	-0.62915	0.78800	0.74653	0.84098	1.20445	0.66972	0.22318	0.28137i
0.46	0.11023	1.28141	0.81393	3.18795	-0.66476	0.79622	0.74917	0.83959	1.19416	0.65081	0.21126	0.25911i
0.44	0.11765	1.28042	0.81503	3.14947	-0.70170	0.80432	0.75167	0.83813	1.18368	0.63217	0.19984	0.23856i
0.42	0.12502	1.27941	0.81621	3.11131	-0.74023	0.81233	0.75404	0.83662	1.17302	0.61375	0.18882	0.21946i
0.40	0.13235	1.27837	0.81747	3.07338	-0.78068	0.82025	0.75630	0.83507	1.16220	0.59546	0.17812	0.20159i
0.38	0.13962	1.27732	0.81881	3.03560	-0.82339	0.82809	0.75847	0.83349	1.15120	0.57724	0.16768	0.18479i
0.36	0.14684	1.27627	0.82023	2.99788	-0.86878	0.83586	0.76055	0.83188	1.14002	0.55900	0.15744	0.16891i
0.34	0.15400	1.27522	0.82173	2.96011	-0.91734	0.84358	0.76256	0.83025	1.12863	0.54068	0.14736	0.15385i
0.32	0.16110	1.27418	0.82332	2.92216	-0.96969	0.85126	0.76450	0.82860	1.11700	0.52217	0.13739	0.13952i
0.30	0.16814	1.27314	0.82500	2.88389	-1.02658	0.85890	0.76638	0.82694	1.10509	0.50341	0.12749	0.12583i
0.28	0.17510	1.27210	0.82678	2.84516	-1.08898	0.86654	0.76822	0.82526	1.09285	0.48427	0.11762	0.11271i
0.26	0.18199	1.27108	0.82868	2.80578	-1.15813	0.87417	0.77001	0.82356	1.08023	0.46465	0.10776	0.10013i
0.24	0.18880	1.27006	0.83071	2.76554	-1.23568	0.88182	0.77176	0.82185	1.06716	0.44441	0.09785	0.08803i
0.22	0.19553	1.26906	0.83290	2.72420	-1.32389	0.88950	0.77348	0.82011	1.05355	0.42339	0.08788	0.07637i
0.20	0.20217	1.26806	0.83527	2.68145	-1.42589	0.89725	0.77517	0.81835	1.03929	0.40140	0.07779	0.06515i
0.18	0.20871	1.26707	0.83787	2.63692	-1.54628	0.90508	0.77685	0.81657	1.02424	0.37816	0.06757	0.05434i
0.16	0.21514	1.26610	0.84074	2.59011	-1.69203	0.91303	0.77851	0.81475	1.00821	0.35336	0.05719	0.04397i
0.14	0.22144	1.26514	0.84395	2.54035	-1.87436	0.92114	0.78017	0.81288	0.99096	0.32653	0.04663	0.03406i
0.12	0.22761	1.26418	0.84762	2.48674	-2.11255	0.92947	0.78184	0.81096	0.97212	0.29703	0.03593	0.02472i
0.10	0.23363	1.26325	0.85188	2.42801	-2.44283	0.93810	0.78354	0.80897	0.95122	0.26393	0.02524	0.01615i
0.08	0.23945	1.26233	0.85698	2.36244	-2.94102	0.94717	0.78527	0.80687	0.92758	0.22596	0.01499	0.00874i
0.06	0.24505	1.26147	0.86320	2.28808	-3.78871	0.95697	0.78707	0.80457	0.90044	0.18157	0.00627	0.00322i

The kinetic energy $\mathcal{T}$ of the drop corresponding to nonviscous irrotational flow can be written in the form

$$\mathcal{T} = \tfrac{1}{2} \sum_{i=1}^{6} \sum_{j=1}^{6} M(q)_{ij}\, \dot{q}_i\, \dot{q}_j \quad , \tag{8}$$

where we use the six-component vector

$$q = \begin{pmatrix} q_2 \\ q_4 \\ q_6 \\ q_1 \\ q_3 \\ q_5 \end{pmatrix} = \begin{pmatrix} \sigma_1 \\ \sigma_2 \\ \sigma_3 \\ \alpha_1 \\ \alpha_2 \\ \alpha_3 \end{pmatrix}$$

to denote collectively the three symmetrical deformation coordinates and the three asymmetrical ones (for later convenience we regard q as a column vector, and use even numbers for the symmetrical coordinates and odd numbers for the asymmetrical ones). The time rate of change of q_i is denoted by $\dot{q}_i$, etc. The elements M_{ij} of the inertia (effective mass) matrix are functions of the shape of the drop, but are independent of the time derivatives $\dot{q}_i$. The matrix M is symmetrical ($M_{ij} = M_{ji}$) and of dimension 6×6. However, for a symmetrical shape ($\alpha_1 = \alpha_2 = \alpha_3 = 0$) the couplings between the components describing symmetrical and asymmetrical distortions disappear, and for such shapes the matrix simplifies to the form

$$M = \begin{pmatrix} M_{sym} & 0 \\ 0 & M_{asym} \end{pmatrix} \quad ,$$

where M_{sym} and M_{asym} are each symmetrical matrices of dimension 3×3.

From the system's Lagrangian

$$\mathcal{L} = \mathcal{T} - \mathcal{V}$$

it follows that the generalized conjugate momenta are

$$p_i = \frac{\partial \mathcal{L}}{\partial \dot{q}_i} = \sum_{j=1}^{6} M(q)_{ij}\, \dot{q}_j \quad , \quad i = 1, 2, \ldots, 6 \quad .$$

Then the Hamiltonian is given by

$$\mathcal{H} = \sum_{i=1}^{6} \dot{q}_i p_i - \mathcal{L} = \tfrac{1}{2} \sum_{i=1}^{6} \sum_{j=1}^{6} M^{-1}(q)_{ij}\, p_i p_j + \mathcal{V}(q) \quad . \qquad (9)$$

The inertia matrix M can be calculated exactly in a straightforward way by solving Laplace's equation for the velocity potential, subject to the appropriate boundary condition on the drop's surface. This method of calculating the inertia matrix has been discussed in refs. [20-22], and we list in appendix 6.4.1 the formulas that we have used. This exact method has been used to calculate M for a variety of shapes and is satisfactory so long as the drop's deformation is not too large. For very deformed shapes, such as shapes close to scission, the method used to solve Laplace's equation (an expansion of the velocity potential in terms of solid harmonics) breaks down, and it is no longer possible to calculate M accurately with this method. For this reason, and also because a fairly long time is required for computing M exactly, it is desirable to have available a faster method for computing M with fair accuracy.

We use for this purpose the approximate method of Werner and Wheeler[12], which is discussed in refs. [1,19]. The method consists of approximating the internal hydrodynamical flow by the flow of circular layers of fluid. That is, as the drop deforms, the fluid inside an infinitesimally thin circular layer of fluid perpendicular to the symmetry axis always remains inside that layer—the layer simply changes its linear position, thickness and radius. This type of motion, which Werner and Wheeler call a "ρ-independent transport and shear," is consistent with the displacements of the drop's surface, but may deviate internally from irrotational flow. From Kelvin's minimum-energy theorem regarding irrotational motion [see for example ref. [43]], the kinetic energy calculated by this approximate method will be larger than or equal to the exact kinetic energy (for irrotational flow), the error being of second order in the deviation of the approximate circular-layer motion from irrotational motion. For the kinetic energy associated

with the motions of fluid constrained to certain simple geometrical shapes, such as a spheroid or a cylinder, the Werner-Wheeler method yields the exact results.

Formulas for the inertia matrix M on the basis of the Werner-Wheeler approximation are given in appendix 6.4.2, and in appendix 6.4.3 we compare for several different shapes (both symmetrical and asymmetrical) the results calculated with this method and the exact method. The general conclusion of the comparisons is that the Werner-Wheeler method is sufficiently accurate for calculating the kinetic energy associated with the distortions of primary interest in fission, and we have therefore adopted this method.

3. Solution

In our study of the solution of the Hamiltonian we consider first the motion of the system in the vicinity of the saddle-point, and later the motion from the saddle point to scission. The transition-state method is used to obtain the probability that the system is in a given state of motion when it passes through the vicinity of the saddle point. This probability is then converted by the motion from the saddle point onward into probability distributions for the observable quantities of interest, namely fission-fragment masses and energies. To first order these distributions are of Gaussian shape, and we compute their most probable values and widths.

3.1. NORMAL MODES AT SADDLE POINT

Since the general motion of the system in the vicinity of the saddle point can be written as a superposition of the independent normal modes of oscillation about the saddle-point shape, a study of the normal modes is of particular importance. In the determination of the normal modes the potential and kinetic energies are first expanded about the position of the saddle point, with terms higher than quadratic neglected, i.e.

$$\mathcal{V} - \hat{\mathcal{V}} = \tfrac{1}{2} \sum_{i=1}^{6} \sum_{j=1}^{6} \hat{K}_{ij} (q_i - \hat{q}_i)(q_j - \hat{q}_j) \quad ,$$

$$\mathcal{T} = \tfrac{1}{2} \sum_{i=1}^{6} \sum_{j=1}^{6} \hat{M}_{ij} \dot{q}_i \dot{q}_j \quad .$$

A caret denotes that the indicated quantity is evaluated at the saddle-point shape. The elements of the stiffness and inertia matrices are given by

$$\hat{K}_{ij} = \widehat{\frac{\partial^2 \mathcal{V}}{\partial q_i \partial q_j}} = \frac{\partial^2 \mathcal{V}(\hat{q})}{\partial q_i \partial q_j} \quad , \tag{10a}$$

$$\hat{M}_{ij} = M(\hat{q})_{ij} \quad , \tag{10b}$$

which are evaluated for a given saddle-point shape by use of the formulas given in appendices 6.3.1, 6.3.2 and 6.4.2. (The second partial derivatives of $\mathcal{V}$ are obtained by differentiating numerically the expressions for the first partial derivatives.) For symmetrical saddle-point shapes the elements of both K and M that couple the symmetrical and asymmetrical distortions are zero, and for such shapes we have the simplification

$$\hat{K} = \begin{pmatrix} \hat{K}_{sym} & 0 \\ 0 & \hat{K}_{asym} \end{pmatrix} \quad ,$$

$$\hat{M} = \begin{pmatrix} \hat{M}_{sym} & 0 \\ 0 & \hat{M}_{asym} \end{pmatrix} \quad ,$$

where each of the submatrices is symmetrical and of dimension 3×3.

Once $\hat{K}$ and $\hat{M}$ are calculated the normal modes are determined in a standard way [see for example ref. [44])] by solving the homogeneous system of 6 linear equations

$$(\hat{K} - \omega^2\hat{M})v = 0$$

for the six frequencies ω_n and eigenvectors $v^{(n)}$, $n = 1, 2, \ldots, 6$. This system of equations was solved here by using Eberlein's method[45]) to diagonalize the (nonsymmetrical) matrix $\hat{M}^{-1}\hat{K}$, which one obtains by multiplying the above equation from the left by $\hat{M}^{-1}$. Because for symmetrical shapes both the stiffness and inertia matrices separate into symmetrical and asymmetrical components, it is possible in practice to solve two uncoupled systems of dimensions 3 each, rather than the original system of dimension 6.

The eigenvalues of the matrix $\hat{M}^{-1}\hat{K}$ give the frequencies (squared) of the oscillations about the saddle-point shape, and the eigenvectors give the transformation from the original set of coordinates $q = \mathrm{col}(q_2, q_4, q_6, q_1, q_3, q_5) = \mathrm{col}(\sigma_1, \sigma_2, \sigma_3, \alpha_1, \alpha_2, \alpha_3)$ to the normal coordinates, which we denote by the use of capital letters, $Q = \mathrm{col}(Q_2, Q_4, Q_6, Q_1, Q_3, Q_5) = \mathrm{col}(\Sigma_1, \Sigma_2, \Sigma_3, A_1, A_2, A_3)$. The values of the normal coordinates are defined to be zero at the saddle-point shape. Explicitly the normal-coordinate transformation is

$$q - \hat{q} = VQ \quad ,$$

where V denotes the matrix of dimension 6×6 whose columns are the eigenvectors $v^{(2)}, v^{(4)}, v^{(6)}, v^{(1)}, v^{(3)}, v^{(5)}$. The numbering of the six normal modes coincides with the scheme used in ref. [20]), where for shapes close to a sphere the nth normal mode consists primarily of a Legendre-polynomial P_n distortion. Thus for a symmetrical saddle-point shape the even modes represent symmetrical oscillations and the odd modes asymmetrical oscillations. For symmetrical shapes that are far removed from a sphere (i.e. dumbbell-like saddle-point shapes for small values of x) each mode consists of a mixture of many (either even or odd) Legendre-polynomial distortions. For such saddle-point shapes descriptive names have been applied[1]) to the five lowest normal modes, and these are given in table 2, where we also

Table 2

Characteristics of normal modes of oscillation about symmetrical saddle-point shapes

n	Mode	Symmetry	Stability
1	Center-of-mass shift	Asymmetrical	Neutral
2	Fission	Symmetrical	Unstable
3	Mass asymmetry	Asymmetrical	$\begin{cases}\text{Stable for } x > x_{BG} \\ \text{Unstable for } x < x_{BG}\end{cases}$
4	Stretching	Symmetrical	Stable
5	Distortion asymmetry	Asymmetrical	Stable
6		Symmetrical	Stable

indicate the symmetry and stability of the modes. Reference [20]) contains a description of the normal modes, which we will not repeat.

Since we are concerned primarily with oscillations about symmetrical saddle-point shapes, for which three of the elements of each eigenvector are zero, we number the nonzero elements of both the symmetrical and asymmetrical eigenvectors by 1, 2, 3. Thus for symmetrical saddle-point shapes the normal-coordinate transformation is

$$\begin{pmatrix} \sigma_1 - \hat{\sigma}_1 \\ \sigma_2 - \hat{\sigma}_2 \\ \sigma_3 - \hat{\sigma}_3 \\ \alpha_1 \\ \alpha_2 \\ \alpha_3 \end{pmatrix} = \begin{pmatrix} v_1^{(2)} & v_1^{(4)} & v_1^{(6)} & 0 & 0 & 0 \\ v_2^{(2)} & v_2^{(4)} & v_2^{(6)} & 0 & 0 & 0 \\ v_3^{(2)} & v_3^{(4)} & v_3^{(6)} & 0 & 0 & 0 \\ 0 & 0 & 0 & v_1^{(1)} & v_1^{(3)} & v_1^{(5)} \\ 0 & 0 & 0 & v_2^{(1)} & v_2^{(3)} & v_2^{(5)} \\ 0 & 0 & 0 & v_3^{(1)} & v_3^{(3)} & v_3^{(5)} \end{pmatrix} \begin{pmatrix} \Sigma_1 \\ \Sigma_2 \\ \Sigma_3 \\ A_1 \\ A_2 \\ A_3 \end{pmatrix}$$

The normalization of the eigenvectors is chosen so that

$$\sum_{i=1}^{3} \left[v_i^{(n)} \right]^2 = 1 \quad , \quad n = 1, 2, \ldots, 6 \quad .$$

The stiffness matrix $\hat{K}$ and inertia matrix $\hat{M}$ are each separately diagonalized by the normal-coordinate transformation, and the orthogonality relations

$$v^{(m)\prime} \hat{K} v^{(n)} = K_n \delta_{mn} \quad ,$$

$$v^{(m)\prime} \hat{M} v^{(n)} = M_n \delta_{mn}$$

define the stiffness constants K_n and inertia constants M_n corresponding to the nth normal mode. The quantity $v^{(m)\prime}$ is the transpose of the column vector $v^{(m)}$, and

$$\delta_{mn} = \begin{cases} 1, & m = n \\ 0, & m \neq n \end{cases} .$$

In terms of the normal coordinates and momenta the Hamiltonian in the neighborhood of the saddle point contains no cross terms coupling different coordinates and momenta, and is given by

$$\mathcal{H} = \hat{\mathcal{V}} + \tfrac{1}{2} \sum_{i=1}^{6} \left(K_i Q_i^2 + \frac{P_i^2}{M_i} \right) , \qquad (11)$$

where the conjugate momenta are

$$P_i = M_i \dot{Q}_i \quad , \quad i = 1, 2, \ldots, 6 \quad .$$

Because the values of K_n and M_n depend upon the choice of eigenvector normalization, they have only relative meaning, whereas their quotient gives the (normalization-independent) frequency (squared) for the nth mode, i.e.

$$\omega_n^2 = K_n / M_n \quad .$$

We present in figs. 7 and 8 the results of our calculation of the frequencies of the oscillations about the symmetrical saddle-point shapes. Figure 7 gives the squares of the frequencies in natural liquid-drop units, and fig. 8 the magnitudes of the frequencies in MeV for nuclei along the line of beta stability.† In each figure we compare our present results with previous results obtained by expanding the drop's radius vector in a series

†When conventional experimental units are used our complete results cannot be displayed easily, and in such cases we specialize to nuclei along the line of beta stability. For this purpose we use Green's approximation to the line of beta stability[46]). The use of conventional units also requires specialization to a particular set of constants for the semi-empirical mass formula, and we use the second set of Myers and Swiatecki[28]).

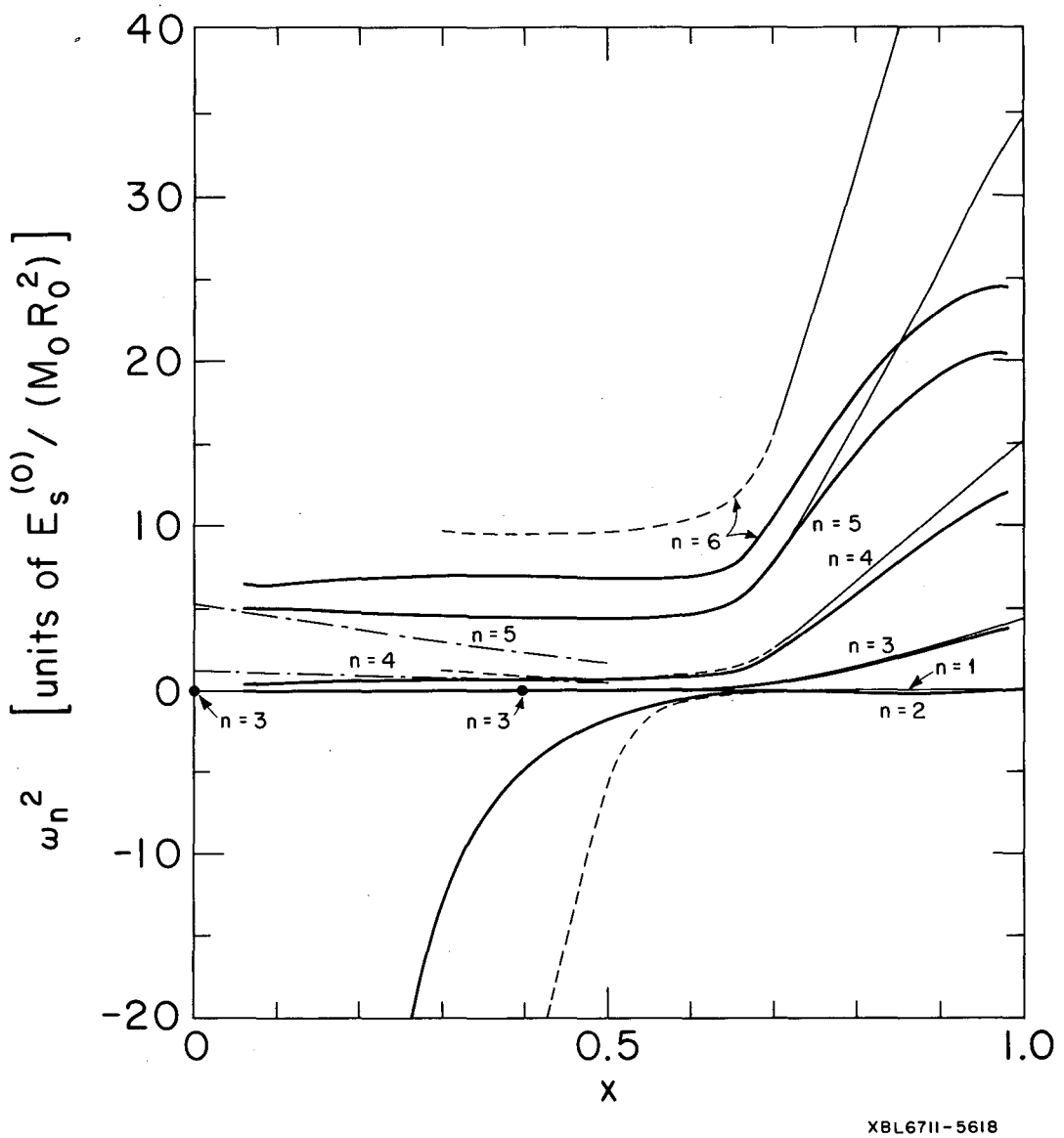

Fig. 7. Squares of frequencies in natural liquid-drop units of $\Omega_0^2 = E_s^{(0)}/(M_0R_0^2)$ as functions of the fissility parameter x. The heavy solid curves give the present results calculated on the basis of the Werner-Wheeler kinetic-energy approximation and the three-quadratic-surface parameterization. The results of ref. [20]) are shown by thin solid and short-dashed lines, the latter indicating that as x decreases below 0.7 the numerical accuracy of the results becomes progressively more questionable. The two-spheroid estimates[1]) are shown by thin dot-dashed lines. The solid points give the locations of the known zeros of the n = 3 curve.

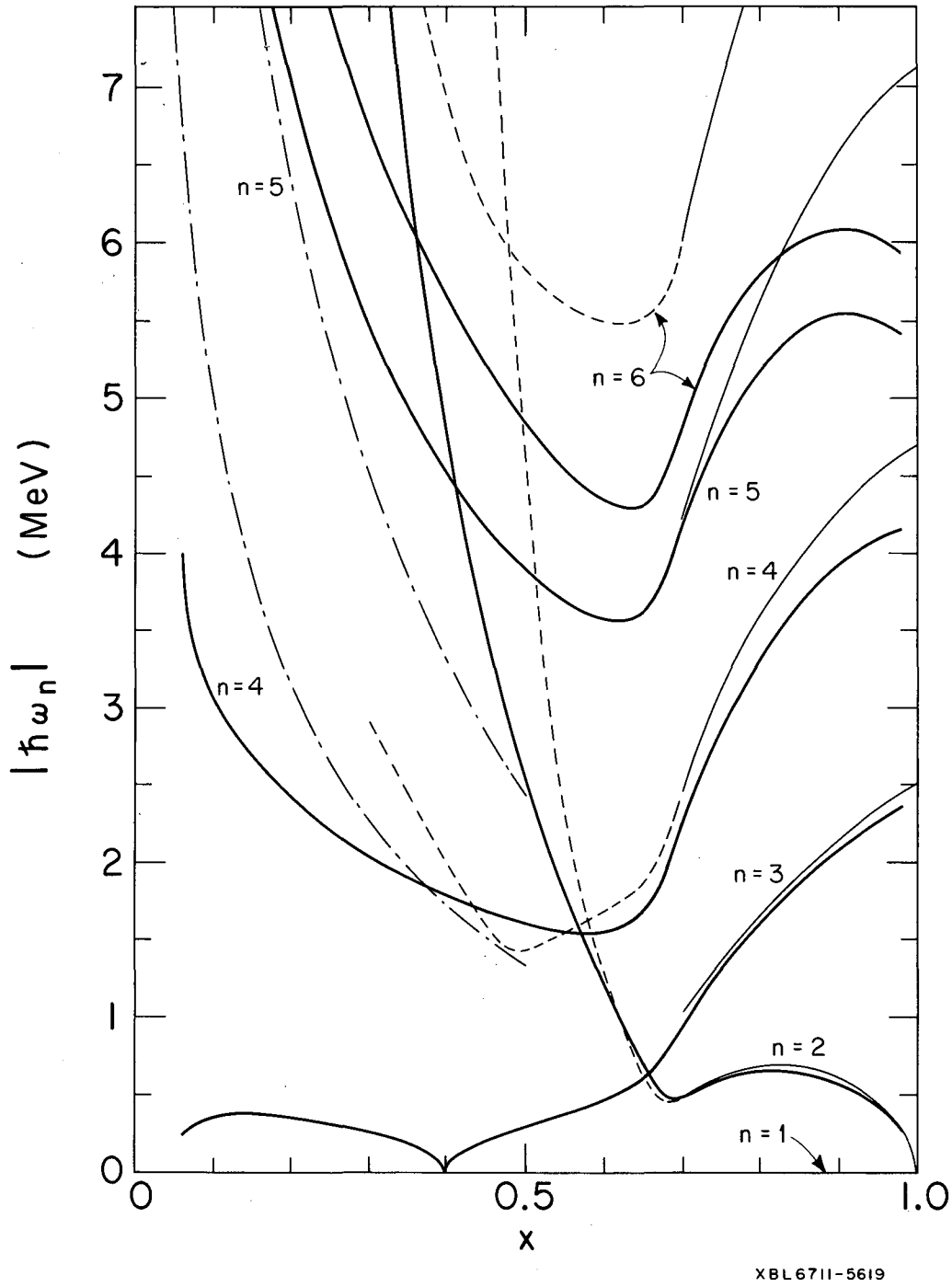

Fig. 8. Magnitudes of the frequencies in MeV for nuclei along the line of beta stability as functions of the fissility parameter x. The heavy solid curves give the present results calculated on the basis of the Werner-Wheeler kinetic-energy approximation and the three-quadratic-surface parameterization. The results of ref. [20]) are shown by thin solid and short-dashed lines, the latter indicating that as x decreases below 0.7 the numerical accuracy of the results becomes progressively more questionable. The two-spheroid estimates[1]) are shown by thin dot-dashed lines.

of 18 Legendre polynomials[20]) and also estimates on the basis of the two-spheroid approximation[1]). It is seen that the frequencies of the four lowest modes are reproduced well by the use of the three-quadratic-surface parameterization and the Werner-Wheeler method for the kinetic energy, whereas the n = 5 and n = 6 modes are not so well reproduced. This is because for the higher modes the hydrodynamical flow corresponding to the Werner-Wheeler approximation has a fairly large curl, which means the inertia constants are somewhat larger than those corresponding to irrotational flow, and consequently the frequencies are somewhat smaller. This deficiency of the Werner-Wheeler approximation is not so serious here because, as we will see later, the properties of mass and energy distributions are almost independent of the n = 5 and n = 6 modes.

Because the normal-coordinate stiffness and inertia constants and eigenvectors have meaning only with respect to a given parameterization of the nuclear shape, we present our results for these quantities in appendix 6.5 rather than here.

3.2. TRANSITION-STATE METHOD

The above discussion of the normal modes at the saddle point leads us naturally to the concept of a transition state, which was first introduced[47]) in connection with the calculation of molecular reaction rates. It has since been used extensively for this purpose [see for example refs. [48-52])] and in the calculation of nuclear reaction rates, including the rate at which compound nuclei undergo fission[53,54]). However, we are interested here in using the transition-state method for a somewhat different purpose—to determine the probability that the nucleus is in a given state of motion when it passes through the vicinity of its saddle point[1,20]).

The transition-state method consists of dividing a system of N degrees of freedom into two systems at its saddle point: a system having a single degree of freedom that represents unstable motion and a second system associated with the remaining N - 1 degrees of freedom. The total wave function for the original system is then the product of the wave function for the first system in one degree of freedom and the wave function for the second system in the remaining N - 1 degrees of freedom.

The standard assumption of the transition-state method is that statistical equilibrium is established by the time the system arrives in the vicinity of its saddle point[47,48]. A compound nucleus undergoing fission typically executes about 10^6 oscillations between formation and reaching the saddle point[55]. This provides ample opportunity for many interchanges of energy, and unless the Hamiltonian has some unexpected property (e.g. a potential-energy "funnel") immediately preceding the saddle point that would prevent the system from arriving there randomly, the assaults at the barrier should be random enough to assure statistical equilibrium at the saddle point. By making this standard assumption we can calculate the probability that each of the N - 1 normal coordinates of the second system are displaced from their equilibrium values by given amounts and that their conjugate momenta have specified values when the nucleus passes through the vicinity of its saddle point. These probability distributions can then be used in the sense of initial conditions for the dynamical calculations that we describe in the next subsection.

In classical statistical mechanics the probability N that the system possesses a given set of coordinates and momenta as it passes through the vicinity of the saddle point is given by the usual Boltzman factor

$$N = C \exp(-\mathcal{H}/\Theta) \quad ,$$

where $\mathcal{H}$ is the Hamiltonian, Θ is the nuclear temperature at the saddle point (measured in energy units), and C is a normalization constant. In the harmonic approximation, in which eq. (11) is used for $\mathcal{H}$, the probability that a given normal coordinate or its conjugate momentum has a specified value is then a Gaussian distribution in that coordinate or momentum. For high nuclear temperatures it is valid to use classical statistical mechanics for determining the probability distributions for the initial conditions, but for low temperatures the classical result is incorrect. As the temperature approaches zero, the widths of the classical distributions approach zero, whereas we know from the Heizenberg uncertainty principle that simultaneous localization of the system in both a position coordinate and in its conjugate momentum can be achieved only within limits. The widths of the distributions are, in general, nonzero as a result of quantal zero-point vibrations. Because quantal effects on the probability distributions can

be important at typical nuclear temperatures, and because we are able to take them into account, we calculate the probability distributions for the initial states of motion according to quantal rather than classical statistical mechanics.

It should be emphasized, however, that we use classical mechanics to describe the division of the drop beyond the vicinity of the saddle point. The use of classical mechanics for discussing the division of the nucleus and the separation of the fragments can be partially justified on the grounds that a short distance from the saddle point the de Broglie wavelength for motion in the fission direction becomes relatively small. The use of a mixture of quantal and classical methods cannot be so easily justified, and although it is the same as that used in ref. [1]), a formal justification would be desirable.

We do not need to consider probability distributions in all the normal coordinates and momenta. Since the observable quantities of interest are calculated in the center-of-mass system, we may disregard the distributions for the n = 1 center-of-mass-shift normal mode. Furthermore, for our purposes here we need not consider probability distributions for the n = 2 fission mode because to first order the final mass and energy distributions are independent of the initial values of the fission coordinate Q_2 and the fission momentum P_2 (see subsects. 3.3 and 3.4).

The quantal probabilities for the remaining normal modes at the saddle point (n = 3, 4, 5, 6) are Gaussian distributions in the normal coordinates and momenta[1,20,56,57]), viz.

$$N(Q_n) = (2\pi\sigma_n^{\,2})^{-\frac{1}{2}} \exp[-Q_n^{\,2}/(2\sigma_n^{\,2})] \quad , \tag{12a}$$

$$N(P_n) = (2\pi\sigma_n'^{\,2})^{-\frac{1}{2}} \exp[-P_n^{\,2}/(2\sigma_n'^{\,2})] \quad , \tag{12b}$$

where the temperature-dependent variances $\sigma_n^{\,2}$ and $\sigma_n'^{\,2}$ are given explicitly by

$$\sigma_n^{\,2} = \frac{1}{2}\frac{\hbar\omega_n}{K_n} \coth\left(\frac{\hbar\omega_n}{2\Theta}\right) \rightarrow \begin{cases} \Theta/K_n \quad , & \Theta \gg \hbar\omega_n \\ \frac{1}{2}\hbar\omega_n/K_n \quad , & \Theta \ll \hbar\omega_n \quad , \end{cases} \tag{13a}$$

$$\sigma_n'^2 = \frac{1}{2} M_n \hbar\omega_n \coth\left(\frac{\hbar\omega_n}{2\Theta}\right) \rightarrow \begin{cases} M_n\Theta \quad , & \Theta \gg \hbar\omega_n \\ \frac{1}{2} M_n \hbar\omega_n \quad , & \Theta \ll \hbar\omega_n \end{cases} . \tag{13b}$$

The normal-mode frequencies ω_n, stiffnesses K_n, and inertias M_n have all been given as functions of x in the preceding subsection, and the nuclear temperature Θ (measured in energy units) is calculated in terms of the known internal excitation energy at the saddle point. The temperature dependence of the variances can be seen from the graph of $\coth[\hbar\omega/(2\Theta)]$ versus $2\Theta/(\hbar\omega)$ in fig. 9, which is reproduced from ref. [1]). It is noted that for high temperatures the quantal expressions (12) and (13) reduce to the classical results (given by the usual Boltzman factor), whereas in the low-temperature limit they reduce to the distributions for the quantal zero-point motions of harmonic oscillators.

The desired probability distribution is the joint probability for simultaneously observing the system with a given set of initial coordinates and momenta. For a general Hamiltonian (of one degree of freedom) the joint probability is not given quantally by the product of the individual probabilities for the coordinate and momentum (because of the noncommutativity of the coordinate and its conjugate momentum). However, for the special case of a harmonic oscillator the product of the coordinate and momentum probabilities does give the correct joint probability[26,58]). Because of this and because the normal modes are independent of one another, the desired probability for observing the system with a given set of initial coordinates and momenta is given by the product of the individual probabilities (12) for each coordinate and momentum.

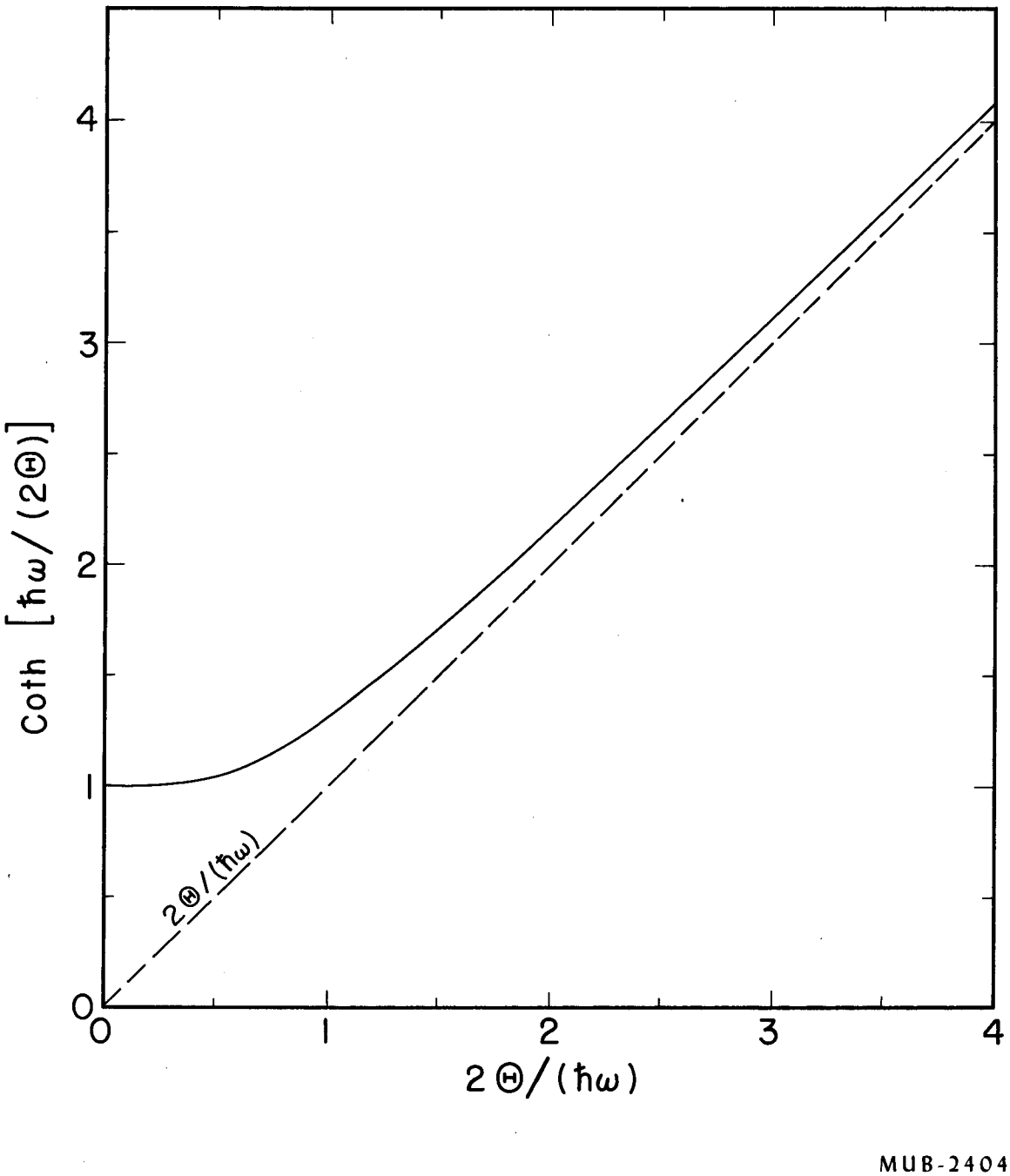

Fig. 9. The function coth[ħω/(2Θ)] versus 2Θ/(ħω). The dashed line gives the function's asymptote.

3.3 DYNAMICAL CALCULATIONS

Now that we have determined the probability distributions for the initial conditions near the saddle point, the next step is to perform the dynamical calculations which tell us how the nucleus divides for a given set of initial conditions. This we do by solving Hamilton's equations of motion, which follow immediately from eq. (9):

$$\dot{q}_i = \frac{\partial \mathcal{H}}{\partial p_i} = \sum_{j=1}^{6} M^{-1}(q)_{ij}\, p_j \quad , \quad i = 1, 2, \ldots, 6 \quad ,$$

$$\dot{p}_i = -\frac{\partial \mathcal{H}}{\partial q_i} = -\frac{\partial \mathcal{V}(q)}{\partial q_i} - \tfrac{1}{2} \sum_{j=1}^{6} \sum_{k=1}^{6} \frac{\partial M^{-1}(q)_{jk}}{\partial q_i}\, p_j p_k \quad , \quad i = 1, 2, \ldots, 6 \quad .$$

This system of 12 first-order differential equations is integrated numerically by use of a fourth-order Adams-Moulton predictor-corrector method, with the starting procedure based on a modified fourth-order Runge-Kutta method[59]. The matrix $M^{-1}(q)$ is obtained by use of Wilkinson's matrix-inversion method[60] from the inertia matrix $M(q)$, whose calculation is described in appendix 6.4.2. The partial derivatives $\partial M^{-1}(q)_{jk}/\partial q_i$ are evaluated numerically, whereas the derivatives $\partial \mathcal{V}(q)/\partial q_i$ are calculated according to the formulas of appendices 6.3.1 and 6.3.2.

The equations of motion have been solved for hundreds of sets of initial conditions. As examples, we present in figs. 10 and 11 certain aspects of the solutions corresponding to starting from the saddle point with 1 MeV of kinetic energy in the fission mode and 1 MeV in the mass-asymmetry mode, for three values of the fissility parameter x (0.62, 0.70 and 0.78). Figure 10, which is reproduced from ref. [61], illustrates the drops' shapes during their descents from saddle to scission, and fig. 11 gives the corresponding time dependences of three of the more important geometrical properties associated with the drops. The nuclei (taken along the line of beta stability) that correspond approximately to the chosen values of x are indicated in parentheses in fig. 10. These nuclei, which differ from one another by ten protons, span the region from medium nuclei, where symmetrical mass divisions are observed experimentally, to heavy nuclei, where asymmetrical mass divisions are observed.

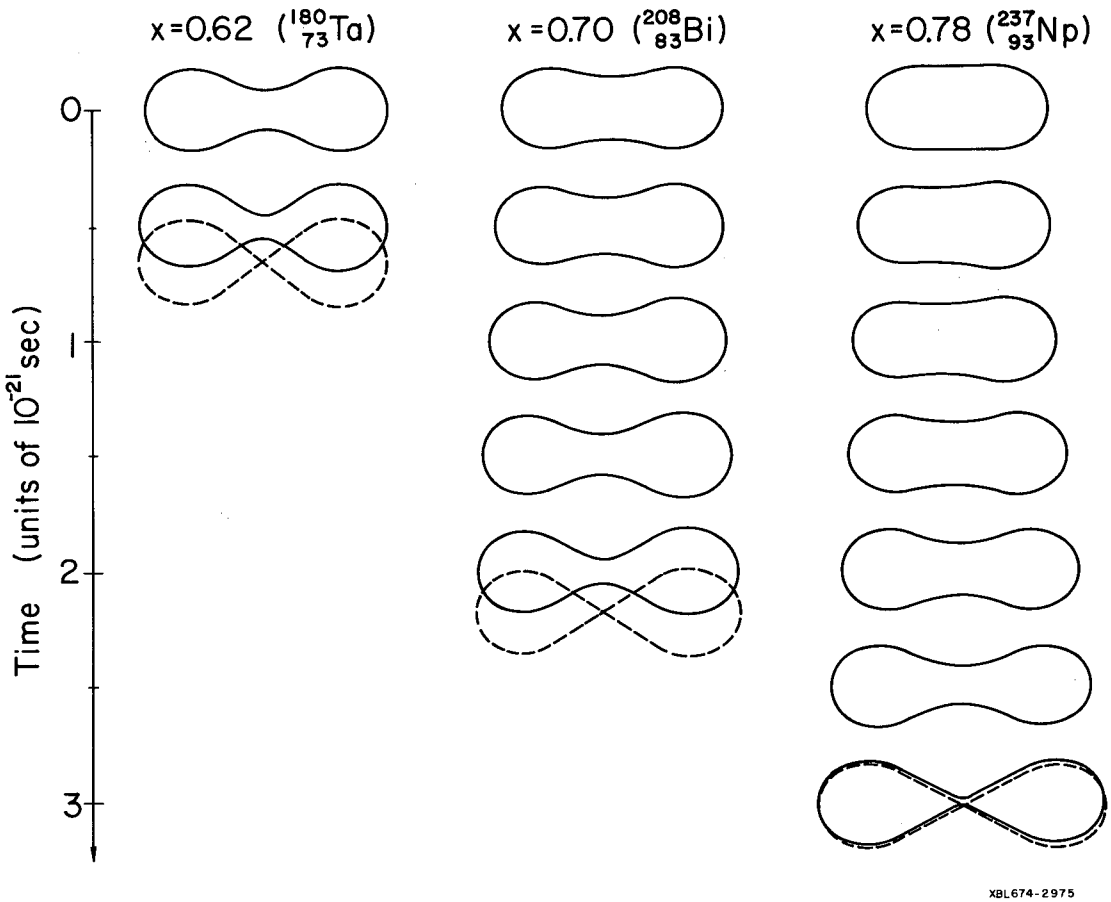

Fig. 10. Illustrations of the shape of the drop during the descent from saddle to scission. The initial conditions correspond to starting from the saddle point with 1 MeV of kinetic energy in the fission mode and 1 MeV in the mass-asymmetry mode. The scission shapes are drawn with dashed lines. (The sign of the initial mass-asymmetrical motion is taken to be negative.)

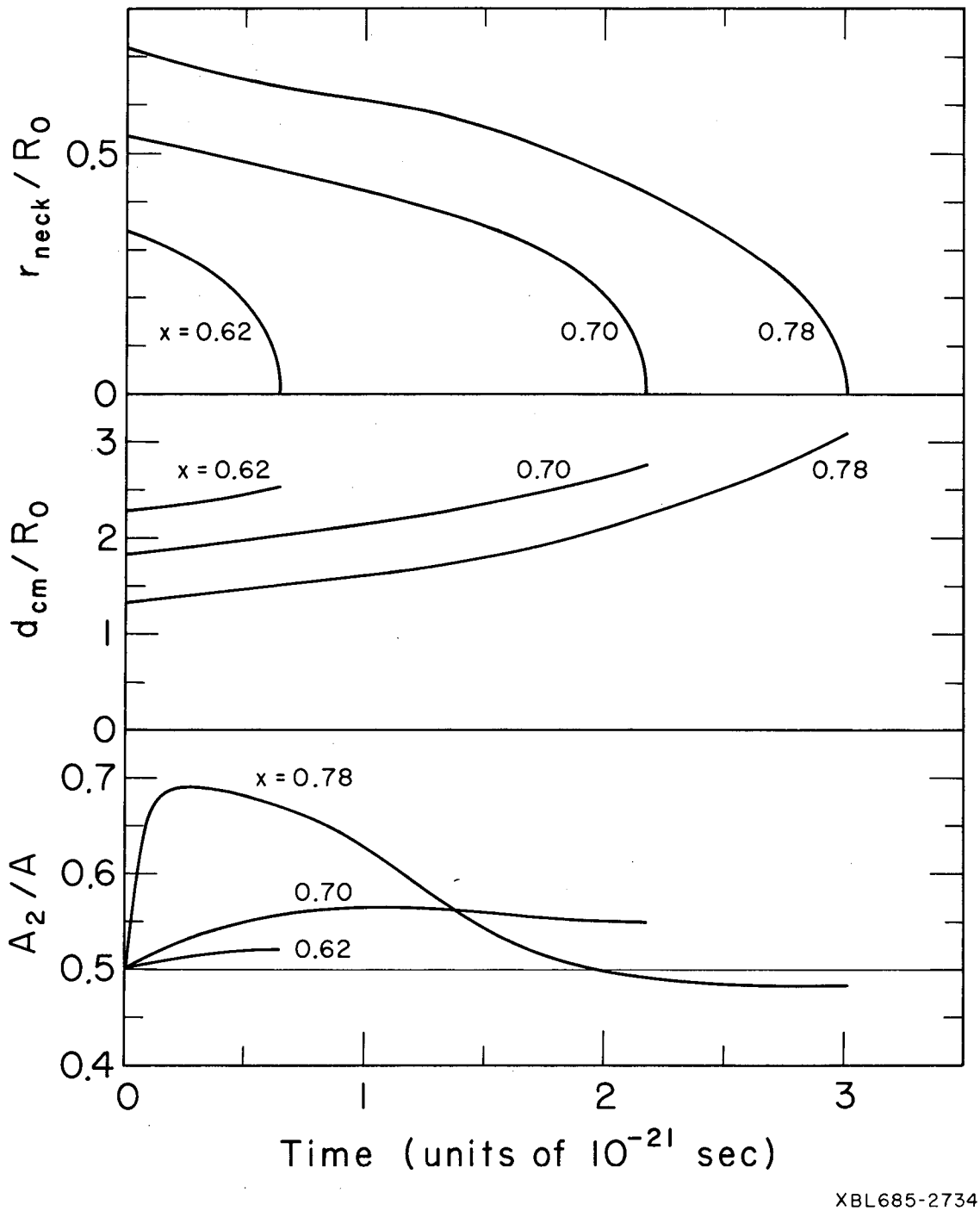

Fig. 11. Examples of the time dependence of the minimum neck radius (top), the distance between the centers of mass of the nascent fragments (middle), and the mass of the right-hand nascent fragment (bottom). The initial conditions are the same as those in fig. 10. The dividing point between the two nascent fragments is taken to be the position of the minimum neck radius. (For shapes close to a cylinder this is not a particularly useful definition. For such shapes small changes in the asymmetrical coordinates lead to large changes in the relative masses of the nascent fragments, as can be seen from the initial rapid increase in A_2/A for x = 0.78.)

Figures 10 and 11 illustrate three important results that have emerged from a consideration of all the solutions obtained: (1) For a constant amount of energy in the fission mode the time from saddle to scission increases substantially with increasing x. This is partly due to the increase in distance between saddle and scission as x increases, but is also associated with the following point. (2) For small values of x the motion in the fission mode consists primarily of a constriction of the drop's neck, whereas for large x the drop also elongates substantially during the descent. Thus a larger amount of mass is displaced in the fission mode for large values of x than for small x. For small values of x the centers of mass of the fragments are moving slowly at scission, whereas for large x they are moving rapidly. (3) The mass-asymmetrical component of motion is not amplified into a large mass asymmetry during the descent as proposed by Hill[3,4]) and by Hill and Wheeler[5]), but instead represents stable oscillations about a symmetrical division.† This means that, within the limitations of the Werner-Wheeler approximation for the kinetic energy and a parameterization that permits only binary division, the most probable mass division is a split into two equal parts.

We next consider the most probable energies associated with the division process, which are obtained by solving the equations of motion for initial conditions corresponding to starting from rest at the saddle point. Since the saddle point is a position of (unstable) equilibrium, a classical system with zero kinetic energy would remain there for an infinite length

---

†As the system approaches the scission point (i.e. as the neck radius approaches zero) it becomes more difficult to transfer mass from one nascent fragment to the other, and the mass ratio approaches a constant value (appropriate to the particular set of initial conditions). This can be seen in the bottom portion of fig. 11.

of time.[†] However, even though an infinite time is required for the drop to divide, there exists a well-defined limiting orbit corresponding to starting from rest at the saddle point. The normal-coordinate transformation tells us both the initial direction of motion from the saddle point (i.e. the fission direction) and the fission-mode potential and kinetic energies [in the harmonic approximation; see eq. (11)]. Thus, even though an infinite time is involved, we can determine analytically the initial motion from the saddle point, and begin the numerical integrations where we stop the analytical solution.

The calculated most probable energies are shown in fig. 12 in natural units of $E_s^{(0)}$, and in fig. 13 in MeV for nuclei along the line of beta stability. The figures show how the available energy, which consists of the sum of the energy release E_{rel} and the fission-barrier height B_f, is divided among the fragments at infinity. The division is into kinetic energy of translation E_{trans}^{∞} and vibrational energy E_{vib}^{∞}. The translational kinetic energy at infinity is shown further divided into the energy E_{trans}^{scis} acquired prior to scission and the energy $E_{trans}^{post\ scis}$ acquired after scission. The pre-scission translational kinetic energy is seen to increase rapidly as x increases above about 0.7. Similarly, the vibrational energy is shown further divided into the energy $E_{vib\ kin}^{scis}$ acquired prior to scission and the energy $E_{vib}^{post\ scis}$ acquired after scission. The sum of E_{trans}^{scis} and $E_{vib\ kin}^{scis}$, which is denoted by E_{kin}^{scis}, represents the system's total kinetic energy at scission, and hence gives the most probable decrease in potential energy in going from the saddle point to scission.

In constructing figs. 12 and 13 an approximation is made in the determination of the division of the available energy after scission into translational kinetic energy and vibrational energy. After scission the frag-

---

[†] Kelson[19]) tabulates for various values of x the time from saddle to scission for initial conditions corresponding to starting from rest at the saddle point. Since the time should be infinite these numbers and the associated discussion are meaningless. Presumably the explanation is a relatively large error either in the determination of the saddle point or in the integration of the equations of motion (or possibly in both).

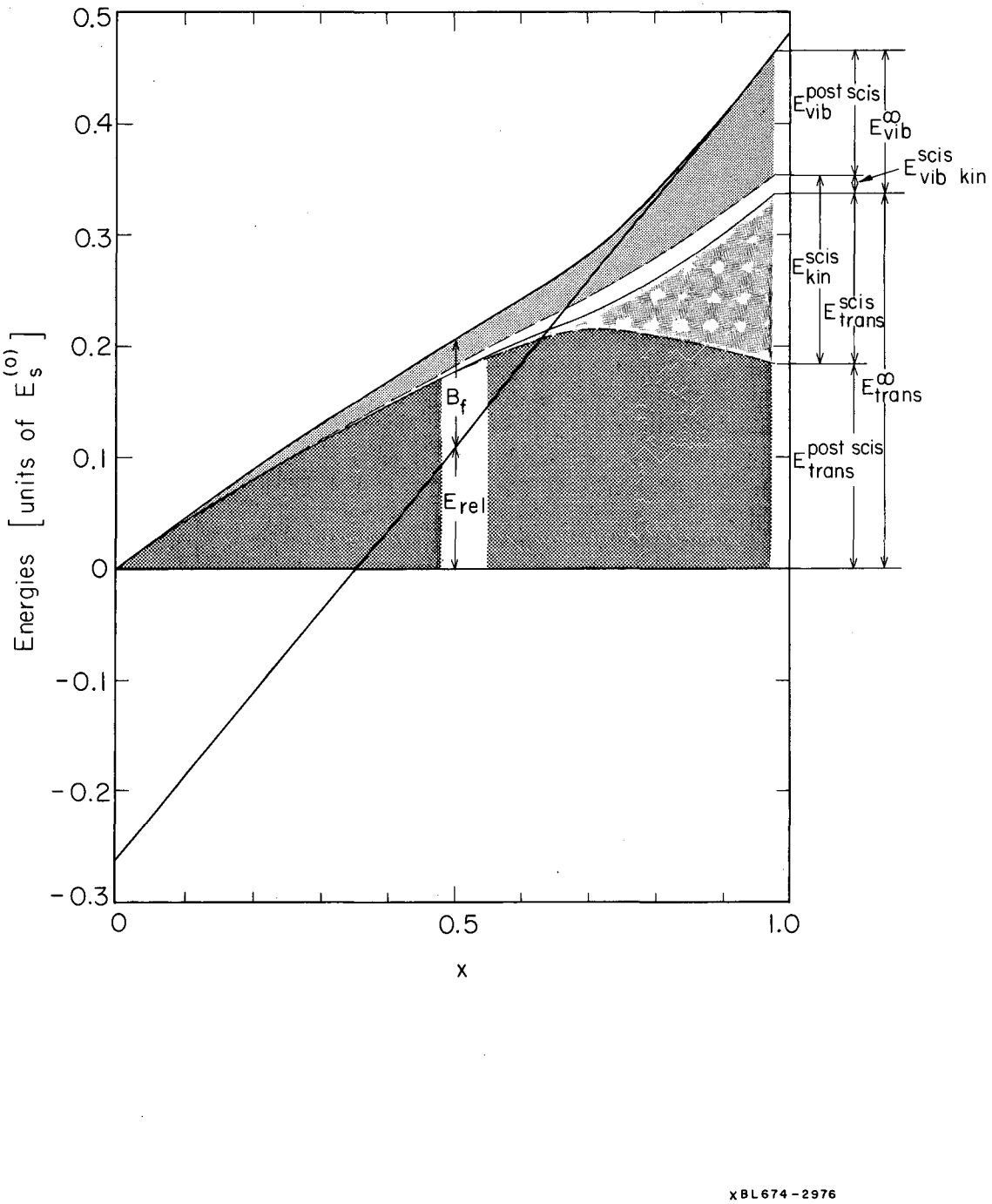

Fig. 12. Most probable fission-fragment energies in natural units of $E_s^{(o)}$, as functions of the fissility parameter x. The symbols are explained in the text.

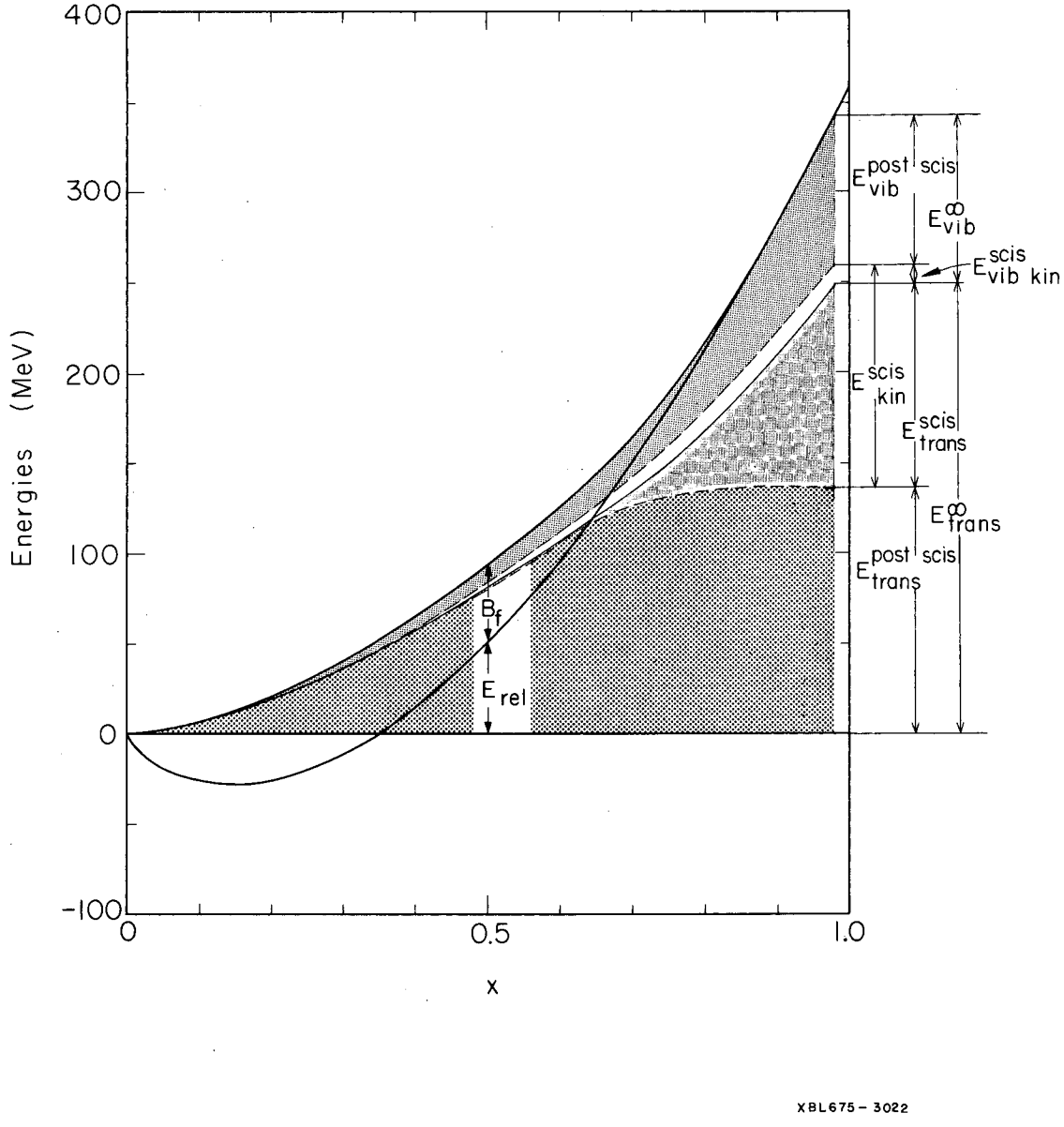

Fig. 13. Most probable fission-fragment energies in MeV for nuclei along the line of beta stability, as functions of the fissility parameter x. The symbols are explained in the text.

ments oscillate fairly rapidly about their centers of mass as they separate. The fragments experience a greater acceleration during the period of time when they are prolate than when they are oblate. Because the fairly rapid oscillations of the fragments tend to cancel the opposing effects of the prolate and oblate shapes, the acquired translational kinetic energy is approximately what it would have been had the fragments remained spherical as they separated. We therefore approximate the translational kinetic energy $E_{trans}^{post\ scis}$ acquired after scission by the interaction energy of two spheres whose centers coincide with the centers of charge of the fragments at scission. The results of refs. [1,62]) [see in particular fig. 18 of ref. [1]) or fig. 3 of ref. [62])] suggest that this approximation should be excellent for smaller values of x, but that it may underestimate somewhat the true post-scission translational kinetic energy for $x \gtrsim 0.7$. The reason for using an approximation for the post-scission kinetic energy is that the post-scission dynamical motion affects only slightly the final kinetic energy at infinity and does not affect the mass division at all (since classically it is impossible to transfer mass after scission), whereas its exact calculation would require an effort comparable to that associated with the pre-scission motion.

We may note that had we approximated the kinetic energy by the interaction energy of the two fragments at scission this would have overestimated the post-scission translational kinetic energy (for nonviscous irrotational flow), since a portion of the interaction energy is converted into vibrational energy of the oscillating fragments as they separate[1,62]). On the other hand, for the limiting case of fragments with infinite viscosities and/or infinite vibrational inertias the interaction energy at scission represents the exact post-scission translational kinetic energy. However, the scission configuration for this case differs from the scission configuration corresponding to nonviscous irrotational hydrodynamical flow, particularly for large values of x.

Second in importance to the most probable mass division and most probable energies are the widths of the mass and energy distributions, and we turn now to the determination of these widths. For this purpose we work to first order in the effects of the displacements of the normal coordinates at the saddle from their equilibrium values and in the deviations from zero of the normal momenta at the saddle point. This simplifies the treatment

considerably, because to first order the dynamical motion from saddle to scission can be discussed in terms of small deviations from the known most probable solution. [See for example ref. [63]), which discusses dynamical orbits in the neighborhood of a known orbit for particles in a circular magnetic accelerator.]

For our purposes we are interested primarily in the first-order effects of the initial conditions on the masses and energies at infinity rather than on the specific path taken from saddle to infinity. We therefore expand the general transformation equations that relate the final masses and energies at infinity to the initial conditions near the saddle point, retaining only linear terms. To avoid writing subscripts and superscripts, for the remainder of our discussion we denote the total translational kinetic energy at infinity by the symbol E, and the total vibrational energy at infinity by the symbol X. As usual A_1 denotes the mass number of the left-hand fragment. The general transformation equations and the first-order expansions are then written as

$$A_1 = A_1(Q_2, P_2; Q_3, P_3, Q_4, P_4, Q_5, P_5, Q_6, P_6)$$

$$= \tfrac{1}{2}A + \frac{\partial A_1}{\partial Q_3} Q_3 + \frac{\partial A_1}{\partial P_3} P_3 + \frac{\partial A_1}{\partial Q_5} Q_5 + \frac{\partial A_1}{\partial P_5} P_5 + \mathcal{O}(2) \quad , \qquad (14a)$$

$$E = E(Q_2, P_2; Q_3, P_3, Q_4, P_4, Q_5, P_5, Q_6, P_6)$$

$$= E_0 + \frac{\partial E}{\partial Q_4} Q_4 + \frac{\partial E}{\partial P_4} P_4 + \frac{\partial E}{\partial Q_6} Q_6 + \frac{\partial E}{\partial P_6} P_6 + \mathcal{O}(2) \quad , \qquad (14b)$$

$$X = X(Q_2, P_2; Q_3, P_3, Q_4, P_4, Q_5, P_5, Q_6, P_6)$$

$$= X_0 + \frac{\partial X}{\partial Q_4} Q_4 + \frac{\partial X}{\partial P_4} P_4 + \frac{\partial X}{\partial Q_6} Q_6 + \frac{\partial X}{\partial P_6} P_6 + \mathcal{O}(2) \quad ; \qquad (14c)$$

terms that are quadratic and higher in the coordinates and momenta are denoted by $\mathcal{O}(2)$. The general transformation equations are strictly independent of the center-of-mass-shift normal coordinate Q_1 and momentum P_1, and we have

omitted these in the general argument lists. The final mass and energy distributions are to first order independent of the initial values of the fission coordinate Q_2 and momentum P_2, and the transformation equations are consequently not expanded with respect to these two quantities. Instead, the expansions refer to constant values of Q_2 and P_2, which are assumed to be small. In practice a value of zero is used for Q_2 and a small (positive) but nonzero value is used for P_2. Since the mass number A_1 is an asymmetrical quantity it depends to first order only upon the n = 3 and 5 asymmetrical normal coordinates and momenta; similarly, the energies E and X depend to first order only upon the n = 4 and 6 symmetrical normal coordinates and momenta. The total energy E + X is to first order constant; in particular,

$$E + X = E_{rel} + B_f \quad . \tag{15}$$

It therefore follows that the partial derivatives of eq. (14c) are related to those of eq. (14b) by

$$\frac{\partial X}{\partial Q_i} = - \frac{\partial E}{\partial Q_i} \quad , \quad i = 4, 6 \quad , \tag{16a}$$

$$\frac{\partial X}{\partial P_i} = - \frac{\partial E}{\partial P_i} \quad , \quad i = 4, 6 \quad . \tag{16b}$$

The various first partial derivatives appearing in eqs. (14) are evaluated at the saddle point with zero momentum in each mode except the fission mode. In practice each derivative is determined numerically from the solutions of the equations of motion for initial conditions in which all the normal coordinates and momenta are zero except the desired coordinate or momentum (and the fission momentum). For example, we calculate $\frac{\partial E}{\partial Q_4}$ from the result

$$\frac{\partial E}{\partial Q_4} = [E(Q_2, P_2; 0, 0, + \Delta Q_4, 0, 0, 0, 0, 0)$$

$$- E(Q_2, P_2; 0, 0, - \Delta Q_4, 0, 0, 0, 0, 0)]/(2 \Delta Q_4) \quad ,$$

where Q_2 is zero, P_2 is a small (positive) quantity, and where ΔQ_4 is determined optimally so that the number of significant figures remaining in the numerator after the subtractions are performed is consistent with the truncation error.

Each of the partial derivatives is a very sensitive function of the coordinate Q_2 and momentum P_2 in the fission direction. In particular, as both Q_2 and P_2 approach zero simultaneously each partial derivative oscillates about zero with a period that approaches zero. However, we will see in the next subsection that these derivatives enter as squares in the first-order expressions for the widths of the distributions. The particular combinations of squares are to first order independent of Q_2 and P_2, as are also the energies E_0 and X_0. The energies E_0 and X_0 have been given as functions of x in figs. 12 and 13 (designated there by E^{∞}_{trans} and E^{∞}_{vib}, respectively), and the appropriate combinations of the partial derivatives will be presented in the next subsection.

3.4. FISSION-FRAGMENT MASS AND ENERGY PROBABILITY DISTRIBUTIONS

By combining the transformation equations that relate the masses and energies at infinity to the initial conditions near the saddle point with the probability distributions for the initial conditions near the saddle point, we arrive at probability distributions for the masses and energies at infinity. Since to first order the transformation equations are linear and the probability distributions for the initial conditions are Gaussian in shape, the resulting distributions for the masses and energies at infinity are also Gaussian in shape, with widths that are related in a simple way to the widths of the initial distributions and the coefficients of the transformation equations.

The probability distribution $N(A_1)$ in the mass of a fragment at infinity is obtained from the fundamental equation expressing the transformation of probabilities[†]

[†] We use the same symbol N to denote each of several probability distributions; the argument of N indicates which explicit function is being referred to.

$$\int N(A_1)dA_1 = \iiiint N(Q_3)dQ_3\, N(P_3)dP_3\, N(Q_5)dQ_5\, N(P_5)dP_5 \quad . \qquad (17)$$

We omit writing the integrals over the initial probability distributions for the symmetrical coordinates and momenta, since A_1 is independent of these quantities and the integrals are therefore unity. Into this equation we substitute the expression for one of the initial coordinates or momenta, say

$$Q_3 = Q_3(A_1;\, P_3,\, Q_5,\, P_5)$$

$$= \left[A_1 - \tfrac{1}{2}A - \frac{\partial A_1}{\partial P_3} P_3 - \frac{\partial A_1}{\partial Q_5} Q_5 - \frac{\partial A_1}{\partial P_5} P_5 - \mathcal{O}(2)\right] \Big/ \frac{\partial A_1}{\partial Q_3} \quad ,$$

which is obtained from eq. (14a). We then have

$$N(A_1) = \iiiint N\left[Q_3(A_1;\, P_3,\, Q_5,\, P_5)\right] \left|\frac{\partial Q_3}{\partial A_1}\right| N(P_3)dP_3\, N(Q_5)dQ_5\, N(P_5)dP_5 \quad ,$$

with the initial probability distributions $N(Q_n)$ and $N(P_n)$ given by eqs. (12). A straightforward three-fold integration of this equation (between the limits $-\infty$ and $+\infty$) gives the result

$$N(A_1) = (2\pi\sigma_{A_1}{}^2)^{-\frac{1}{2}} \exp\left[-(A_1 - \tfrac{1}{2}A)^2/(2\sigma_{A_1}{}^2)\right] \quad ,$$

where the variance $\sigma_{A_1}{}^2$ is given explicitly by

$$\sigma_{A_1}{}^2 = \sigma_3{}^2\left(\frac{\partial A_1}{\partial Q_3}\right)^2 + \sigma_3'{}^2\left(\frac{\partial A_1}{\partial P_3}\right)^2 + \sigma_5{}^2\left(\frac{\partial A_1}{\partial Q_5}\right)^2 + \sigma_5'{}^2\left(\frac{\partial A_1}{\partial P_5}\right)^2 \quad .$$

Inserting into this expression eqs. (13) for the variances of the initial distributions yields

$$\sigma_{A_1}^2 = \tfrac{1}{2}\frac{\hbar\omega_3}{K_3}\left[\left(\frac{\partial A_1}{\partial Q_3}\right)^2 + K_3 M_3\left(\frac{\partial A_1}{\partial P_3}\right)^2\right]\coth\left(\frac{\hbar\omega_3}{2\Theta}\right)$$

$$+ \tfrac{1}{2}\frac{\hbar\omega_5}{K_5}\left[\left(\frac{\partial A_1}{\partial Q_5}\right)^2 + K_5 M_5\left(\frac{\partial A_1}{\partial P_5}\right)^2\right]\coth\left(\frac{\hbar\omega_5}{2\Theta}\right) \quad .$$

We now define the quantities $\sigma_{A_1 n}^2(0)$ by

$$\sigma_{A_1 n}^2(0) = \tfrac{1}{2}\frac{\hbar\omega_n}{K_n}\left[\left(\frac{\partial A_1}{\partial Q_n}\right)^2 + K_n M_n\left(\frac{\partial A_1}{\partial P_n}\right)^2\right] \quad , \quad n = 3, 5 \quad ,$$

in terms of which the variance of the mass distribution at a given nuclear temperature Θ at the saddle point can be written as

$$\sigma_{A_1}^2 = \sigma_{A_1 3}^2(0)\coth\left(\frac{\hbar\omega_3}{2\Theta}\right) + \sigma_{A_1 5}^2(0)\coth\left(\frac{\hbar\omega_5}{2\Theta}\right) \quad . \qquad (18a)$$

It is seen that the quantity $\sigma_{A_1 n}^2(0)$ represents physically the contribution of the nth normal mode to the variance of the mass distribution at zero nuclear temperature. The quantities $\sigma_{A_1 n}^2(0)$ are to first order independent of the fission coordinate Q_2 and momentum P_2, although, as discussed in the previous subsection, the individual partial derivatives $\frac{\partial A_1}{\partial Q_n}$ and $\frac{\partial A_1}{\partial P_n}$ are sensitive functions of Q_2 and P_2.

Analogous derivations can be given for the total translational kinetic-energy distribution N(E) and the vibrational-energy distribution N(X). For example, from eqs. (14b), (12) and (13) we find that

$$N(E) = \iiint N\left[Q_4(E;\, P_4,\, Q_6,\, P_6)\right]\left|\frac{\partial Q_4}{\partial E}\right| N(P_4)dP_4\, N(Q_6)dQ_6\, N(P_6)dP_6$$

$$= (2\pi\sigma_E^2)^{-\frac{1}{2}}\exp\left[-(E - E_0)^2/(2\sigma_E^2)\right] \quad ,$$

with

$$\sigma_E^2 = \sigma_{E4}^2(0) \coth\left(\frac{\hbar\omega_4}{2\Theta}\right) + \sigma_{E6}^2(0) \coth\left(\frac{\hbar\omega_6}{2\Theta}\right) \tag{18b}$$

and

$$\sigma_{En}^2(0) = \tfrac{1}{2} \frac{\hbar\omega_n}{K_n}\left[\left(\frac{\partial E}{\partial Q_n}\right)^2 + K_n M_n \left(\frac{\partial E}{\partial P_n}\right)^2\right] \quad ; \quad n = 4, 6 \quad .$$

Because of the equality of the partial derivatives expressed by eqs. (16), it follows that to first order the vibrational-energy distribution

$$N(X) = (2\pi\sigma_X^2)^{-\frac{1}{2}} \exp\left[-(X - X_0)^2/(2\sigma_X^2)\right]$$

has the same variance

$$\sigma_X^2 = \sigma_E^2 \tag{18c}$$

as the translational kinetic-energy distribution.

We present in figs. 14 and 15 graphs of the remaining quantities that enter the calculated mass and energy distributions. (The most probable energies E_0 and X_0 have already been presented in figs. 12 and 13, labeled there by E^{∞}_{trans} and E^{∞}_{vib}, respectively.) Figure 14 gives the zero-temperature contributions $\sigma_{A_1 n}^2(0)$ of the n = 3 and 5 modes to the variance of the mass distribution. Since mass-asymmetrical oscillations are unstable for $x \leq x_{BG}$, the n = 3 contribution is infinite for this range of x. As x increases above x_{BG} the n = 3 contribution at first decreases, and the minimum in the curve merely reflects the tendency of the mass distribution to broaden with increasing x for large values of x.

Results for the quantities $\sigma_{A_1 n}^2(0)$ have been obtained only for $x \leq 0.78$. The reason for this is the following: For $x > 0.78$ the middle surface is a spheroid at the saddle point, and consequently during the descent it undergoes a transition from a spheroid to a hyperboloid of revolution. Because of a lack of foresight a numerical difficulty arises at this transition point when the shape is asymmetrical (symmetrical shapes are treated properly). The difficulty arises because for asymmetrical shapes the posi-

tion ℓ_3 of the center of the middle quadratic surface and its transverse semiaxis squared a_3^2, as well as the first partial derivatives of ℓ_3 and a_3^2 with respect to the generalized coordinates approach infinity at this transition point. The difficulty is purely numerical in nature and could be eliminated by not using ℓ_3 and a_3^2 (and their derivatives) as auxiliary quantities in the calculation of the final quantities of interest (see appendices 6.1 and 6.2). The effort that would be required to remove the difficulty has not been made in view of two circumstances. First, for large values of x division into more than two bodies releases more energy than division into two[64]), but any tendency during the dynamical descent to form more than two bodies is not allowed by the restriction of our parameterization to binary division. It is therefore doubtful that for large values of x our parameterization adequately describes all the relevant degrees of freedom. Second, because the distance from saddle to scission increases with increasing x the accuracy of the numerical solutions of the equations of motion decreases as x increases, and the values that we would obtain for $\sigma_{A_1 n}^2(0)$ for $x > 0.78$ would be of questionable numerical accuracy.

The zero-temperature contributions $\sigma_{En}^2(0)$ of the n = 4 and 6 modes to the variances of the distributions in total translational kinetic energy and vibrational energy are shown in fig. 15. It is seen that these energy distributions broaden with increasing x. Although for symmetrical shapes no difficulty arises at the transition of the middle surface from a spheroid to a hyperboloid of revolution, at about this same point the numerical accuracy of the solutions of the equations of motion begins to deteriorate as x increases, because of the increased distance from saddle to scission. This is indicated in the figure by the use of short-dashed lines for $x > 0.78$.

It is seen from fig. 14 that the primary contribution to the variance of the mass distribution is from the n = 3 mass-asymmetry mode, and from fig. 15 that the primary contribution to the variances of the energy distributions is from the n = 4 stretching mode. The relative smallness of the contributions from the n = 5 and 6 modes suggests that the still higher modes (which are disregarded in our parameterization) would contribute negligible amounts. It also indicates that the discrepancy between our results and the exact results for ω_5^2 and ω_6^2 (cf. figs. 7 and 8) does not seriously affect the widths of the mass and energy distributions.

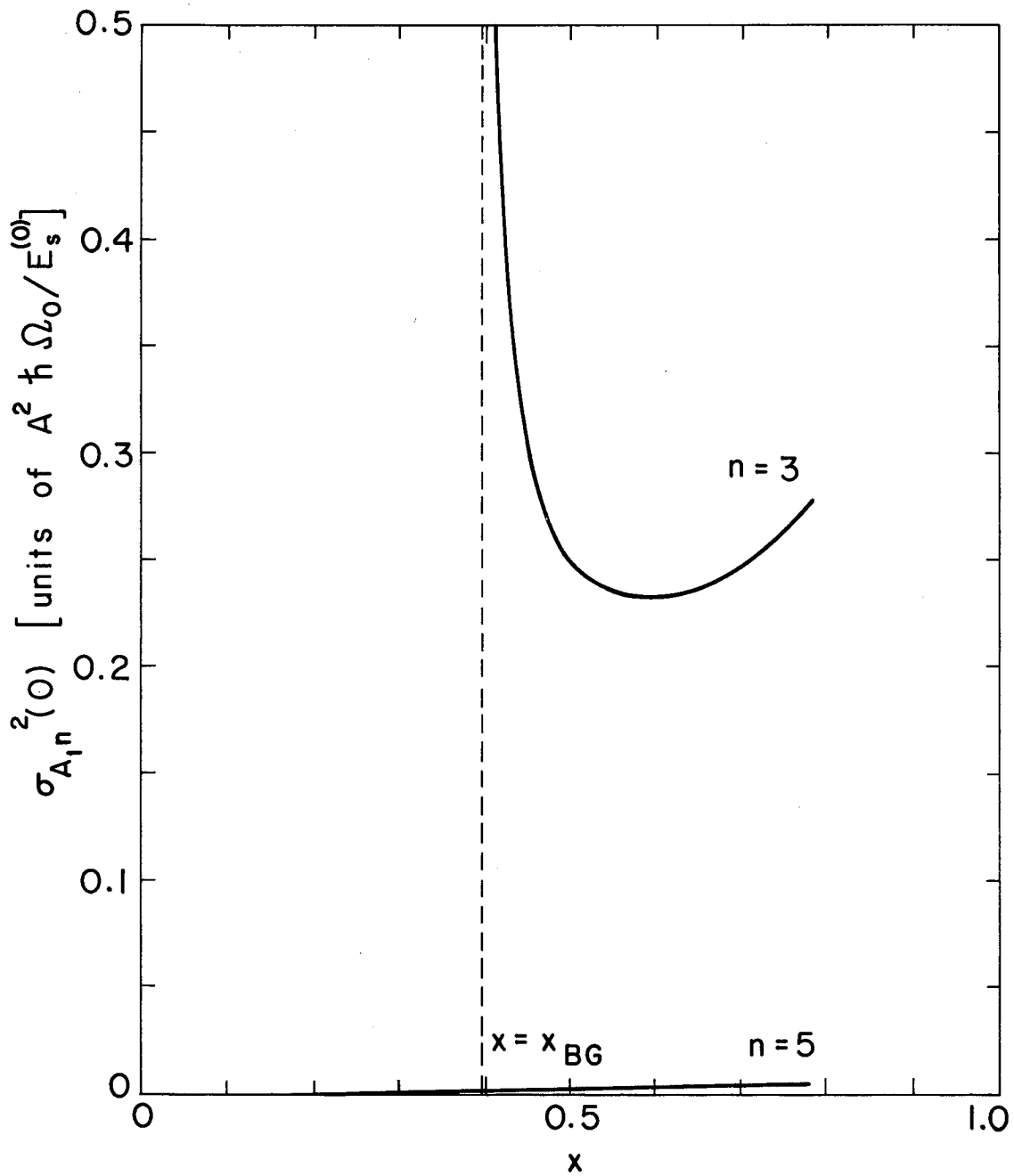

Fig. 14. The zero-temperature contributions $\sigma_{A_1 n}^2(0)$ of the n = 3 and 5 modes to the variance of the mass distribution, as functions of the fissility parameter x. The dashed line marks the critical Businaro-Gallone point, below which the n = 3 contribution is infinite.

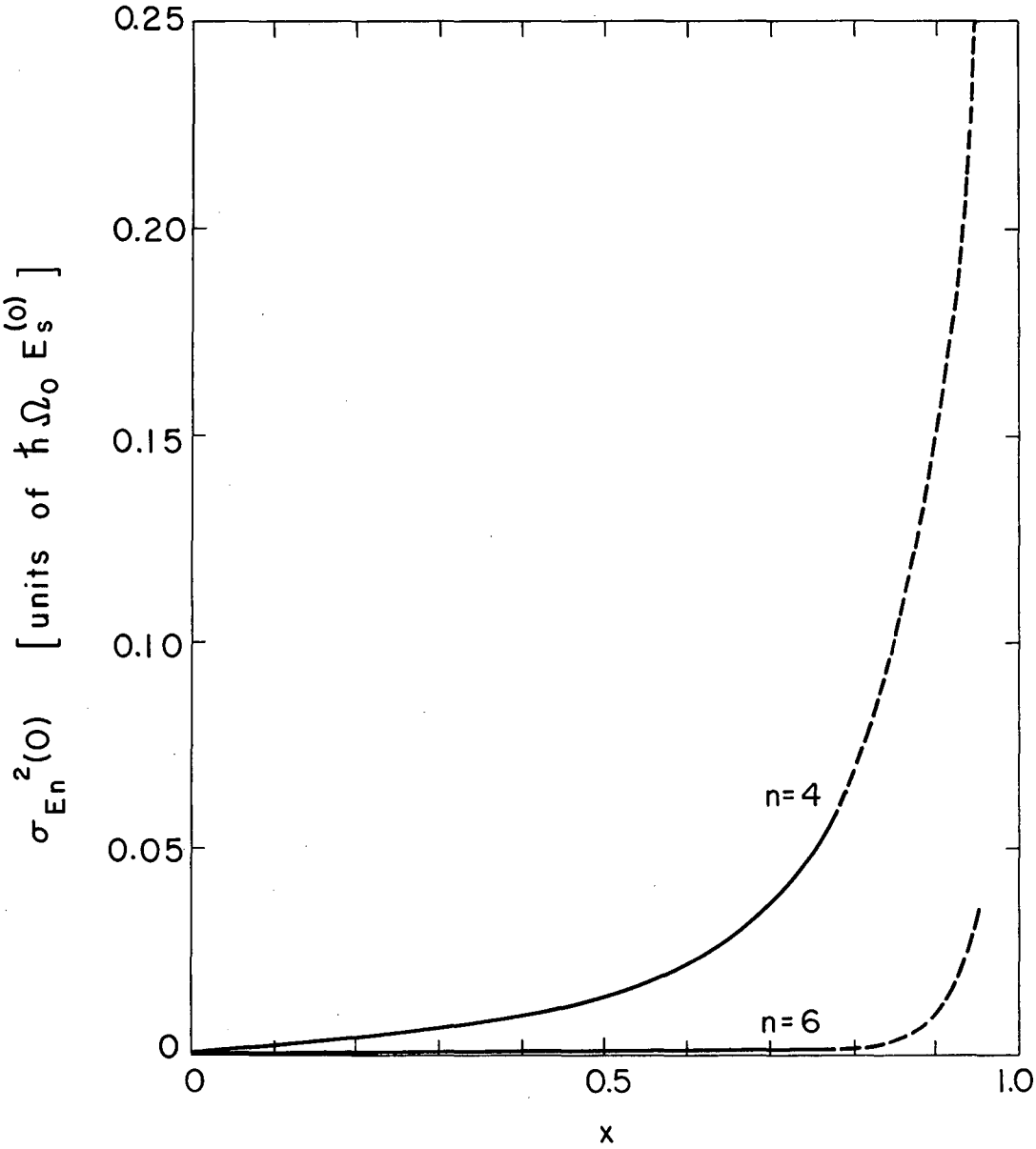

Fig. 15. The zero-temperature contributions $\sigma_{En}^2(0)$ of the n = 4 and 6 modes to the variances of the distributions in total translational kinetic energy and vibrational energy, as functions of the fissility parameter x. As x increases above 0.78 the numerical accuracy of these results becomes progressively more questionable, and this is indicated by the use of dashed lines.

The results of figs. 14 and 15 are presented in natural liquid-drop units so that the variances of the mass and energy distributions can be determined readily for a given compound nucleus at a given nuclear temperature Θ at the saddle point. In addition to figs. 14 and 15 the determination involves in general the use of figs. 7 (or 8) and 9, as well as eqs. (18), (11), (2) and (3).

For nuclei along the line of beta stability, we present in fig. 16 the variances of the mass distribution in $(\text{amu})^2$, and in fig. 17 the variances of the energy distributions in $(\text{MeV})^2$, for several values of the nuclear temperature Θ at the saddle point. It is observed that, apart from values of Θ close to zero, the general trend is that the variances of the mass distribution decrease with increasing x. The general trend of the variances of the energy distributions is an increase with increasing x, although it is seen that for large values of Θ the variances become relatively flat and even experience a local minimum at $x \approx 0.7$. This behavior, as well as the structure shown in fig. 16 for $\Theta \neq 0$, arises from the dependence on x of the normal-mode frequencies (see again fig. 8). For convenience, we also show the full widths at half maximum of the mass distribution in fig. 18, and of the energy distributions in fig. 19, again for nuclei along the line of beta stability and for several values of Θ. (For a Gaussian distribution the full width at half maximum is equal to the square root of the variance multiplied by 2.3548.)

4. Comparisons of Theoretical and Experimental Results

We are now ready to compare our calculated distributions in fission-fragment masses and energies with experimental results. The calculated distributions are for the division of idealized liquid drops, and the purpose of the comparisons is to tell us whether or not the properties of the division of real nuclei are similar to those of idealized drops whose charge, surface tension, mass and size are equal to those of nuclei. The comparisons are made for nuclei throughout the periodic table and as functions of the internal nuclear excitation energy of the compound nuclei undergoing fission. Thus from the comparisons we will learn for what range of nuclei and at what excitation energies the liquid-drop theory of fission applies to real nuclei.

It should be emphasized that the point of the comparisons is not to determine the values of any parameters by arbitrarily adjusting the data to the theory. The values of all constants that enter the theoretical distributions are taken from previous analyses of experimental results that do not include fission [with one exception: fission-barrier heights were used in the analysis of ref. [28]) in the determination of the ratio of the surface-energy constant to the Coulomb-energy constant]. Thus the calculated and experimental distributions are not normalized to each other in any way.

In converting from natural liquid-drop units to conventional units we use the second set of values of Myers and Swiatecki[28]) for the constants of the semi-empirical mass formula. The conversion from excitation energy to nuclear temperature at the saddle point is made according to the semi-empirical nuclear equation of state[65])

$$E_{ex}^{SP} = a\Theta^2 - \Theta \quad ,$$

where the level-density parameter a is taken equal to A/(8 MeV) [refs. [65,66])]. The determination of Θ by use of this equation involves an appreciable uncertainty because, first of all, the value of the level-density parameter at the saddle point may be different than the value at the equilibrium deformation, and, second, the level-density parameter for a given nucleus (at its equilibrium deformation) can differ considerably from the average result that we use.

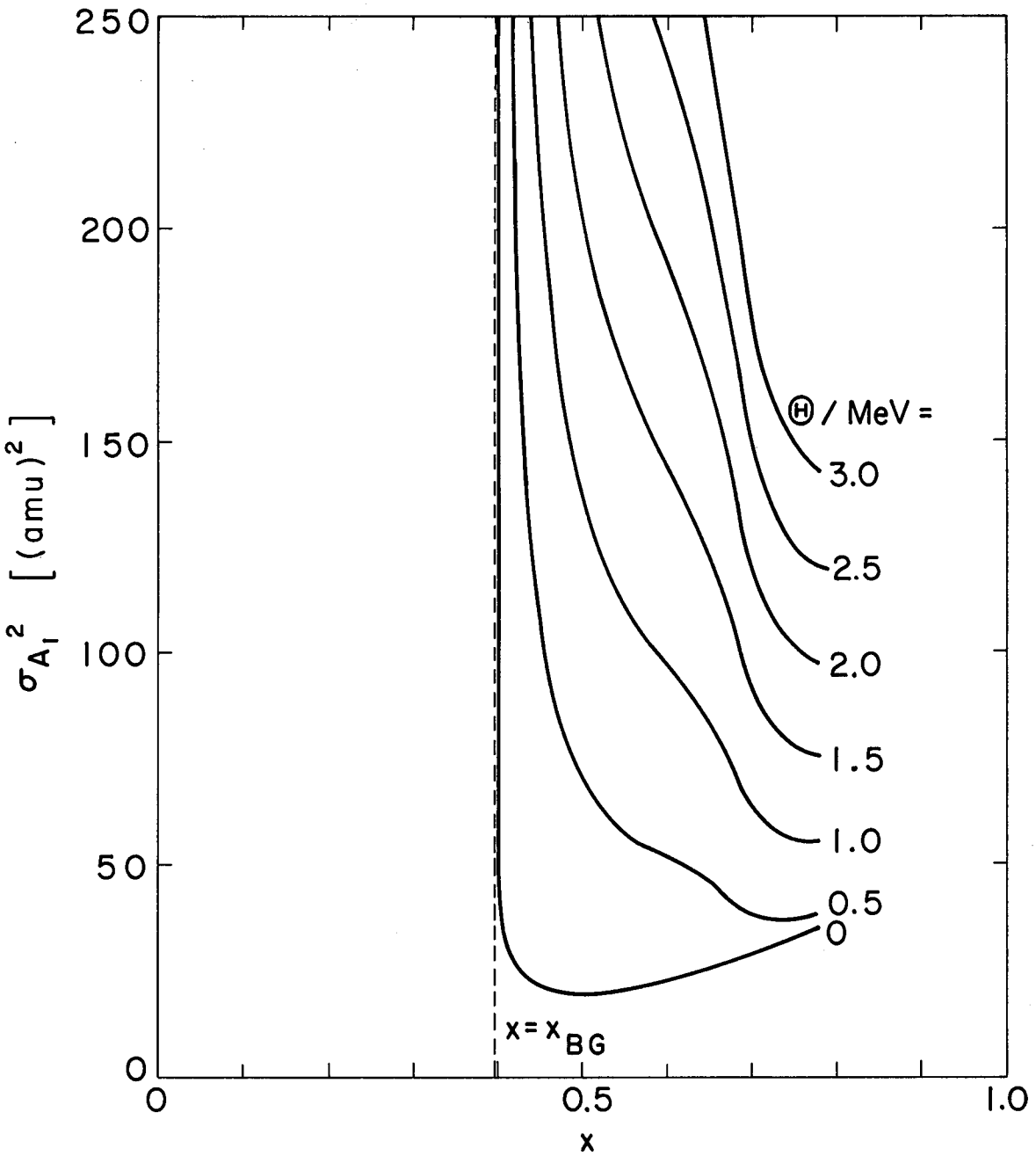

XBL678-3837

Fig. 16. Variances of the mass distribution for nuclei along the line of beta stability, as functions of the fissility parameter x. The curves are for various values of the nuclear temperature Θ at the saddle point. The dashed line marks the critical Businaro-Gallone point, below which the variances are infinite.

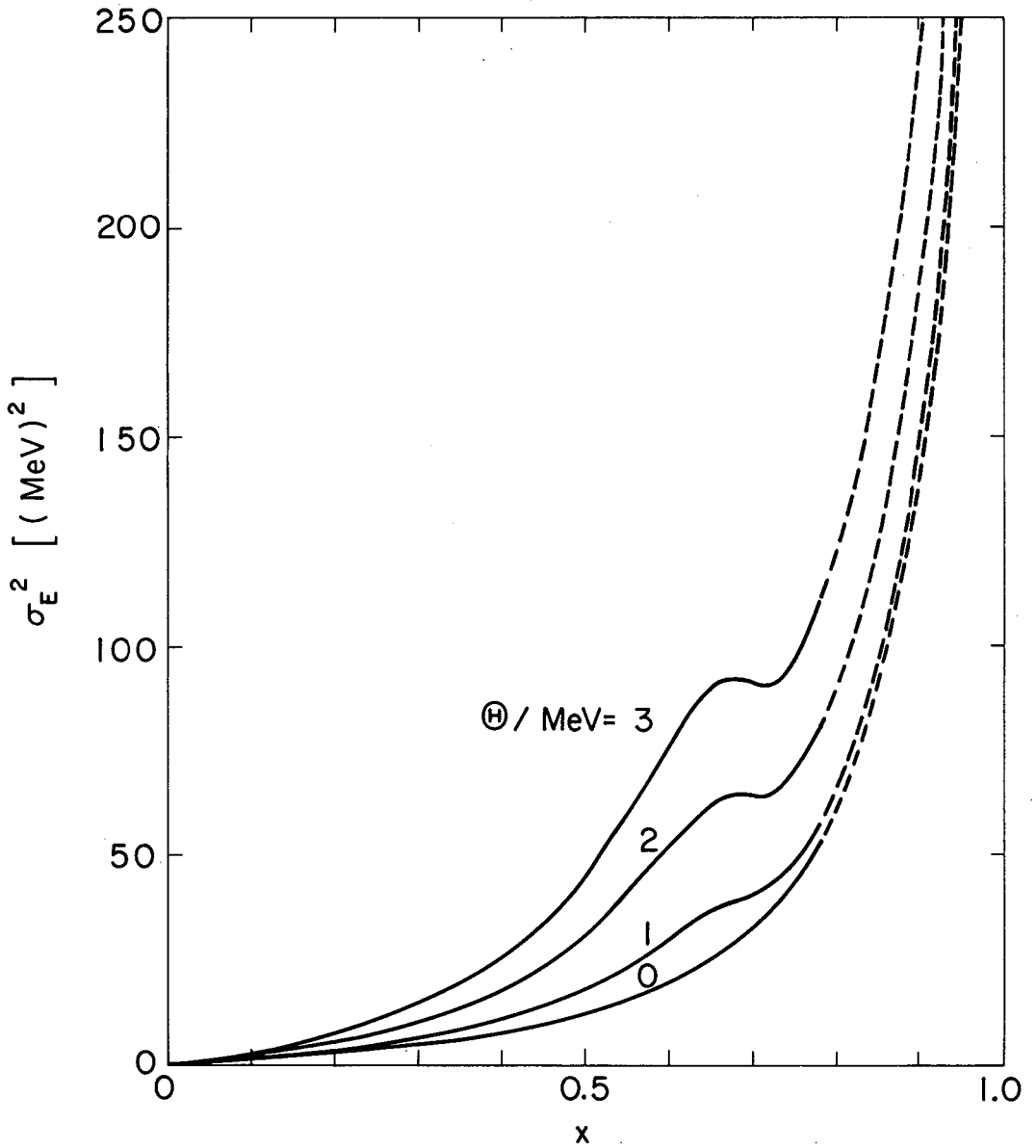

Fig. 17. Variances of the distributions in total translational kinetic energy and vibrational energy for nuclei along the line of beta stability, as functions of the fissility parameter x. The curves are for various values of the nuclear temperature Θ at the saddle point. As x increases above 0.78 the numerical accuracy of these results becomes progressively more questionable, and this is indicated by the use of dashed lines.

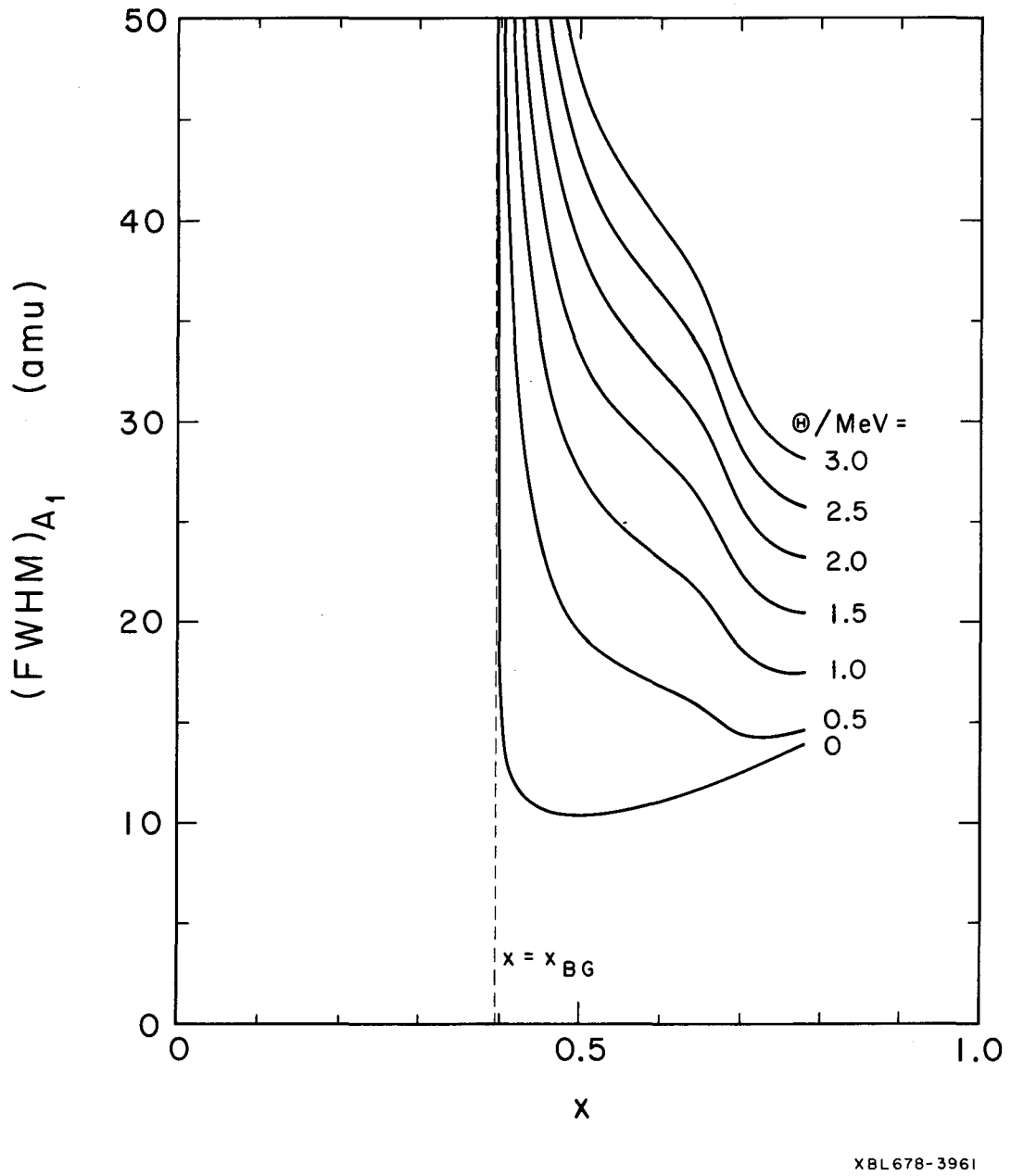

Fig. 18. Full widths at half maximum of the mass distribution for nuclei along the line of beta stability, as functions of the fissility parameter x. The curves are for various values of the nuclear temperature Θ at the saddle point. The dashed line marks the critical Businaro-Gallone point, below which the widths are infinite.

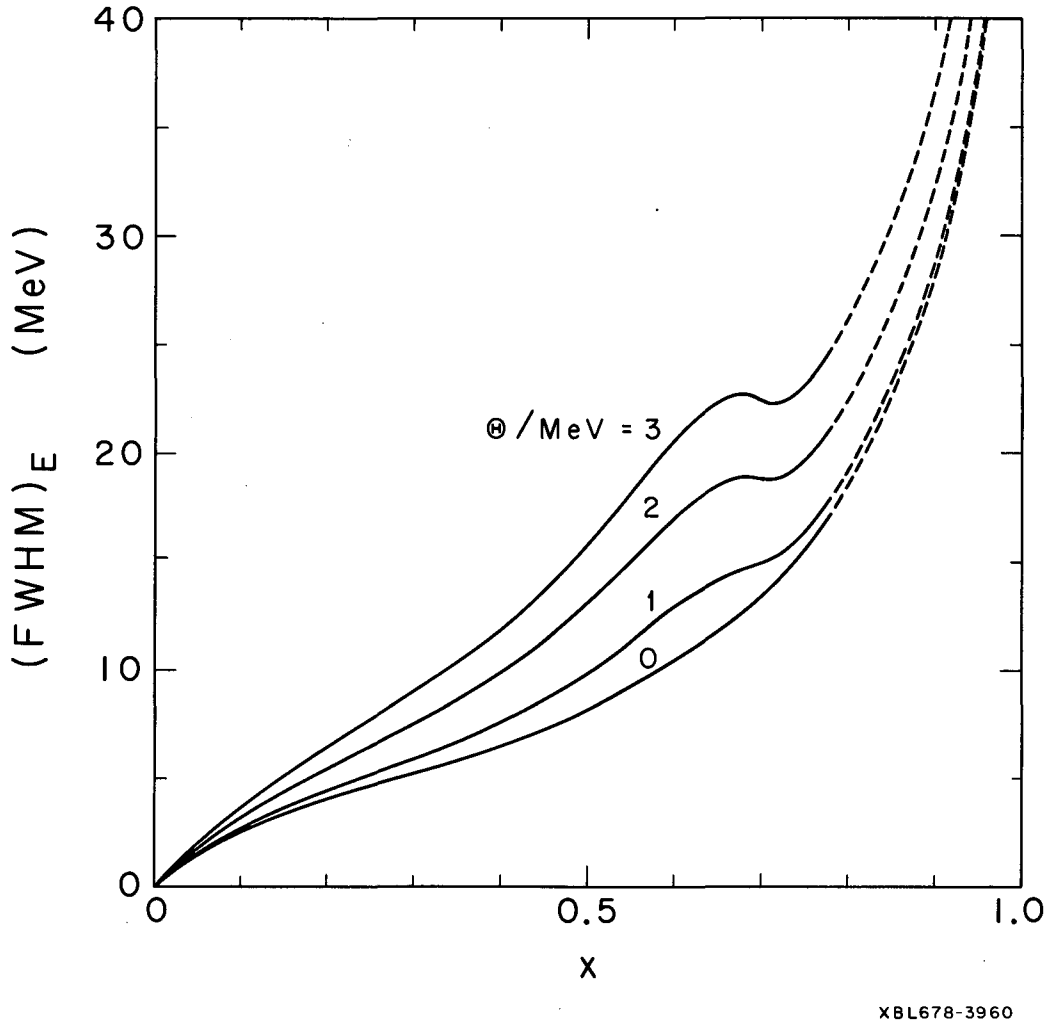

Fig. 19. Full widths at half maximum of the distributions in total translational kinetic energy and vibrational energy for nuclei along the line of beta stability, as functions of the fissility parameter x. The curves are for various values of the nuclear temperature Θ at the saddle point. As x increases above 0.78 the numerical accuracy of these results becomes progressively more questionable, and this is indicated by the use of dashed lines.

The excitation energy E_{ex}^{SP} at the saddle point equals the excitation energy at the ground state minus the height of the fission barrier. The height of the fission barrier can in turn be expressed approximately as the height of the liquid-drop portion of the barrier [which is calculated here and in refs. [2,33])], plus the shell correction at the saddle point, minus the shell correction at the ground state[28,30]). Values for the shell correction at the ground state are given in ref. [30]), and the shell correction at the saddle point, which is believed to be small[30]), is neglected here.

Our procedure for making the comparisons is to discuss first the most probable values for the masses and energies, and second the widths of the distributions in these quantities.

Within the limitations of the Werner-Wheeler approximation for the kinetic energy and a parameterization that permits only binary division, we have seen that the calculated most probable mass division for idealized nonviscous irrotational liquid drops is into two equal parts, for all excitation energies and for all values of the fissility parameter $x > x_{BG} = 0.396$. (Strictly speaking, this was demonstrated only for $x \leq 0.78$, and the situation could change for larger values of x.)

Experimentally, the most probable mass division is into two equal parts for the fission of nuclei lighter than about radium at all excitation energies[†] and for the fission of nuclei heavier than radium at high excitation energies, but is into two unequal parts for the fission of nuclei heavier than radium at low excitation energies. The experimental mass distribution for radium itself is peaked both at divisions corresponding to equal parts and unequal parts; the frequency of the unequal divisions decreases as the excitation energy increases. [See for example refs. [67,68]) for illustrations of the dependence of experimental mass distributions upon compound nuclei and excitation energy.] Thus the experimental most probable mass division of heavy nuclei at low excitation energies does not correspond to that of an idealized nonviscous irrotational liquid drop, whereas the

[†]Because the difficulty of observing the fission of medium nuclei increases with decreasing excitation energy, most experimental mass distributions for medium nuclei are for compound nuclei having at least a small amount of excitation energy at the saddle point.

most probable mass divisions for the other situations do correspond to those of idealized drops.

The next comparison that we make concerns the most probable translational kinetic energies of the fragments and is presented in fig. 20, which is an updated version of fig. 2 of ref. [61]). The dot-dashed curve gives the calculated translational kinetic energy acquired by the fragments prior to scission, the short-dashed curve that acquired after scission, and the solid curve the total at infinity. The experimental total translational kinetic energies at infinity are from a variety of sources[69-75]) but include only cases in which the mass distributions are symmetrical. The kinetic energies were obtained by the use of solid-state detectors and have been corrected (in the original works) for the effects of neutron emission. The open symbols represent most probable values, and the solid symbols average values. The calculations (with no adjustable parameters) are seen to reproduce both the correct order of magnitude and the correct trend with x of the total kinetic energies, but a systematic difference of about 5% is evident.

Attempts have been made to deduce the most probable translational kinetic energy acquired by the fragments prior to scission from experimental data on long-range alpha particles emitted during fission[76,77]). Such estimates are obtained by comparing the experimental angular distributions and kinetic-energy distributions of the long-range alpha particles with distributions calculated on the basis of simple models[76,77]). Since the calculated distributions depend sensitively upon the assumptions made regarding the initial conditions for the alpha particle, the conclusions are rather uncertain. Also, the experimental pre-scission kinetic energies obtained in this way refer to the most probable (asymmetrical) mass division, whereas our calculated energies are for a symmetrical mass division. Even with these deficiencies, we nevertheless compare in fig. 20 the two available estimates with our calculated most probable pre-scission kinetic energies. The experimental result for ^{236}U [open diamond[76])] is somewhat lower than the calculated value, whereas the result for ^{252}Cf [open hexagon[77])] agrees almost exactly with the calculated value. If the comparisons of the pre-scission kinetic energies are taken at face value, the results indicate that the fragments associated with the fission of heavy nuclei are already in substantial motion by the time they arrive at the scission point.

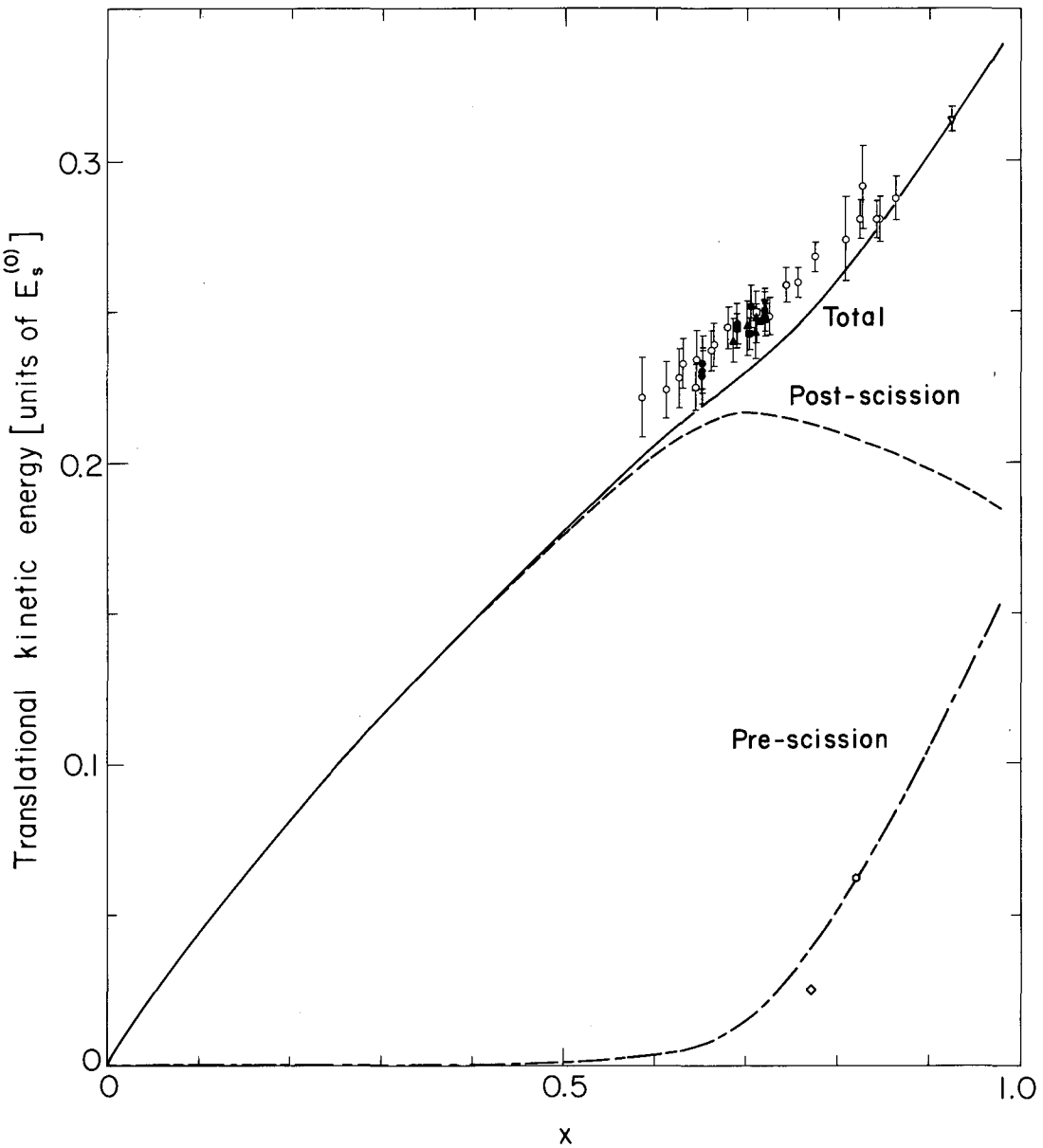

Fig. 20. Comparisons of calculated and experimental most-probable fission-fragment translational kinetic energies, as functions of the fissility parameter x. The dot-dashed curve gives the calculated most-probable translational kinetic energy acquired by the fragments prior to scission, the short-dashed curve that acquired after scission, and the solid curve the total at infinity. The experimental total kinetic energies are from the following sources: ○,[69]); □,[70]); ▽,[71]); ●,[72]); ■,[73]); ▼,[74]) and ▲,[75]). The experimental pre-scission kinetic energies are from ◇,[76]) and ⬡,[77]).

The calculated most probable kinetic energies both at scission and at infinity are to lowest order independent of the nuclear excitation energy. There is experimental evidence only for the energies at infinity; this indicates that to within experimental errors the most probable total translational kinetic energies are independent of excitation energy [see for example refs. [69,72])], which confirms the prediction.

The next comparison that should logically be made is for the most probable vibrational energies. Experimental values for these quantities can be deduced most directly from measurements of the numbers of neutrons emitted from the fragments [see for example refs. [78,79])]. The comparison is not made explicitly because the available data is for the fission of heavy nuclei at low excitation energies, for which we have already seen that the liquid-drop theory does not predict the correct most probable mass division. However, to first order the sum of the translational kinetic energy and the vibrational energy equals the height of the fission barrier plus the energy release [see eq. (15)], which is given correctly (apart from fluctuations due to shell structure) by the liquid-drop semi-empirical mass formula. We can therefore conclude directly from fig. 20 that the calculations should give the correct order of magnitude and the correct trend with x of the most probable vibrational energies, but that the experimental vibrational energies should be systematically low, to correspond to the experimental translational energies being systematically high. It would nevertheless be worthwhile experimentally to verify directly this conclusion by explicitly determining the number of neutrons emitted by the fragments as a function of x.

We turn now to comparisons between the calculated and experimental widths of the mass and energy distributions. The widths depend upon both the fissility parameter x and the temperature Θ, and a complete comparison would require plotting (in a three-dimensional diagram) the calculated and experimental widths versus x and Θ. Both because of the difficulty in constructing such a diagram and because of the unevenness of the experimental results, we divide the comparisons into three parts: (1) widths as functions of x for zero or small values of Θ, (2) widths as functions of Θ for selected medium nuclei, and (3) widths for various heavy nuclei at moderate and large values of Θ.

We have already seen that for heavy nuclei at low excitation energies the shapes of the calculated and experimental mass distributions are not the same: the calculated distributions are Gaussian in shape and are centered at a division into equal parts, whereas the experimental distributions have two peaks centered at divisions into unequal parts. Because of this, a comparison of the widths of these distributions is subject to some ambiguity. At least five different approaches can be taken: (1) The actual width at half-maximum probability of the complete (asymmetrical) experimental distribution can be compared with the calculated width. (2) The variance of the complete experimental distribution can be compared with the calculated variance. (3) The experimental distribution can be decomposed into a symmetrical and an asymmetrical component, and the width of the symmetrical component compared with the calculated width. Such decompositions have been made in refs. [73,80,81]) for induced fission of radium, where the distributions have three distinct peaks. In practice this method is not applicable to the fission of heavier nuclei because the symmetrical component cannot be extracted accurately. (4) The width of the complete experimental distribution can be obtained by fitting a single Gaussian curve through the wings of the distribution. (A particularly simple way of doing this is to plot the logarithm of the mass yield versus the square of the difference between the mass number and its value at symmetry. The slope in the region of the wings is then related to the width.) (5) Finally, the width of a single peak of the experimental distribution can be compared with the calculated width. Of these five approaches we use and compare methods (1) and (4) for target nuclei heavier than radium, and method (3) for induced fission of radium, where there are three distinct peaks.

Shown in fig. 21 is a comparison as a function of x of the full widths at half maximum of mass distributions, divided by the square root of $\coth[\hbar\omega_3/(2\Theta)]$. From eq. (18a) and the first-order relationship between the full width at half maximum and the variance, the plotted function is seen to be

$$(\mathrm{FWHM})_{A_1}\Big/\left[\coth\left(\frac{\hbar\omega_3}{2\Theta}\right)\right]^{\frac{1}{2}} = 2.3548\left[\sigma_{A_1 3}{}^2(0) + \sigma_{A_1 5}{}^2(0)\,\coth\left(\frac{\hbar\omega_5}{2\Theta}\right)\Big/\coth\left(\frac{\hbar\omega_3}{2\Theta}\right)\right]^{\frac{1}{2}} \quad . \quad (19)$$

This quantity is approximately independent of Θ for small values of Θ since the temperature dependence enters as a ratio of two hyperbolic cotangents that multiplies a term much smaller than the first term (see again fig. 14). The theoretical curve is evaluated for $\Theta = 0$, although any small value of Θ would give a result that is indistinguishable on a graph of this scale. Dividing by the square root of the hyperbolic cotangent, which is unity for $\Theta = 0$, permits an approximate extraction of the temperature dependence of the experimental widths for medium nuclei, for which there are no measurements at zero temperature.

The mass distributions whose widths are given in fig. 21 were obtained by a variety of methods: simultaneous measurements of fragment energies by use of solid-state detectors[72-75,81,82,88-90]), simultaneous measurements of fragment velocities[87]), and radiochemical techniques[83-86]). The data (as well as those of the next figure) have been corrected for the effects of fragment neutron emission and finite counter resolution only when the appropriate corrections were made by the original investigators. The relationship that holds for a Gaussian distribution has been used to convert from variances to full widths at half maximum when the former quantity is reported[72,73]).

It is seen from fig. 21 that the experimental widths are systematically larger than the calculated ones. The discrepancy is about 25% for medium nuclei, and increases to about 100% for heavy nuclei when method 4 is used to extract the widths. The widths for heavy nuclei extracted by method 1 are roughly four times as large as the calculated widths and in addition show the opposite dependence upon x. Thus experimental mass distributions for heavy nuclei are both of a different shape (at low excitation energies) and also have widths that are significantly larger than the distributions for idealized liquid drops (that are constrained to shapes described in terms of three smoothly joined portions of quadratic surfaces of revolution and therefore having a single neck). We postpone our discussion of the significance of this result until the next section.

We present in fig. 22 a comparison as a function of x of the full widths at half maximum of fission-fragment total translational kinetic-energy distributions, divided by the square root of $\coth[\hbar\omega_4/(2\Theta)]$. The plotted function, which is analogous to that of fig. 21 and eq. (19), is also approximately independent of Θ for small values of Θ. The data of fig. 22

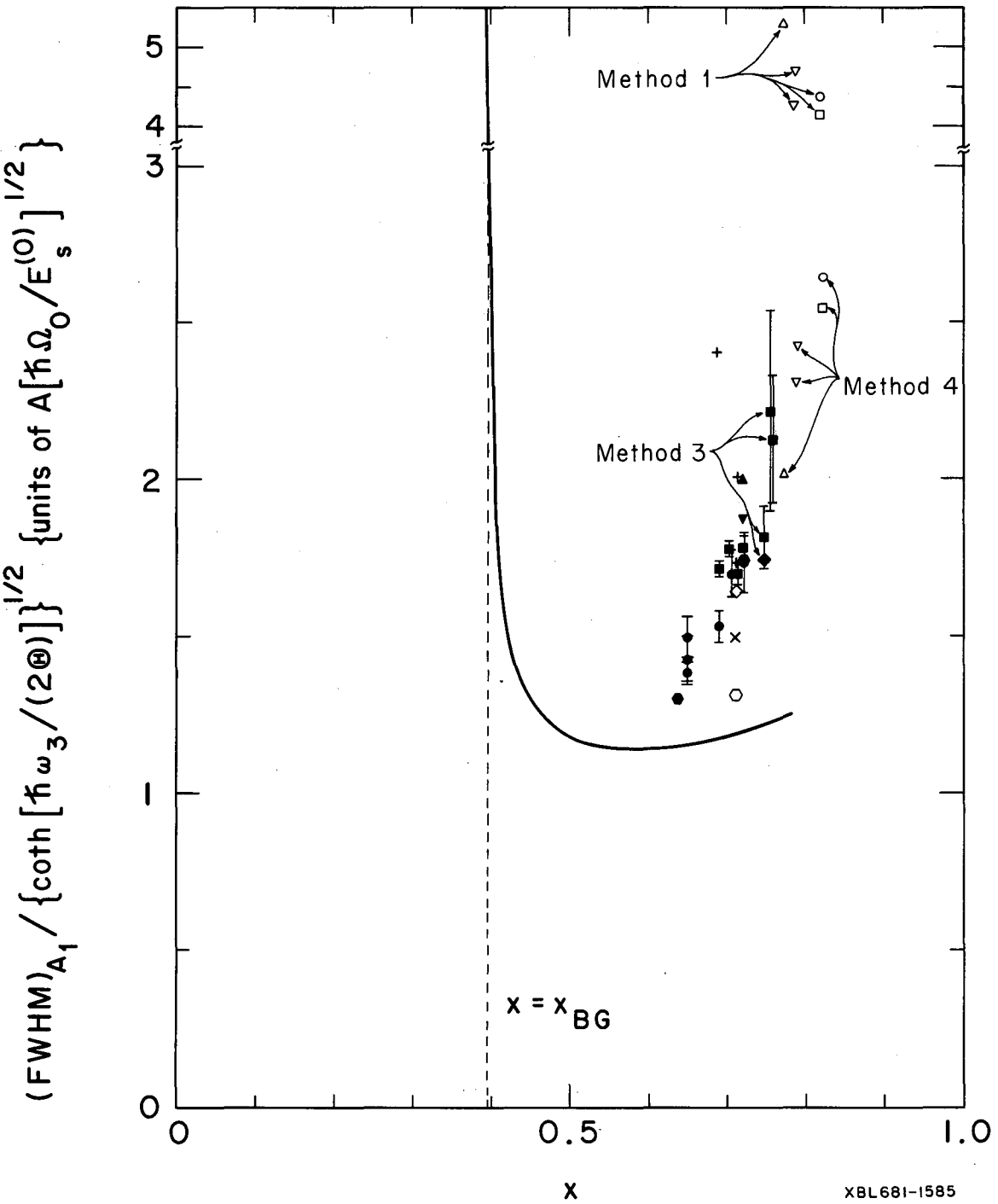

Fig. 21. A comparison of calculated and experimental full widths at half maximum of mass distributions, as a function of the fissility parameter x. Division of the widths by $\{\coth[\hbar\omega_3/(2\Theta)]\}^{\frac{1}{2}}$ extracts approximately their temperature dependence. The various methods used to determine the widths for the fission of heavy nuclei are discussed in the text. Note that the scale is discontinuous and that the experimental widths determined by method 1 are roughly twice as large as those determined by method 4. The dashed line marks the critical Businaro-Gallone point, below which the calculated widths are infinite. The experimental data are from the following sources: ●,[72]); ■,[73]); ▼,[74]); ▲,[75]); ◆,[81]); ⬢,[82]); ◇,[83]); ⬡,[84]); +,[85]); ×,[86]); ○,[87]); □,[88]); ▽,[89]) and △,[90]).

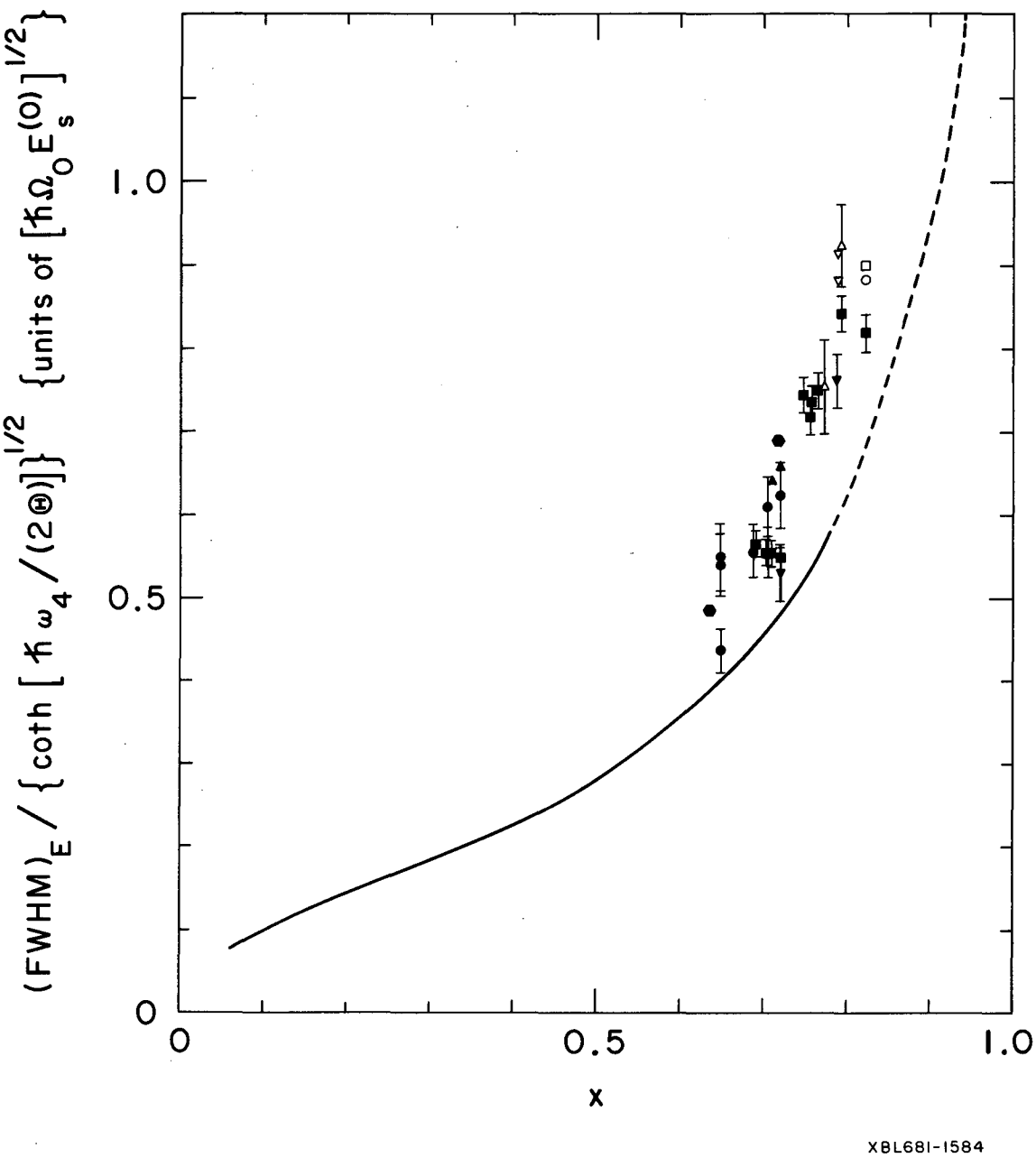

Fig. 22. A comparison of calculated and experimental full widths at half maximum of total translational kinetic-energy distributions, as a function of the fissility parameter x. Division of the widths by $\{\coth[\hbar\omega_4/(2\Theta)]\}^{\frac{1}{2}}$ extracts approximately their temperature dependence. As x increases above 0.78 the numerical accuracy of the calculated curve becomes progressively more questionable, and this is indicated by the use of a dashed line. Below x = 0.06 the curve was not calculated but is known to pass through the origin. The experimental data are from the following sources: ●,[72]); ■,[73]); ▼,[74]); ▲,[75]); ,[82]); ○,[87]); ▽,[89]); △,[91]) and □,[92]).

have been obtained both from fragment-energy measurements with solid state detectors[72-75,82,89,91]) and fragment-velocity measurements[87,92]). From the figure we see that the widths of the experimental kinetic-energy distributions are systematically about 25% larger than the calculated widths for idealized drops and that the trends with the fissility parameter x are approximately the same.

Comparisons of the widths of the distributions in masses and translational kinetic energies as functions of the nuclear temperature Θ at the saddle point are made in figs. 23 and 24, respectively, for four medium nuclei. Since the experimental data, which are those of Plasil et al.[72]), are reported in terms of variances, these quantities are plotted rather than full widths at half maximum.

The theoretical distributions are calculated for systems with zero total angular momentum. The compound nuclei ^{201}Tl and ^{213}At of figs. 23 and 24 were formed by bombardments with alpha particles, and consequently have only a small amount of angular momentum. On the other hand, the compound nuclei ^{186}Os and ^{198}Pb were formed by the use of heavy-ion-induced reactions (with two exceptions), and hence are characterized by a fairly large amount of angular momentum. The comparisons for these two compound nuclei must therefore be made with the reservation that the large angular momentum present could possibly affect the experimental distributions.

In the determination of the nuclear temperature Θ at the saddle point, account was taken of two complications[72]). First, the possibility of the compound nucleus emitting neutrons prior to fission was included by calculating the competition between fission and neutron emission during its de-excitation. Second, the effect of angular momentum on Θ [arising from the dependence of the fission-barrier height on angular momentum[32])] was taken into account by integrating over the distribution of angular momentum.

From figs. 23 and 24 certain observations are apparent: (1) The experimental variances of both the mass and kinetic-energy distributions are consistently higher than the calculated ones by roughly 40%. This means the experimental widths are higher than the calculated ones by roughly 20%. (2) For the three compound nuclei ^{186}Os, ^{201}Tl and ^{213}At the experimental and calculated slopes of the variances of the mass distributions are approximately the same, whereas the experimental slopes of the variances of the kinetic-energy distributions are smaller than the calculated ones.

(3) For the compound nucleus ^{198}Pb the experimental slopes of the variances of both the mass distribution and the kinetic-energy distribution are larger than the calculated ones.

For heavy nuclei at high excitation energies the experimental most probable mass division is into two equal parts, but the mass distribution has a flatter top than a Gaussian curve. Although the determination of the experimental widths at high excitation energies appears straightforward, a complication exists associated with the possibility of the compound nucleus partially de-exciting by neutron emission and then fissioning. If this occurs the measured mass distribution contains an asymmetrical component corresponding to low-energy fission, which broadens the observed distribution. Because of the difficulty of accurately unfolding the measured mass distribution into low-energy and high-energy components, we are not able to make definitive comparisons between our calculated widths and experimental widths corresponding to true high-energy fission. Nevertheless, disregarding this complication, we compare in table 3 calculated and experimental widths of mass distributions for various heavy nuclei at moderate and high excitation energies. It is seen from the table that the experimental widths are roughly three times as large as the calculated widths. However, it must be emphasized that this conclusion depends upon the assumption that the entire observed mass distribution results from fission with no prior emission of neutrons.

A similar comparison is made in table 4 of the variances (or widths) of kinetic-energy distributions for heavy nuclei at moderate and high excitation energies. In examining the table it should be pointed out that for the same experimental situation variances obtained from time-of-flight measurements of fragment velocities[101]) are significantly larger than those obtained from solid-state-detector measurements of fragment energies[100]). This systematic discrepancy is illustrated in for example ref. [73]). The comparisons made in the table indicate that the experimental widths are roughly one and one-half times as large as the calculated widths.

We turn now to the widths of vibrational-energy distributions. We do not make detailed comparisons concerning the widths of these distributions, for reasons similar to those discussed in connection with most probable vibrational energies. However, we do compare our calculations with two experimental data. Terrell[78]) has deduced from distributions of fission

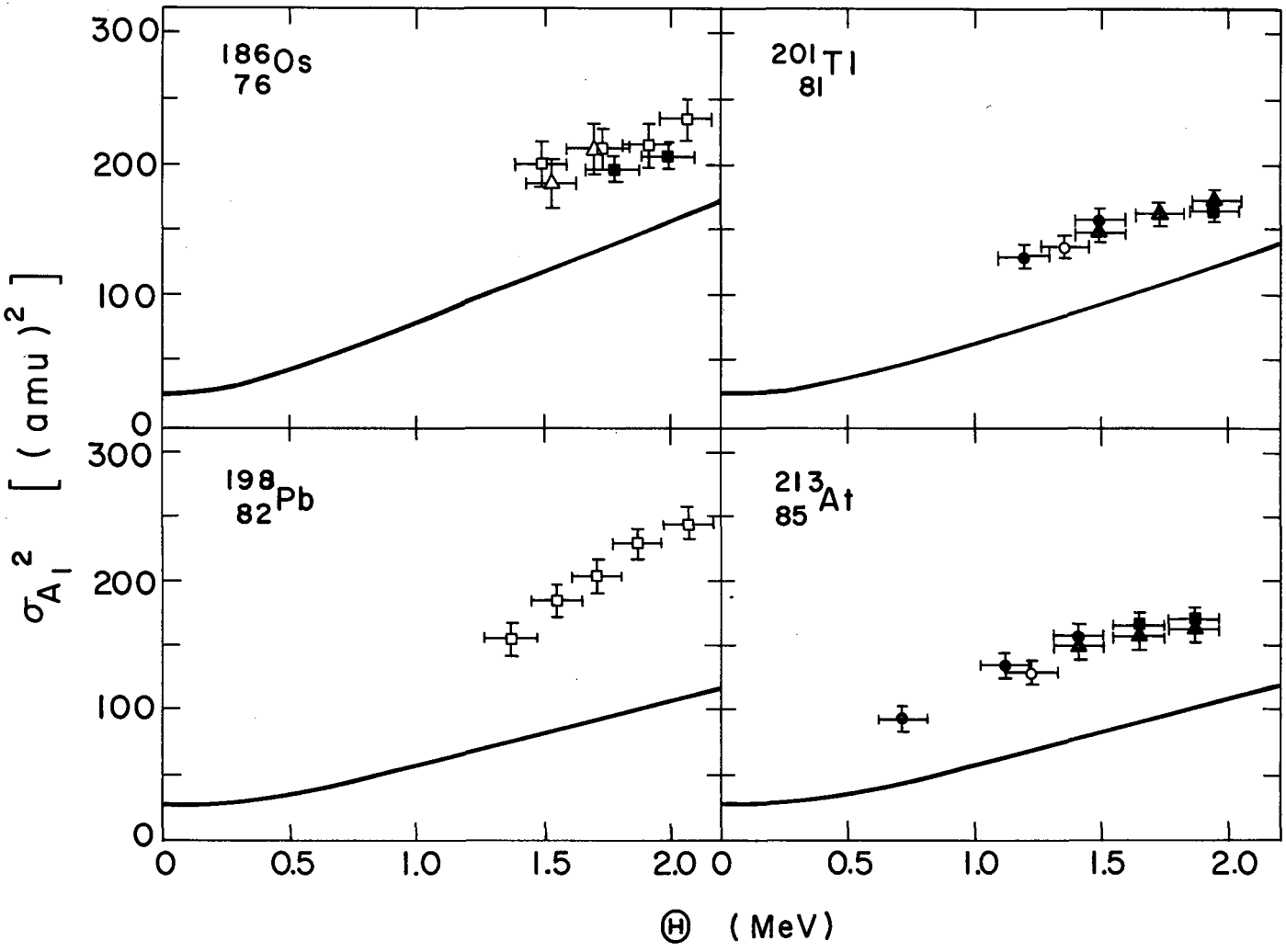

Fig. 23. Comparisons of calculated and experimental variances of fission-fragment mass distributions for four medium compound nuclei, as functions of the nuclear temperature Θ at the saddle point. The data are those of Plasil et al.[72]) and have been corrected for neutron-emission effects. The compound nucleus ^{186}Os was formed from the following reactions: △, $^{174}Yb + ^{12}C$; □, $^{170}Er + ^{16}O$ and ■, $^{182}W + ^{4}He$. The compound nucleus ^{198}Pb was formed from the reaction $^{182}W + ^{16}O$. The compound nuclei ^{201}Tl and ^{213}At were formed by bombarding ^{197}Au and ^{209}Bi, respectively, with ^{4}He. The different symbols in these two cases represent different experiments.

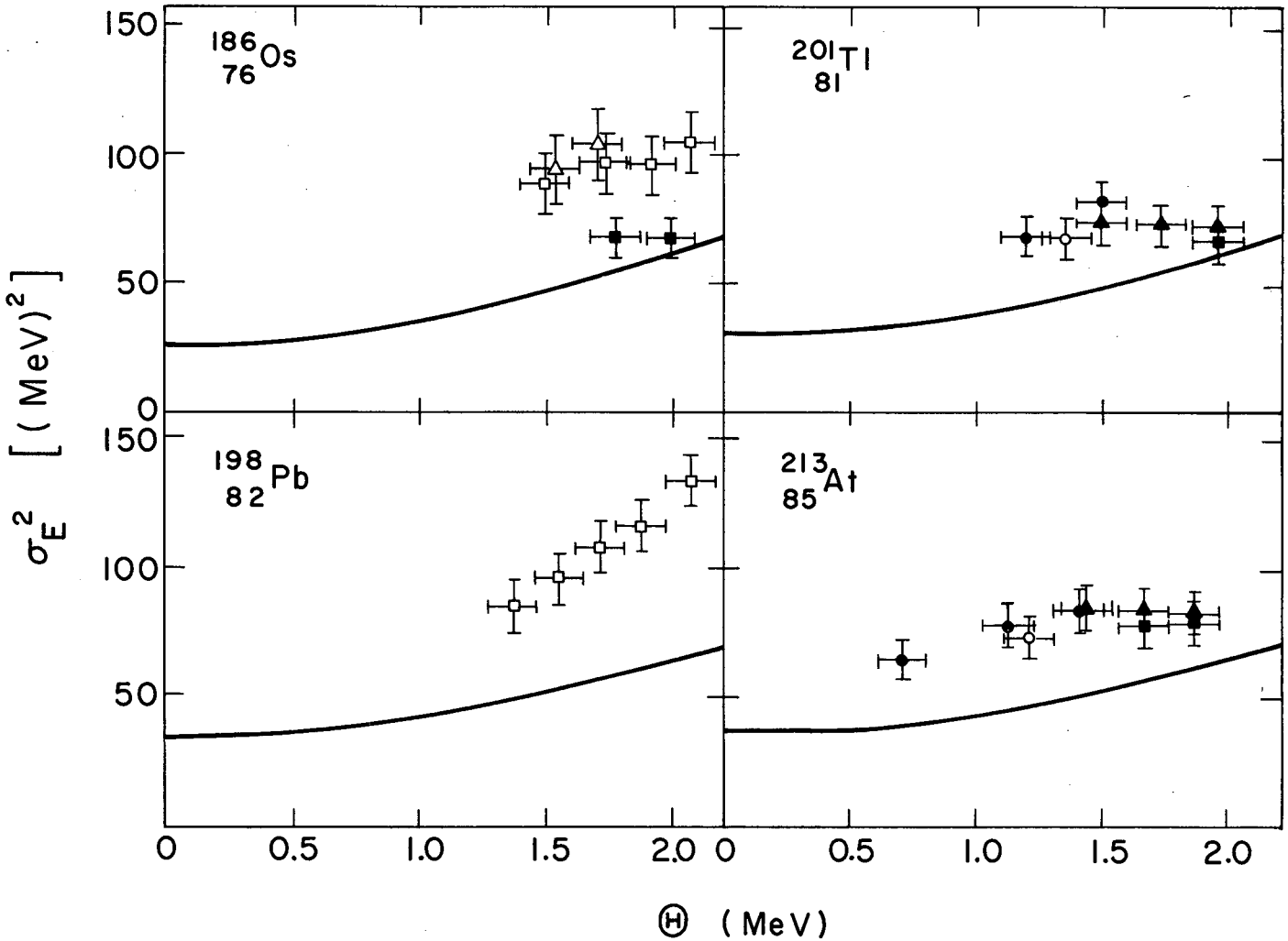

Fig. 24. Comparisons of calculated and experimental variances of fission-fragment total translational kinetic-energy distributions for four medium compound nuclei, as functions of the nuclear temperature Θ at the saddle point. The data are those of Plasil et al.[72]) and have been corrected for neutron-emission effects. The compound nuclei were formed from the same reactions as those in fig. 23.

Table 3

Widths of mass distributions for heavy nuclei at moderate and high excitation energies

Target	Projectile	Compound nucleus	x	Bombarding energy (MeV)	Θ (MeV)	$(FWHM)_{A_1}$ Theory (amu)	Exp.	Ref.
^{232}Th	α	^{236}U	0.772	65.0	1.44	21	57	91)
^{233}U	d	^{235}Np	0.784	23.4	1.00	17	56	93)
^{233}U	α	^{237}Pu	0.793	44.3	1.10	18	54	94)
^{233}U	α	^{237}Pu	0.793	77.3	1.52	21	49	82)
^{235}U	α	^{239}Pu	0.791	45	1.08	18	57	94)
^{238}U	p	^{239}Np	0.780	150	2.28	25	52	95)
^{238}U	d	^{240}Np	0.778	125	2.09	24	54	95)
^{238}U	α	^{242}Pu	0.787	45.4	1.23	19	56	94)
^{238}U	α	^{242}Pu	0.787	65.0	1.47	21	56	91)
^{238}U	^{16}O	^{254}Fm	0.842	138	1.72	22	66	96)
^{237}Np	α	^{241}Am	0.800	45.7	1.07	18	50	97)
^{238}Pu	α	^{242}Cm	0.810	42.2	1.05	18	42	98)
^{239}Pu	d	^{241}Am	0.800	23.4	0.94	17	61	97)
^{239}Pu	α	^{243}Cm	0.809	47.5	1.12	18	45	98)
^{240}Pu	d	^{242}Am	0.799	21.2	0.88	17	56	99)

Table 4

Variances (or widths) of kinetic-energy distributions for heavy nuclei at moderate and high excitation energies

Target	Projectile	Compound nucleus	x	Bombarding energy (MeV)	Θ (MeV)	σ_E^2 [(MeV)^2] Theory	σ_E^2 [(MeV)^2] Exp.	$(FWHM)_E$ (MeV) Theory	$(FWHM)_E$ (MeV) Exp.	Ref.
^{230}Th	α	^{234}U	0.774	29.5	0.82	53	110±6			100)
^{230}Th	α	^{234}U	0.774	29.7	0.82	53	174			101)
^{232}Th	α	^{236}U	0.772	29.5	0.82	52	107±6			100)
^{232}Th	α	^{236}U	0.772	29.5	0.82	52	164			101)
^{232}Th	α	^{236}U	0.772	65.0	1.44	63	154±15			91)
^{233}U	α	^{237}Pu	0.793	29.5	0.83	62	123±6			100)
^{233}U	α	^{237}Pu	0.793	29.7	0.84	62	213			101)
^{233}U	α	^{237}Pu	0.793	77.3	1.52	74	175			82)
^{238}U	α	^{242}Pu	0.787	65.0	1.47	70	141±15			91)
^{238}U	α	^{242}Pu	0.787	42.0	1.19			19	26±1	74)
^{238}U	^{16}O	^{254}Fm	0.842	138	1.72			25	45	96)

neutron numbers that the full width at half maximum of the excitation-energy distribution for the spontaneous fission of ^{252}Cf is 19 ± 2 MeV and that the widths at low excitation energy for several compound nuclei ranging from U to Cm are 17 ± 2 MeV. These widths are somewhat smaller than the corresponding experimental widths of translational kinetic-energy distributions. Since to first order the widths of excitation-energy and translational kinetic-energy distributions should be equal, a slight inconsistency exists between the experimental results. Our calculated widths for the two sets of nuclei considered by Terrell are, respectively, 20 MeV and about 18 MeV, which agree with his experimental widths of excitation-energy distributions.

Two final comparisons that we would like to mention concern the magnitudes of the (purely imaginary) fission-mode frequency ω_2 and the mass-asymmetry frequency ω_3. In ref. [20]) experimental values of the fission-mode frequency obtained in a variety of ways were compared as a function of x with liquid-drop-model results calculated by use of a parameterization employing an expansion of the drop's radius vector in a series of 18 Legendre polynomials. Further experimental values of $|\omega_2|$ are reported in refs. [102,103]). Since for the range of x for which experimental values exist our present results for ω_2 are practically identical to those of ref. [20]), we do not repeat the analysis here, but instead merely summarize the conclusions. The liquid-drop-model results reproduce the correct order of magnitude of the experimental fission-mode frequencies. Most of the data are not sufficiently accurate to provide a sensitive test of the calculations, but the points derived from spontaneous-fission half lives and fission-barrier heights suggest that possibly 2.8 times as much mass is displaced in the fission mode as would correspond to irrotational flow. This number depends fairly sensitively upon what assumption is made regarding the shape of the fission barrier, and an analysis[42]) that takes into account single-particle effects on the barrier shape near the ground state indicates that the mass displaced in the fission mode is approximately 6.2 times as much as would correspond to irrotational flow.

Experimental information on both the magnitude of the fission frequency ω_2 and the mass-asymmetry frequency ω_3 can be obtained from measurements of fission cross sections and fission-fragment angular distributions as functions of excitation energy. The experimental values of Britt et al.[104]) for the magnitude of ω_2 are roughly 40% lower than the calculated values for

irrotational flow. For ω_3 the calculated values for irrotational flow are about 2 and 3 times as large as the experimental values[104]) for, respectively, ^{240}Pu and ^{236}U. These results suggest that the effective mass in the fission mode is 2.8 times the irrotational value, and that the effective masses in the mass-asymmetry mode for ^{240}Pu and ^{236}U are, respectively, 4 and 9 times the irrotational values[104]). Somewhat similar results for $|\omega_2|$ and ω_3 have been deduced from analyses of fission cross sections as functions of excitation energy[105]).

The conclusions drawn from our comparisons are discussed in the next section.

5. Summary and Conclusion

We have studied the division of an idealized charged liquid drop, using a parameterization of the shape of the nuclear surface in terms of three smoothly joined portions of quadratic surfaces of revolution. The parameterization takes into account six degrees of freedom and is suitable for discussing the masses, translational kinetic energies and vibrational energies of the fission fragments. The general procedure that we have used is similar to that of ref. [1]) and consists of applying standard static, dynamical and statistical methods to the Hamiltonian for the idealized system. Whereas the results of ref. [1]) were limited to the fission of nuclei lighter than about radium, the present parameterization allows us to learn more about the predictions of the liquid-drop model for heavy nuclei as well as medium.

Our study has included, first of all, calculating the surface and Coulomb energies as functions of the six generalized coordinates specifying the shape of the drop. Particular emphasis was given to locating the saddle point and calculating its properties. We learned that the more important static saddle-point properties[2,33,39]) are reproduced with amazing accuracy in the three-quadratic-surface parameterization over the entire range of the fissility parameter x from 0 to 1.

Second, we calculated the kinetic energy as a function of the coordinates and their time derivatives. This was done both exactly (by solving Laplace's equation for the velocity potential) and by use of the Werner-Wheeler method[1,12,19]), which consists of approximating the internal hydro-

dynamical flow by the flow of circular layers of fluid. The Werner-Wheeler method was found to be sufficiently accurate for the distortions of primary interest in fission, and was used for most of the calculations.

Third, the frequencies and eigendisplacements of the normal modes of oscillation of the system about its saddle-point shape were determined. The known properties[20]) of the four lowest modes, which are the ones of primary interest in mass and energy distributions, were reproduced well by the three-quadratic-surface parameterization and the Werner-Wheeler method, whereas the properties of the n = 5 and 6 modes were reproduced less accurately.

Fourth, in the application of statistical mechanics, we made the standard assumption of the transition-state method: that statistical equilibrium is established by the time the system reaches the vicinity of the saddle point. This allows us to calculate the probability for finding the system in a given state of motion as it passes through the vicinity of the saddle point.

Finally, for given initial conditions near the saddle point, we integrated numerically Hamilton's equations of motion, which told us how the system divides from the vicinity of the saddle point onward. This step converts the probability distributions for the states of motion near the saddle point into the probability distributions for the masses and energies of the fragments at infinity.

Comparisons were made between the calculated distributions and experimental distributions resulting from the fission of real nuclei. The comparisons were made for nuclei throughout the periodic table as functions of the excitation energy of the compound nuclei undergoing fission. In making the comparisons we considered first the most probable mass divisions and energies, and second the widths of the distributions in these quantities.

In evaluating the comparisons, it must be borne in mind that the calculated distributions are for the masses and energies of fragments resulting from the fission of idealized nonviscous irrotational liquid drops whose shapes are constrained to three smoothly joined portions of quadratic surfaces of revolution. This parameterization does not permit the formation of more than one neck or division into more than two bodies. The calculated results therefore probably do not represent the true predictions of the liquid-drop model for very heavy nuclei, where division into more than two

bodies becomes energetically more favorable than division into two[64]). For such nuclei it would be very worthwhile to know the true predictions for an unconstrained drop.

The major points brought out by the comparisons, which were made without the use of any adjustable parameters, are the following:

(1) The calculated and experimental most probable mass divisions are not in agreement for the fission of heavy nuclei at low excitation energies, whereas they are in agreement for the fission of heavy nuclei at high excitation energies and medium nuclei at all excitation energies.

(2) The calculated most probable translational kinetic energies of the fragments at infinity reproduce both the correct order of magnitude and the trend with x of the experimental energies, but the calculated energies are systematically about 5% smaller than the experimental ones. The calculated most probable translational kinetic energies at scission agree approximately with the experimental values deduced from analyses of long-range alpha particles emitted during fission, although the analyses leading to the experimental values are subject to considerable uncertainty.

(3) The widths of the experimental mass distributions are larger than the calculated ones by about 25% for medium nuclei and by about 100% for heavy nuclei when a certain method is used for extracting the widths. When an alternative method is used the experimental widths for heavy nuclei at low excitation energies are roughly four times as large as the calculated widths. The experimental widths for heavy nuclei at high excitation energies are roughly three times as large as the calculated widths, although the experimental values are possibly affected by fission following neutron emission. The calculations reproduce correctly the dependence on excitation energy of the experimental widths for three of four medium compound nuclei studied, but predict too small a variation with excitation energy for the fourth compound nucleus.

(4) The trend with x of the widths of the experimental translational kinetic-energy distributions agrees approximately with the calculations, but the experimental widths at low excitation energies are systematically about 25% larger than the calculated widths. For heavy nuclei at high excitation energies the experimental widths are roughly 50% larger than the calculated widths. The experimental widths increase with increasing excitation energy less slowly than the calculations for three of four medium compound nuclei,

and more rapidly for the other.

In all cases the experimental most probable kinetic energies and the widths of both mass and kinetic-energy distributions are larger than the calculated results. What can be learned from this general observation? For heavy nuclei the long descent from saddle to scission makes it difficult to reach any conclusion. However, for medium nuclei the results for the kinetic-energy distributions suggest that in the fission process the flow of nuclear matter is either rotational or viscous. This conclusion is reached from the following considerations:

For medium nuclei a drop with rotational or viscous flow has approximately the same scission shape as a drop with nonviscous irrotational flow (because of the short distance separating the saddle point and scission point). For the same scission shape the translational kinetic energy at infinity is larger for rotational or viscous flow than for nonviscous irrotational flow. This is because rotational or viscous fragments remain deformed longer during their initial acceleration and hence acquire as translational kinetic energy a larger fraction of their scission interaction energy than nonviscous irrotational fragments, which oscillate fairly rapidly as they separate. The results of refs. [1,62]) indicate that for $x \approx 0.7$ infinitely rotational or viscous fragments acquire approximately 8% more kinetic energy from scission to infinity than nonviscous irrotational fragments [see in particular fig. 18 of ref. [1]) or fig. 3 of ref. [62])]. Since the experimental translational kinetic energies are about 5% larger than the calculated energies for nonviscous irrotational flow, the results suggest that the flow is characterized by some curl or some viscosity (or both).

Let us examine a similar argument for the widths of the translational kinetic-energy distributions. The results of ref. [1]) indicate that for $x \geq 0.65$ the widths of the translational kinetic-energy distributions are slightly larger for infinitely rotational or viscous fragments than for nonviscous irrotational fragments [see in particular eq. (19) and figs. 18 and 19 or eqs. (19) and (21) and fig. 21 of ref. [1])]. The difference is zero at $x = 0.65$ and increases to about 5% at $x = 0.8$. For this entire range of x the experimental widths are roughly 25% larger than the calculated widths for nonviscous irrotational flow. Thus neither the over-all magnitude nor the trend with x of the discrepancy is explained by assuming rotational or viscous flow, but the sign of the discrepancy is consistent with this assump-

tion. However, we place little weight upon this particular argument.

We have also seen that analyses of spontaneous-fission half lives and fission-barrier heights and analyses of transition-state spectra suggest that several times as much mass is displaced in both the fission mode and the mass-asymmetry mode as would correspond to irrotational flow. [An experiment that would provide information on vibrational inertias and nuclear viscosity by measuring the amount of flattening experienced by nuclei during head-on collisions is discussed in ref. [106].]

To summarize, the nonviscous irrotational liquid-drop model provides an approximate description of the distributions in fission-fragment masses and energies for the fission of medium nuclei at all excitation energies and heavy nuclei at high excitation energies, but, within the limitation of a parameterization that permits only binary division, it does not reproduce the observed properties of the fission of heavy nuclei at low excitation energies. This conclusion is illustrated schematically in fig. 25. (For definiteness we take about 40 MeV for the excitation energy at which mass distributions for heavy nuclei change from asymmetrical to symmetrical. We assume in designating radium as the transition nucleus that the system's angular momentum is small. For certain purposes an increase in angular momentum has the same effect as an increase in the fissility parameter.) In all cases the experimental translational kinetic energies and widths are larger than the calculated results (for nonviscous irrotational flow), and this, along with other evidence, suggests that in the fission process the flow of nuclear matter is either rotational or viscous.

This concludes our discussion of what has been learned from a simplified version of the nonviscous irrotational liquid-drop model. However, before ending we would like to make some speculative remarks concerning the observed mass asymmetry in the fission of heavy nuclei at low excitation energies.

One possibility that must not be ruled out is that an unconstrained nonviscous irrotational liquid drop could form two necks during the descent from saddle to scission, which could result in an asymmetrical mass division if the drop divided at one neck and the remaining two bodies coalesced to form a single large fragment. However, we feel that this is not the explanation of the observed mass asymmetry because such a mechanism would imply that the larger fragment should possess more deformation energy and

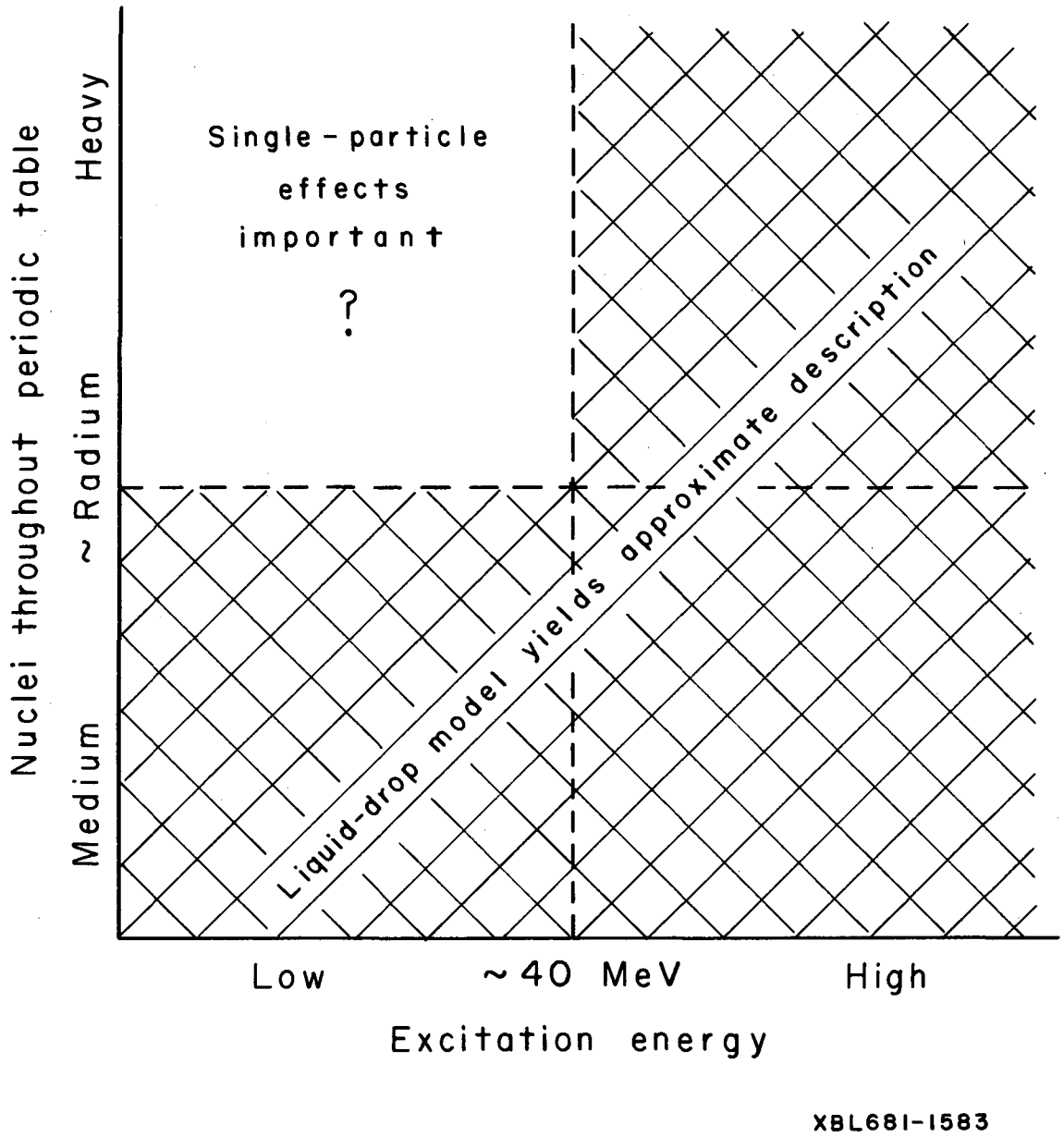

Fig. 25. A schematic illustration of where the liquid-drop model yields an approximate description of nuclear fission. Shown also is the region where single-particle effects are probably important.

hence emit more neutrons than the lighter, whereas the opposite situation is observed experimentally [see for example ref. [79])]. On the other hand, the width of the mass distribution corresponding to the division of an unconstrained drop could be larger than that corresponding to our constrained drop, which could bring the true calculated widths for the division of liquid drops into better agreement with the data of fig. 21.

We have seen some evidence that in the fission process the flow is either rotational or viscous, and a possibility that should be explored by explicit calculations is that in the region of heavy nuclei a rotational or viscous drop would prefer an asymmetrical mass division to a symmetrical one.

Recently Kelson[107]) and Griffin[108,109]) have reintroduced the idea of Hill and Wheeler[5]) that the most probable asymmetrical mass division for heavy nuclei at low excitation energies arises from a quantal suppression of symmetrical mass divisions. They argue that the numbers of gerade and ungerade states (states with even and odd parities, respectively, under reflection at a plane through the origin perpendicular to the symmetry axis) do not change from some characteristic point in the fission process onward. Furthermore, it is argued that for the fragments at infinity the gerade-ungerade ratio is equal to their mass ratio, and that therefore an asymmetrical division will result if the gerade-ungerade ratio is different from unity at the characteristic point in the process. This characteristic point is taken by Kelson to be the ground state of the nucleus undergoing fission, and for the spontaneous fission of ^{252}Cf the mass distribution calculated on this basis is in excellent agreement with the experimental mass distribution. However, at the ground state the gerade-ungerade ratio differs from unity almost as much for medium nuclei as for heavy nuclei, and Kelson's approach is therefore unable to explain (among other things) the existence of symmetrical fission for nuclei lighter than radium.

Griffin takes the characteristic point to be the saddle point and calculates that as a function of the fissility parameter x the gerade-ungerade ratio at the saddle is unity for small values of x and begins to increase fairly rapidly at $x \approx 0.67$, increasing to 1.42 at $x = 1$. With our definition of the fissility parameter the gerade-ungerade ratio is 1.09 for ^{210}Po (where the experimental most probable mass ratio is unity), is 1.13 for deuteron-induced fission of ^{226}Ra (where the experimental mass distribution has three peaks), and is 1.16 for ^{236}U (where the experimental most probable mass ratio

is 1.4). Furthermore, as x increases in the region of heavy nuclei Griffin's gerade-ungerade ratio increases, whereas the experimental most probable mass ratio decreases [see for example ref. [110])]. Thus, Griffin's theory is unable alone to reproduce either the correct magnitude of the mass ratio for heavy nuclei or the correct dependence of the mass ratio upon nuclei (in addition to failing to predict three peaks for radium). Even though the present developments of the idea of a quantal suppression of symmetrical mass divisions are unable to satisfactorily explain observed mass distributions, Griffin points out that it is nevertheless possible that such a suppression would provide a tendency toward an asymmetrical mass division, with the details of the distribution determined by some other mechanism.

A final possibility is the old idea that the mass distribution for the fission of heavy nuclei at low excitation energies is the result of a single-particle perturbation of the liquid-drop-model Hamiltonian. The influence of single particles on the potential energy of a slightly deformed system has been discussed in for example refs. [24,28,111,112]. Such studies show that the nuclear potential energy can be obtained approximately by adding a single-particle correction to the surface and Coulomb energies of the liquid-drop model. This correction depends primarily upon the density of single-particle states near the Fermi surface, and is negative when the density is low and positive when it is high. The correction is therefore an <u>oscillatory</u> function, both of the proton and neutron numbers and of the nuclear deformation. The amplitude of the oscillations in general decreases somewhat (but does not disappear completely) as the nucleus deforms away from the spherical shape. Although single-particle effects have not been adequately studied at the saddle point and beyond, it is reasonable to assume that even at these large deformations they lead to fairly large perturbations of the liquid-drop-model Hamiltonian.

We feel that the inclusion of a single-particle correction to the energy would probably allow for an adequate description of fission-fragment mass and energy distributions. Since the details of such a theory have not been worked out, we will make some qualitative comments on how single-particle effects could be expected to explain the major properties of mass and energy distributions.

The idea on which we base our considerations is a single-particle lowering of the energy near the scission point for selected asymmetrical shapes in

which the larger nascent fragment has nearly constant proton and neutron numbers. Now, in the absence of single-particle effects the energy is a minimum for symmetrical shapes. Since the fragment mass number corresponding to such a symmetrical division increases as the mass number of the fissioning nucleus increases, the number of nucleons separating the symmetrical position of the liquid-drop minimum energy from the asymmetrical position of the single-particle reduction decreases in going from medium nuclei through radium to heavy nuclei. Then, for medium nuclei the energy at the position of the maximum single-particle reduction could still be higher than the energy at symmetry (because of the relatively large distance separating the two positions), and the most probable mass division would be symmetrical. At about radium the distance separating the symmetrical and asymmetrical shapes could be such that the energy is comparable at these two points, and the mass distribution would be peaked at both symmetrical and asymmetrical divisions. For heavy nuclei the distance becomes sufficiently small that the energy could be lower at the asymmetrical shape, which would produce an asymmetrical most probable mass division. With increasing mass number of the fissioning nucleus the distance continues to decrease, which would imply a decreasing most probable mass ratio, as is observed experimentally [see for example ref. [110])].

At what deformations of the nascent fragments should the deepest minimum in the energy occur? Three arguments suggest that it should occur for somewhat deformed nascent fragments: (1) In the fission of heavy nuclei at low excitation energies the average number of neutrons emitted by each of the most probable fragments is greater than 1 [see for example ref. [79])], which implies that the most probable fragments possess some deformation energy at scission. (2) If the fragments were nearly spherical at scission their translational kinetic energies at infinity would be much larger than is observed experimentally [see for example ref. [69])]. (3) The dynamical paths calculated on the basis of the liquid-drop model correspond to fairly large fragment deformations near scission. Therefore, secondary shells at larger deformations[111]) rather than primary shells at spherical configurations are probably responsible for the deepest minimum in the energy.

However, one would also expect a local decrease in the energy corresponding to a nearly spherical nascent fragment that has "magic" numbers of protons and neutrons (50 + 82 = 132). [Favoring the exploitation of this minimum is the relative "softness" of a liquid drop with respect to the distortion-

asymmetry degree of freedom[1]).] This could be responsible for the small number of neutrons emitted by the near-magic fragment and the large number emitted by the complementary fragment [see for example ref. [79])], as well as the increased total translational kinetic energy when one of the fragments is near-magic [see for example refs. [73,74])].

When the nucleus reaches the scission point in a somewhat more deformed configuration than its most probable, the single-particle effects would be expected to be reduced in magnitude. This is supported experimentally by the observation that mass distributions for heavy nuclei at low excitation energies change from asymmetrical to symmetrical as the total translational kinetic energy decreases [see for example refs. [74,91])]. Smaller kinetic energy implies in general a larger separation of fragment centers near scission, which means the fragments are more deformed and hence less influenced by single-particle effects, which would result in a symmetrical mass distribution.

At high excitation energies single-particle effects are expected to decrease as the result of a more random population of single-particle levels over a wider range of energy. The transition for heavy nuclei from asymmetrical to symmetrical mass distributions as the excitation energy increases could thus arise partially from such a decrease of single-particle effects with increasing excitation energy. However, another effect that probably contributes to this transition is the population of higher quantum states in the mass-asymmetry degree of freedom as the excitation energy increases. The summation of the squares of a number of such wave functions, weighted according to their statistical probabilities, would produce a more symmetrical division than that given by the square of the ground-state wave function.

To conclude, we have shown that the nonviscous irrotational liquid-drop model reproduces approximately fission-fragment mass and energy distributions of medium nuclei at all excitation energies and heavy nuclei at high excitation energies, and feel that the observed deviations for heavy nuclei at low excitation energies probably arise from a single-particle alteration of the energy for selected shapes near the scission point.

To us the major outstanding problem in fission theory is to check these speculations by including single-particle effects in a realistic way in the calculation of the properties of the fission process. We hope that in such a study our parameterization in terms of three smoothly joined portions of quadratic surfaces of revolution will prove useful for describing the shape

of the nuclear surface, and that our general procedure of systematically considering the statics, dynamics and statistical mechanics will also be applied to the single-particle Hamiltonian.

The major part of this study was made in Stanley G. Thompson's group at the Lawrence Radiation Laboratory, Berkeley, and I would like to express my appreciation to him for his interest in and advice regarding the research. The paper represents a continuation of a Ph. D. Thesis performed under Wladyslaw J. Swiatecki's supervision, and consequently many of the ideas presented here are his. I wish to thank him for the valuable suggestions he has continued to give. I have also benefited from discussions with many others, especially Luciano G. Moretto, William D. Myers, John O. Rasmussen and Chin Fu Tsang at the Lawrence Radiation Laboratory, and Harold C. Britt, Zeev Fraenkel, James J. Griffin, Franz Plasil, Hal W. Schmitt and James Terrell elsewhere.

I would like to thank Esther Coleman for her assistance in writing the computer programs that were used in this study, Paul Concus and Loren Meissner for their advice regarding numerical procedures, and Joan Phillips for her assistance with hand computations, plotting graphs, and preparing the manuscript.

The entire work was performed under the auspices of the U. S. Atomic Energy Commission, with the final stages completed in Group T-9 of the Los Alamos Scientific Laboratory.

6. Appendices

6.1. GEOMETRICAL PARAMETERS OF QUADRATIC SURFACES OF REVOLUTION

The inversion of eqs. (5) and (6) leads immediately to

$$\ell_1 = \tfrac{1}{2}(-\sigma_1 + 2\alpha_1)u \quad , \tag{20a}$$

$$\ell_2 = \tfrac{1}{2}(\sigma_1 + 2\alpha_1)u \quad , \tag{20b}$$

$$a_1^2 = (1 + \tfrac{1}{2}\alpha_2)u^2 \quad , \tag{20c}$$

$$a_2^2 = (1 - \tfrac{1}{2}\alpha_2)u^2 \quad , \tag{20d}$$

$$a_1^2/c_1^2 = \sigma_3 + \tfrac{1}{2}\alpha_3 \quad , \tag{20e}$$

$$a_2^2/c_2^2 = \sigma_3 - \tfrac{1}{2}\alpha_3 \quad , \tag{20f}$$

$$a_3^2/c_3^2 = \sigma_2 \quad . \tag{20g}$$

These formulas give seven of the nine geometrical parameters of the quadratic surfaces of revolution in terms of the six generalized deformation coordinates and the unit of distance u. The two remaining quantities ℓ_3 and a_3^2, as well as the locations z_1 and z_2 of the points of tangency of the middle surface with the two end surfaces, are determined by solving the four equations that express the continuity at z_1 and z_2 of the values of ρ and $\frac{d\rho}{dz}$. From eq. (4) we find that

$$\rho^2(z_i) = a_i^2 - (a_i^2/c_i^2)(z_i-\ell_i)^2 = a_3^2 - (a_3^2/c_3^2)(z_i-\ell_3)^2 \quad , \quad i = 1, 2, \tag{21a}$$

$$-\rho(z_i)\,\frac{d\rho(z_i)}{dz} = (a_i^2/c_i^2)(z_i-\ell_i) = (a_3^2/c_3^2)(z_i-\ell_3) \quad , \quad i = 1, 2 \, . \tag{21b}$$

It follows immediately from (21b) that

$$z_i = \frac{(a_i^2/c_i^2)\ell_i - (a_3^2/c_3^2)\ell_3}{(a_i^2/c_i^2) - (a_3^2/c_3^2)} \quad , \quad i = 1, 2 \quad , \tag{22}$$

but this result still contains the unknown quantity ℓ_3. (Of course for a symmetrical shape, for which $\alpha_1 = \alpha_2 = \alpha_3 = 0$, the value of ℓ_3 is zero.)

Substitution of this result into the equation obtained by eliminating a_3^2 from (21a), i = 1, 2, leads to the quadratic equation

$$A\beta^2 + 2B\beta + C = 0 \quad ,$$

where

$$\beta = (a_3^2/c_3^2)\ell_3$$

and

$$A = (a_1^2/c_1^2) - (a_2^2/c_2^2) \quad , \tag{23a}$$

$$B = (a_1^2/c_1^2)\,[(a_2^2/c_2^2) - (a_3^2/c_3^2)]\ell_1 - (a_2^2/c_2^2)\,[(a_1^2/c_1^2) - (a_3^2/c_3^2)]\ell_2 \quad , \tag{23b}$$

$$C = (a_3^2/c_3^2)\left\{(a_2^2/c_2^2)\,[(a_1^2/c_1^2) - (a_3^2/c_3^2)]\ell_2^2 - (a_1^2/c_1^2)\,[(a_2^2/c_2^2) - (a_3^2/c_3^2)]\ell_1^2\right\} + [(a_1^2/c_1^2) - (a_3^2/c_3^2)]\,[(a_2^2/c_2^2) - (a_3^2/c_3^2)]\,(a_2^2 - a_1^2) \quad . \tag{23c}$$

The solution of this equation, with the proper choice of sign, is

$$\beta = \begin{cases} \left[-B + \text{sign}(B)\,(B^2 - AC)^{\frac{1}{2}}\right]/A \quad , & A \neq 0 \\ -\frac{1}{2}\,\frac{C}{B}\left[1 + \frac{1}{4}\left(\frac{AC}{B^2}\right) + \frac{1}{8}\left(\frac{AC}{B^2}\right)^2 + \frac{5}{64}\left(\frac{AC}{B^2}\right)^3 + \ldots\right] \quad , & |AC| \ll B^2 \quad . \end{cases} \tag{24}$$

Now that $\beta = (a_3^2/c_3^2)\ell_3$ is known the values of z_1 and z_2 can be found from (22). One can also determine ℓ_3 immediately by dividing β by a_3^2/c_3^2, provided that a_3^2/c_3^2 is not zero. Finally, the value of the remaining unknown a_3^2 can be found from either of eqs. (21a), provided that ℓ_3 is not infinite.

It is observed that for asymmetrical shapes ℓ_3 approaches infinity as a_3^2/c_3^2 approaches zero; we will see in appendix 6.2 that the derivatives of ℓ_3 with respect to the generalized deformation coordinates also approach infinity at the same time. This introduces numerical difficulties at the transition of an asymmetrical shape from a spheroid to a hyperboloid of revolution of one sheet. The difficulties could be eliminated by writing the equation of the middle quadratic surface of revolution as, say,

$$\rho^2 = \alpha + 2\beta z - (a_3^2/c_3^2)z^2 \tag{25}$$

and using

$$\alpha = a_3^2 - (a_3^2/c_3^2)\ell_3^2 \tag{26}$$

and β rather than a_3^2 and ℓ_3 as auxiliary quantities in the calculation of the final quantities of interest. When this is done the solution for β is again given by (24), and the result for α is obtained from either of eqs. (21a). Alternatively, a combination of both of eqs. (21a) yields the symmetrical result

$$\alpha = \frac{z_2\rho_1^2 - z_1\rho_2^2}{z_2 - z_1} - (a_3^2/c_3^2)z_1z_2 \quad , \tag{27}$$

where

$$\rho_i^2 = \rho^2(z_i) \quad , \quad i = 1, 2 \quad .$$

Provided that ℓ_3 is finite the value of a_3^2 can of course also be obtained from this result.

The unit of distance u is determined from the requirement that the volume of the deformed drop equal the volume of the spherical drop. By equating the result of a straightforward volume integration to $4\pi R_0^3/3$ we find that

$$u = R_0\left(\tilde{V}_1 + \tilde{V}_2 + \tilde{V}_3\right)^{-\frac{1}{3}} \quad , \tag{28}$$

where $\tilde{V}_i$ (i = 1, 2, 3) is the volume divided by $4\pi/3$ enclosed within the ith surface for an imaginary drop of the same shape but uniformly scaled so that the unit of distance u is unity. Explicitly,

$$\tilde{V}_i = \tfrac{1}{2}\tilde{a}_i^2\tilde{c}_i + (-1)^i\left[\tfrac{3}{4}\tilde{a}_i^2(\tilde{\ell}_i-\tilde{z}_i) - \tfrac{1}{4}(\tilde{a}_i^2/\tilde{c}_i^2)(\tilde{\ell}_i-\tilde{z}_i)^3\right] \quad , \quad i = 1, 2, \tag{29a}$$

$$\tilde{V}_3 = \tfrac{3}{4}\tilde{a}_3^2(\tilde{z}_2-\tilde{z}_1) - \tfrac{1}{4}(\tilde{a}_3^2/\tilde{c}_3^2)\left[(\tilde{\ell}_3-\tilde{z}_1)^3 + (\tilde{z}_2-\tilde{\ell}_3)^3\right] - \tilde{a}_3^2\tilde{c}_3\,\theta(-\tilde{a}_3^2) \; ; \tag{29b}$$

when a_3^2/c_3^2 is close to zero for an asymmetrical shape it is more convenient to express the result for $\tilde{V}_3$ in the alternate form

$$\tilde{V}_3 = \tfrac{3}{4}\tilde{\alpha}(\tilde{z}_2-\tilde{z}_1) + \tfrac{3}{4}\tilde{\beta}(\tilde{z}_2^2-\tilde{z}_1^2) - \tfrac{1}{4}(\tilde{a}_3^2/\tilde{c}_3^2)(\tilde{z}_2^3-\tilde{z}_1^3) - \tilde{a}_3^2\tilde{c}_3\,\theta(-\tilde{a}_3^2) \; . \tag{29c}$$

The tildas denote that the indicated quantities are evaluated for u = 1; for example, it follows from (20) that

$$\tilde{\ell}_1 = \tfrac{1}{2}(-\sigma_1 + 2\alpha_1) \quad ,$$

$$\tilde{c}_1 = \left[\tilde{a}_1^2/(\tilde{a}_1^2/\tilde{c}_1^2)\right]^{\frac{1}{2}}$$

$$= \left[(1 + \tfrac{1}{2}\alpha_2)/(\sigma_3 + \tfrac{1}{2}\alpha_3)\right]^{\frac{1}{2}} \quad .$$

The theta function $\theta(-\tilde{a}_3^2)$ is zero for $\tilde{a}_3^2 > 0$ and unity for $\tilde{a}_3^2 < 0$. Since u is known, the nine geometrical parameters of the quadratic surfaces of revolution are now completely determined in terms of the six generalized deformation coordinates.

The position ℓ_{cm} of the center of mass of the drop can also be obtained by performing a straightforward integration. The result is found to be

$$\ell_{cm} R_o^3 = \frac{3}{8} a_1^2 \left[z_1^2 - (\ell_1 - c_1)^2 \right] - (a_1^2/c_1^2) \left\{ \frac{3}{16} \left[z_1^4 - (\ell_1 - c_1)^4 \right] \right.$$

$$\left. - \tfrac{1}{2} \ell_1 \left[z_1^3 - (\ell_1 - c_1)^3 \right] + \frac{3}{8} \ell_1^2 \left[z_1^2 - (\ell_1 - c_1)^2 \right] \right\}$$

$$+ \frac{3}{8} a_2^2 \left[(\ell_2 + c_2)^2 - z_2^2 \right] - (a_2^2/c_2^2) \left\{ \frac{3}{16} \left[(\ell_2 + c_2)^4 - z_2^4 \right] \right.$$

$$\left. - \tfrac{1}{2} \ell_2 \left[(\ell_2 + c_2)^3 - z_2^3 \right] + \frac{3}{8} \ell_2^2 \left[(\ell_2 + c_2)^2 - z_2^2 \right] \right\}$$

$$+ \frac{3}{8} a_3^2 \left(z_2^2 - z_1^2 \right) - (a_3^2/c_3^2) \left[\frac{3}{16} \left(z_2^4 - z_1^4 \right) \right.$$

$$\left. - \tfrac{1}{2} \ell_3 \left(z_2^3 - z_1^3 \right) + \frac{3}{8} \ell_3^2 \left(z_2^2 - z_1^2 \right) \right] \quad ;$$

when a_3^2/c_3^2 is close to zero for an asymmetrical shape the last one-third of this expression should be written in the alternate form

$$\frac{3}{8} \alpha (z_2^2 - z_1^2) + \tfrac{1}{2} \beta (z_2^3 - z_1^3) - \frac{3}{16} (a_3^2/c_3^2)(z_2^4 - z_1^4) \quad .$$

The two points of intersection z_1 and z_2 must each lie somewhere between the two ends of the drop, and this requirement imposes the constraint on the variables that

$$\ell_1 - c_1 \leq z_1 \leq z_2 \leq \ell_2 + c_2 \quad ,$$

where z_1 and z_2 are given by (22). This constraint becomes more severe as a_i^2/c_i^2 $(i = 1, 2)$ approaches a_3^2/c_3^2, since the numerator of the right-hand side of (22) must then also approach zero in order for z_i to remain finite. This implies that ℓ_i must approach ℓ_3. For the limiting case in which $a_i^2/c_i^2 = a_3^2/c_3^2$, the two surfaces i and 3 actually coincide, and the point of intersection z_i may be taken as any point along their common overlap.

Because of the restrictions imposed by this equation the present parameterization is not particularly well suited for describing small deviations of the system from a spherical or a spheroidal shape.

6.2. DERIVATIVES OF GEOMETRICAL PARAMETERS OF QUADRATIC SURFACES OF REVOLUTION

For the calculation of both the generalized forces acting on the drop (appendix 6.3) and the inertia matrix (appendix 6.4) it is necessary to calculate the first partial derivatives of ℓ_1, ℓ_2, ℓ_3 (or β), a_1^2, a_2^2, a_3^2 (or α), a_1^2/c_1^2, a_2^2/c_2^2, a_3^2/c_3^2, z_1 and z_2 with respect to σ_1, σ_2, σ_3, α_1, α_2 and α_3. Expressions for the geometrical parameters in terms of the coordinates were given in appendix 6.1, and we give here the relevant formulas for the derivatives, listed in an order appropriate for computation. As in the text, we sometimes refer to the symmetrical and asymmetrical coordinates collectively by q_j, $j = 1, 2, \ldots, 6$.

It follows from (20e) and (20f) that

$$\frac{\partial(a_i^2/c_i^2)}{\partial q_j} = \begin{cases} 1 \ , & q_j = \sigma_3 \\ \frac{1}{2}(-1)^{i+1} \ , & q_j = \alpha_3 \\ 0 \ , & \text{otherwise} \end{cases} \quad , \quad i = 1, 2$$

and from (20g) that

$$\frac{\partial(a_3^2/c_3^2)}{\partial q_j} = \begin{cases} 1 \ , & q_j = \sigma_2 \\ 0 \ , & \text{otherwise} \end{cases} .$$

We next compute several auxiliary quantities that enter the expressions for the remaining derivatives. Define by $\tilde{\beta}$ the quantity $\beta/u = (a_3^2/c_3^2)\tilde{\ell}_3$, where $\tilde{\ell}_3 = \ell_3/u$ is the value that ℓ_3 would have for a drop uniformly scaled so that the unit of distance u is unity. Then from (24) we have

$$\frac{\partial\tilde{\beta}}{\partial\tilde{A}} = \begin{cases} -\left\{\tilde{\beta} + \left[\frac{1}{2}\,\mathrm{sign}(\tilde{B})\tilde{C}\right]/(\tilde{B}^2 - \tilde{A}\,\tilde{C})^{\frac{1}{2}}\right\}/\tilde{A} & , \quad \tilde{A} \neq 0 \\ -\frac{1}{8}\frac{\tilde{C}^2}{\tilde{B}^3}\left[1 + \left(\frac{\tilde{A}\,\tilde{C}}{\tilde{B}^2}\right) + \frac{15}{16}\left(\frac{\tilde{A}\,\tilde{C}}{\tilde{B}^2}\right)^2 + \frac{7}{8}\left(\frac{\tilde{A}\,\tilde{C}}{\tilde{B}^2}\right)^3 + \ldots\right] & , \quad |\tilde{A}\,\tilde{C}| \ll \tilde{B}^2 \end{cases} ,$$

$$\frac{\partial\tilde{\beta}}{\partial\tilde{B}} = -\,\mathrm{sign}(\tilde{B})\tilde{\beta}/(\tilde{B}^2 - \tilde{A}\,\tilde{C})^{\frac{1}{2}} ,$$

$$\frac{\partial\tilde{\beta}}{\partial\tilde{C}} = -\,\frac{1}{2}\,\mathrm{sign}(\tilde{B})/(\tilde{B}^2 - \tilde{A}\,\tilde{C})^{\frac{1}{2}} ,$$

where

$$\tilde{A} = A ,$$

$$\tilde{B} = B/u ,$$

$$\tilde{C} = C/u^2$$

are the values of A, B and C [given by (23)] corresponding to a drop uniformly scaled so that u = 1. By use of the chain rule for computing first partial derivatives we find from (23) and (20) that

$$\frac{\partial\tilde{\beta}}{\partial\sigma_1} = -\,\frac{1}{2}\left[\left(\frac{a_1^2}{c_1^2} - \frac{a_3^2}{c_3^2}\right)\frac{a_2^2}{c_2^2} + \left(\frac{a_2^2}{c_2^2} - \frac{a_3^2}{c_3^2}\right)\frac{a_1^2}{c_1^2}\right]\frac{\partial\tilde{\beta}}{\partial\tilde{B}}$$

$$+\left[\left(\frac{a_1^2}{c_1^2} - \frac{a_3^2}{c_3^2}\right)\frac{a_2^2}{c_2^2}\,\ell_2 + \left(\frac{a_2^2}{c_2^2} - \frac{a_3^2}{c_3^2}\right)\frac{a_1^2}{c_1^2}\,\ell_1\right]\frac{a_3^2}{c_3^2}\frac{\partial\tilde{\beta}}{\partial\tilde{C}}\Big/u ,$$

$$\frac{\partial\tilde{\beta}}{\partial\sigma_2} = -\left(\frac{a_1^2}{c_1^2}\ell_1 - \frac{a_2^2}{c_2^2}\ell_2\right)\frac{\partial\tilde{\beta}}{\partial\tilde{B}}\Big/ u$$

$$+\left[\left(\frac{a_1^2}{c_1^2} - 2\frac{a_3^2}{c_3^2}\right)\frac{a_2^2}{c_2^2}\ell_2^2 - \left(\frac{a_2^2}{c_2^2} - 2\frac{a_3^2}{c_3^2}\right)\frac{a_1^2}{c_1^2}\ell_1^2\right.$$

$$\left.-\left(\frac{a_1^2}{c_1^2} + \frac{a_2^2}{c_2^2} - 2\frac{a_3^2}{c_3^2}\right)\left(a_2^2 - a_1^2\right)\right]\frac{\partial\tilde{\beta}}{\partial\tilde{C}}\Big/ u^2 \quad ,$$

$$\frac{\partial\tilde{\beta}}{\partial\sigma_3} = -\left(\frac{a_1^2}{c_1^2} + \frac{a_2^2}{c_2^2} - \frac{a_3^2}{c_3^2}\right)\left(\ell_2 - \ell_1\right)\frac{\partial\tilde{\beta}}{\partial\tilde{B}}\Big/ u$$

$$+\left[\left(\frac{a_1^2}{c_1^2} + \frac{a_2^2}{c_2^2} - \frac{a_3^2}{c_3^2}\right)\frac{a_3^2}{c_3^2}\left(\ell_2^2 - \ell_1^2\right)\right.$$

$$\left.+\left(\frac{a_1^2}{c_1^2} + \frac{a_2^2}{c_2^2} - 2\frac{a_3^2}{c_3^2}\right)\left(a_2^2 - a_1^2\right)\right]\frac{\partial\tilde{\beta}}{\partial\tilde{C}}\Big/ u^2 \quad ,$$

$$\frac{\partial\tilde{\beta}}{\partial\alpha_1} = -\left[\left(\frac{a_1^2}{c_1^2} - \frac{a_3^2}{c_3^2}\right)\frac{a_2^2}{c_2^2} - \left(\frac{a_2^2}{c_2^2} - \frac{a_3^2}{c_3^2}\right)\frac{a_1^2}{c_1^2}\right]\frac{\partial\tilde{\beta}}{\partial\tilde{B}}$$

$$+2\left[\left(\frac{a_1^2}{c_1^2} - \frac{a_3^2}{c_3^2}\right)\frac{a_2^2}{c_2^2}\ell_2 - \left(\frac{a_2^2}{c_2^2} - \frac{a_3^2}{c_3^2}\right)\frac{a_1^2}{c_1^2}\ell_1\right]\frac{a_3^2}{c_3^2}\frac{\partial\tilde{\beta}}{\partial\tilde{C}}\Big/ u \quad ,$$

$$\frac{\partial\tilde{\beta}}{\partial\alpha_2} = -\left(\frac{a_1^2}{c_1^2} - \frac{a_3^2}{c_3^2}\right)\left(\frac{a_2^2}{c_2^2} - \frac{a_3^2}{c_3^2}\right)\frac{\partial\tilde{\beta}}{\partial\tilde{C}} \quad ,$$

$$\frac{\partial\tilde{\beta}}{\partial\alpha_3} = \frac{\partial\tilde{\beta}}{\partial\tilde{A}} + \tfrac{1}{2}\left[\left(\left(\frac{a_1^2}{c_1^2} - \frac{a_2^2}{c_2^2} - \frac{a_3^2}{c_3^2}\right)\ell_2\right.\right.$$

$$\left.\left. + \left(\frac{a_2^2}{c_2^2} - \frac{a_1^2}{c_1^2} - \frac{a_3^2}{c_3^2}\right)\ell_1\right]\frac{\partial\tilde{\beta}}{\partial\tilde{B}}\Big/ u\right.$$

$$\left. - \tfrac{1}{2}\left\{\left[\left(\left(\frac{a_1^2}{c_1^2} - \frac{a_2^2}{c_2^2} - \frac{a_3^2}{c_3^2}\right)\ell_2^2\right.\right.\right.$$

$$\left.\left.\left. + \left(\frac{a_2^2}{c_2^2} - \frac{a_1^2}{c_1^2} - \frac{a_3^2}{c_3^2}\right)\ell_1^2\right]\frac{a_3^2}{c_3^2}\right.\right.$$

$$\left.\left. + \left(\frac{a_1^2}{c_1^2} - \frac{a_2^2}{c_2^2}\right)\left(a_2^2 - a_1^2\right)\right\}\frac{\partial\tilde{\beta}}{\partial\tilde{C}}\Big/ u^2\right. \quad .$$

Provided that a_3^2/c_3^2 is not zero for an asymmetrical shape the derivatives of the (scaled) center of the middle spheroid $\tilde{\ell}_3 = \ell_3/u$ can now be obtained in terms of these quantities from

$$\frac{a_3^2}{c_3^2}\frac{\partial\tilde{\ell}_3}{\partial q_j} = \frac{\partial\tilde{\beta}}{\partial q_j} + \begin{cases} -\tilde{\ell}_3 & , \quad q_j = \sigma_2 \\ 0 & , \quad \text{otherwise} \end{cases} \quad .$$

From (22) and (20) it follows that the derivatives of the (scaled) points of tangency $\tilde{z}_i = z_i/u$ are given by (for i = 1, 2)

$$\left(\frac{a_i^2}{c_i^2} - \frac{a_3^2}{c_3^2}\right)\frac{\partial \tilde{z}_i}{\partial q_j} = -\frac{\partial \tilde{\beta}}{\partial q_j} + \begin{cases} \frac{1}{2}(-1)^i\, a_i^2/c_i^2 \ , & q_j = \sigma_1 \\ \tilde{z}_i \ , & q_j = \sigma_2 \\ \tilde{\ell}_i - \tilde{z}_i \ , & q_j = \sigma_3 \\ a_i^2/c_i^2 \ , & q_j = \alpha_1 \\ 0 \ , & q_j = \alpha_2 \\ \frac{1}{2}(-1)^{i+1}\,(\tilde{\ell}_i - \tilde{z}_i) \ , & q_j = \alpha_3 \ . \end{cases}$$

As we discussed near the end of appendix 6.1 the present parameterization is deficient for shapes in which a_3^2/c_3^2 is close to a_i^2/c_i^2 (i = 1, 2). It is seen from this equation that for such shapes $\partial \tilde{z}_i/\partial q_j$ is able to approach infinity.

We use the notation $\tilde{\rho}_i^2 = \rho^2(z_i)/u^2$ and from (21a) and (20) find that (for i = 1, 2)

$$\frac{\partial\tilde{\rho}_i^{\,2}}{\partial q_j} = 2\,\frac{a_i^{\,2}}{c_i^{\,2}}\,(\tilde{\ell}_i - \tilde{z}_i)\,\frac{\partial\tilde{z}_i}{\partial q_j} + \begin{cases} (-1)^{i+1}\,(a_i^{\,2}/c_i^{\,2})(\tilde{\ell}_i - \tilde{z}_i) \quad , & q_j = \sigma_1 \\ 0 \quad , & q_j = \sigma_2 \\ -(\tilde{\ell}_i - \tilde{z}_i)^2 \quad , & q_j = \sigma_3 \\ -2(a_i^{\,2}/c_i^{\,2})(\tilde{\ell}_i - \tilde{z}_i) \quad , & q_j = \alpha_1 \\ \tfrac{1}{2}(-1)^{i+1} \quad , & q_j = \alpha_2 \\ \tfrac{1}{2}(-1)^{i}\,(\tilde{\ell}_i - \tilde{z}_i)^2 \quad , & q_j = \alpha_3 \end{cases}.$$

We denote by $\tilde{\alpha}$ the quantity α/u^2, where α is defined by (26). Then from (27) and (20) we find that

$$\begin{aligned} \frac{\partial\tilde{\alpha}}{\partial q_j} = {} & \left(\tilde{z}_2\,\frac{\partial\tilde{\rho}_1^{\,2}}{\partial q_j} - \tilde{z}_1\,\frac{\partial\tilde{\rho}_2^{\,2}}{\partial q_j}\right)\Big/(\tilde{z}_2 - \tilde{z}_1) \\ & + (\tilde{\rho}_2^{\,2} - \tilde{\rho}_1^{\,2})\left(\tilde{z}_1\,\frac{\partial\tilde{z}_2}{\partial q_j} - \tilde{z}_2\,\frac{\partial\tilde{z}_1}{\partial q_j}\right)\Big/(\tilde{z}_2 - \tilde{z}_1)^2 \\ & - \left(\tilde{z}_1\,\frac{\partial\tilde{z}_2}{\partial q_j} + \tilde{z}_2\,\frac{\partial\tilde{z}_1}{\partial q_j}\right)\frac{a_3^{\,2}}{c_3^{\,2}} \\ & + \begin{cases} -\tilde{z}_1\tilde{z}_2 \quad , & q_j = \sigma_2 \\ 0 \quad , & \text{otherwise} \end{cases}. \end{aligned}$$

We further denote by $\tilde{a}_3^{\,2}$ the quantity $a_3^{\,2}/u^2$; provided that $\tilde{\ell}_3$ is finite it then follows from (26) and (20) that

$$\frac{\partial \tilde{a}_3^{\,2}}{\partial q_j} = \frac{\partial \tilde{\alpha}}{\partial q_j} + 2\tilde{\ell}_3 \frac{\partial \tilde{\beta}}{\partial q_j} + \begin{cases} -\tilde{\ell}_3^{\,2} , & q_j = \sigma_2 \\ 0 , & \text{otherwise} \end{cases} .$$

The final auxiliary derivatives that we compute are associated with the unit of distance u. From (28), (29) and (20) we find that

$$\frac{1}{u}\frac{\partial u}{\partial q_j} = R_0^{-3} \sum_{i=1}^{2} \tfrac{1}{4}(-1)^{i+1} z_i u \left(z_i \frac{\partial \tilde{\beta}}{\partial q_j} + u \frac{\partial \tilde{\alpha}}{\partial q_j} \right)$$

$$+ \tfrac{1}{4} c_3 u^2 \frac{\partial \tilde{a}_3^{\,2}}{\partial q_j} \theta(-\tilde{a}_3^{\,2})$$

$$+ \begin{cases} -\frac{1}{8}\rho_i^{\,2} u , & q_j = \sigma_1 \\ \frac{1}{12}(-1)^i z_i^{\,3} - \frac{1}{12} c_3^{\,3} \theta(-\tilde{a}_3^{\,2}) , & q_j = \sigma_2 \\ \frac{1}{12}[c_i^{\,3} + (-1)^i (\ell_i - z_i)^3] , & q_j = \sigma_3 \\ -\frac{1}{4}(-1)^i \rho_i^{\,2} u , & q_j = \alpha_1 \\ \frac{1}{8}(-1)^i [c_i + (-1)^i (\ell_i - z_i)] u^2 , & q_j = \alpha_2 \\ -\frac{1}{24}(-1)^i [c_i^{\,3} + (-1)^i (\ell_i - z_i)^3] , & q_j = \alpha_3 , \end{cases}$$

where the summation is taken over all the terms in the complete expression. As before, the theta function $\theta(-\tilde{a}_3^{\,2})$ is zero for $\tilde{a}_3^{\,2} > 0$ and unity for $\tilde{a}_3^{\,2} < 0$.

We are at last in a position to give the formulas for the remaining first partial derivatives of actual interest in terms of these auxiliary quantities. From (20) we have (for i = 1, 2)

$$\frac{\partial \ell_i'}{\partial q_j} = \ell_i \frac{1}{u} \frac{\partial u}{\partial q_j} + \begin{cases} \frac{1}{2}(-1)^i u \ , & q_j = \sigma_1 \\ u \ , & q_j = \alpha_1 \\ 0 \ , & \text{otherwise} \end{cases} ,$$

$$\frac{\partial \beta}{\partial q_j} = \beta \frac{1}{u} \frac{\partial u}{\partial q_j} + u \frac{\partial \tilde{\beta}}{\partial q_j} \ ,$$

$$\frac{\partial \ell_3}{\partial q_j} = \ell_3 \frac{1}{u} \frac{\partial u}{\partial q_j} + u \frac{\partial \tilde{\ell}_3}{\partial q_j} \ , \quad \ell_3 \text{ finite} \ ,$$

$$\frac{\partial a_i^2}{\partial q_j} = 2a_i^2 \frac{1}{u} \frac{\partial u}{\partial q_j} + \begin{cases} \frac{1}{2}(-1)^{i+1} u^2 \ , & q_j = \alpha_2 \\ 0 \ , & \text{otherwise} \end{cases} ,$$

$$\frac{\partial \alpha}{\partial q_j} = 2\alpha \frac{1}{u} \frac{\partial u}{\partial q_j} + u^2 \frac{\partial \tilde{\alpha}}{\partial q_j} \ ,$$

$$\frac{\partial a_3^2}{\partial q_j} = 2a_3^2 \frac{1}{u} \frac{\partial u}{\partial q_j} + u^2 \frac{\partial \tilde{a}_3^2}{\partial q_j} \ , \quad a_3^2 \text{ finite} \ ,$$

$$\frac{\partial z_i}{\partial q_j} = z_i \frac{1}{u} \frac{\partial u}{\partial q_j} + u \frac{\partial \tilde{z}_i}{\partial q_j} \ .$$

6.3. POTENTIAL ENERGY AND GENERALIZED FORCES

We consider in this appendix the computation of the relative surface energy $B_s = E_s/E_s^{(0)}$ and relative Coulomb energy $B_c = E_c/E_c^{(0)}$ that appear in eq. (7). Also, we give formulas for the generalized surface and Coulomb forces acting on the drop, obtained by taking the negative of the first partial derivatives of B_s and B_c with respect to the six generalized deformation coordinates that specify the shape of the drop.

6.3.1. Surface energy and forces.

Because the shape of the drop is specified in terms of portions of quadratic surfaces of revolution, the relative surface energy B_s (equal to the surface area divided by $4\pi R_0^2$) can be expressed in terms of elementary transcendental functions. We write B_s in the form of the sum

$$B_s = \sum_{i=1}^{2} \{G(a_i^2/R_0^2, a_i^2/c_i^2) + F[a_i^2/R_0^2, a_i^2/c_i^2, (-1)^i(\ell_i - z_i)/R_0]$$

$$+ F[a_3^2/R_0^2, a_3^2/c_3^2, (-1)^i(z_i - \ell_3)/R_0]\} \quad . \tag{30}$$

The physical meaning of the individual terms can be best understood by referring back to fig. 1. Consider first the case when the summation index i is 1. Then the first term within the curly braces gives the relative surface area from the end of the left-hand spheroid to its center ℓ_1, the second term gives the relative surface area from the center of the left-hand spheroid to the tangency point z_1, and the third term gives the relative surface area from the tangency point z_1 to the center ℓ_3 of the middle quadratic surface of revolution. When the summation index i is 2 the three terms have analogous meanings for the right-hand portions of the drop. (For a symmetrical shape one could of course eliminate the summation and simply multiply the three terms for the left-hand side by 2.) As should be clear from the physical meanings of the two functions F and G, the latter can be expressed in terms of the former according to the relationship

$$G(a_i^2/R_0^2, a_i^2/c_i^2) = F(a_i^2/R_0^2, a_i^2/c_i^2, c_i/R_0) \quad , \quad i = 1, 2 \quad .$$

The functions F and G are obtained by straightforward surface integrations over portions of quadratic surfaces of revolution. For actual computation it is best to write the resulting expressions in different forms depending upon the signs and magnitudes of the arguments of F and G. There are a total of seven regions that need to be considered for F, corresponding physically to the cases where the quadratic surface of revolution is an oblate spheroid (region 1), is close to a sphere (region 2), is a prolate spheroid (region 3), is close to a cylinder (region 4), is a hyperboloid of revolution of one sheet (region 5), is two tangent collinear cones (region 6), or is a hyperboloid of revolution of two sheets (region 7). These seven regions are illustrated in fig. 26, which should be consulted simultaneously with fig. 2. It turns out that the formulas for F are identical in regions 1 and 5 and also in regions 2 and 4. It is necessary to calculate G only in regions 1, 2 and 3, and neither F nor G is needed on the boundaries of the unphysical region (defined by $x = 0$, $y \geq 0$ and $x \leq 0$, $y = 0$). For reasons discussed in appendices 6.1 and 6.2 the expressions we use for calculating the surface energy and forces are not applicable when a_3^2/c_3^2 is close to zero (region 4) for an asymmetrical shape.

In writing the expressions for F and G we use the dimensionless dummy arguments x, y and z, which refer to, respectively, a_i^2/R_0^2, a_i^2/c_i^2 ($i = 1, 2, 3$) and the distances divided by R_0 from the centers to the tangency points (or ends) of the quadratic surfaces of revolution. (There should arise no confusion between our use of the symbol x here and its previous use to denote the fissility parameter.) We use the symbol ϵ to denote the quantity $1 - y$. When the quadratic surface of revolution is a prolate spheroid or a hyperboloid of revolution of two sheets, $\epsilon^{\frac{1}{2}}$ is the eccentricity as it is usually defined, but this is not the case when it is an oblate spheroid or a hyperboloid of revolution of one sheet.

The relevant formulas for F are

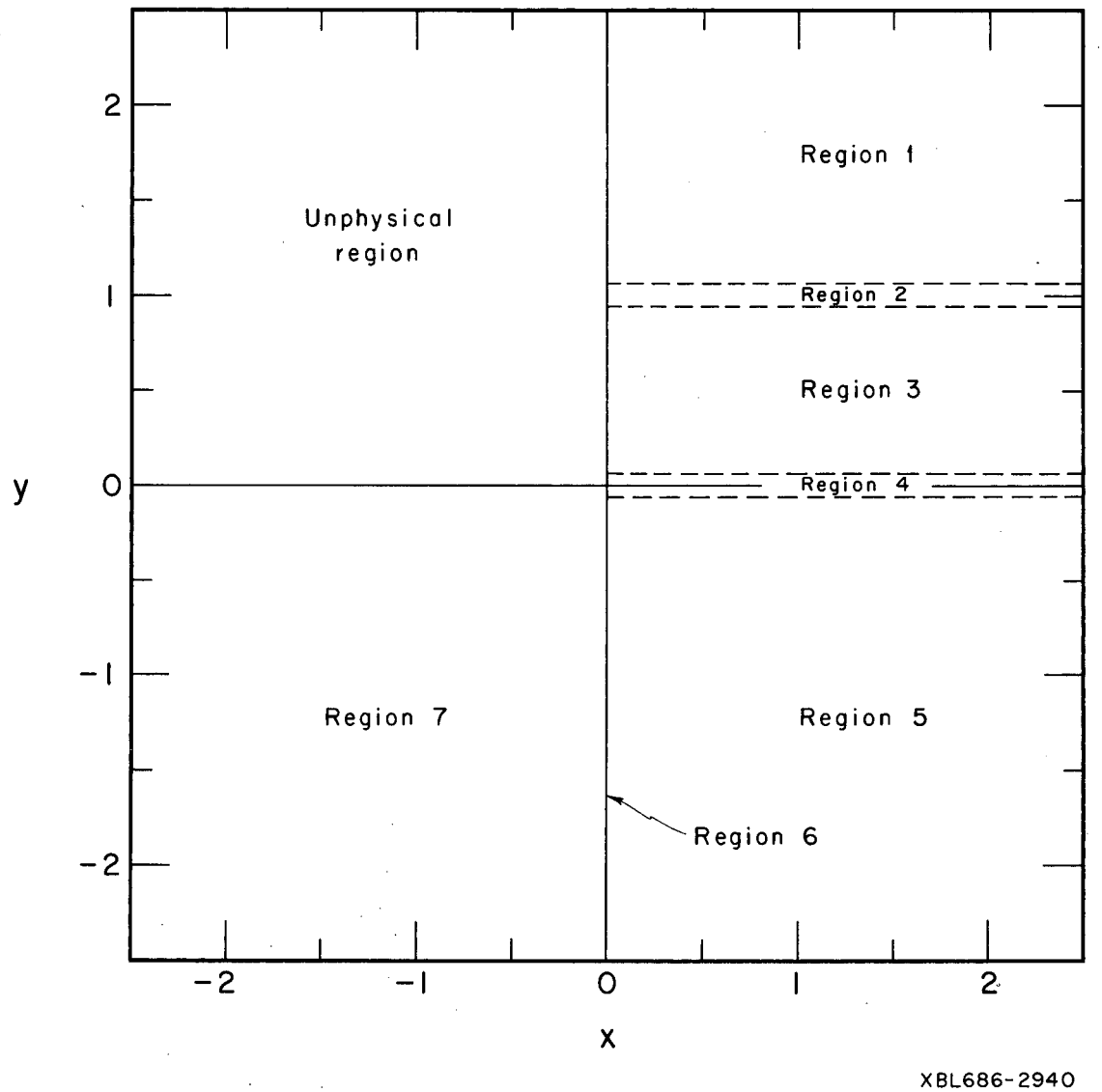

Fig. 26. An illustration of the regions considered in connection with the surface-energy functions $F(x,y,z)$ and $G(x,y)$ and their first partial derivatives. The dimensionless arguments x and y refer to, respectively, a_i^2/R_0^2 and a_i^2/c_i^2 $(i = 1, 2, 3)$.

$$F(x, y, z) = \begin{cases} \frac{1}{4}\left(z(x - \epsilon yz^2)^{\frac{1}{2}} + x(-\epsilon y)^{-\frac{1}{2}} \ln\left\{z(-\epsilon y/x)^{\frac{1}{2}} + [1 - (\epsilon yz^2/x)]^{\frac{1}{2}}\right\}\right) , & \text{regions 1, 5} \\ \frac{1}{2} z(x)^{\frac{1}{2}} \left[1 - \frac{1}{6}(\epsilon yz^2/x) - \frac{1}{40}(\epsilon yz^2/x)^2 - \frac{1}{112}(\epsilon yz^2/x)^3 + \ldots\right] , & \text{regions 2, 4} \\ \frac{1}{4}\left\{z(x - \epsilon yz^2)^{\frac{1}{2}} + x(\epsilon y)^{-\frac{1}{2}} \arcsin\left[z(\epsilon y/x)^{\frac{1}{2}}\right]\right\} , & \text{region 3} \\ \frac{1}{4} z^2(-\epsilon y)^{\frac{1}{2}} , & \text{region 6} \\ \frac{1}{4}\left(z(x - \epsilon yz^2)^{\frac{1}{2}} + x + x(-\epsilon y)^{-\frac{1}{2}} \ln\left\{\frac{z(\epsilon y/x)^{\frac{1}{2}} + [-1 + (\epsilon yz^2/x)]^{\frac{1}{2}}}{\epsilon^{\frac{1}{2}} + (-y)^{\frac{1}{2}}}\right\}\right) , & \text{region 7} , \end{cases}$$

and for G are

$$G(x, y) = \begin{cases} \frac{1}{4} x\left\{1 + (-\epsilon y)^{-\frac{1}{2}} \ln\left[(-\epsilon)^{\frac{1}{2}} + y^{\frac{1}{2}}\right]\right\} , & \text{region 1} \\ \frac{1}{4} x\left[1 + y^{-\frac{1}{2}}\left\{1 + \frac{1}{6}\epsilon + \frac{3}{40}\epsilon^2 + \frac{5}{112}\epsilon^3 + \ldots\right\}\right] , & \text{region 2} \\ \frac{1}{4} x\left[1 + (\epsilon y)^{-\frac{1}{2}} \arcsin\left(\epsilon^{\frac{1}{2}}\right)\right] , & \text{region 3} . \end{cases}$$

In calculating the generalized surface forces we use the chain rule for partial differentiation. We denote by F_x the first partial derivative of F with respect to the first argument, at constant values of the remaining arguments, etc. Then from (30) it follows that the generalized surface forces are

$$
\begin{aligned}
-\frac{\partial B_s}{\partial q_j} = -\sum_{i=1}^{2} \Bigg\{ & G_x(a_i^2/R_0^2, a_i^2/c_i^2)\, \frac{\partial a_i^2}{\partial q_j}\Big/ R_0^2 + G_y(a_i^2/R_0^2, a_i^2/c_i^2)\, \frac{\partial (a_i^2/c_i^2)}{\partial q_j} \\
& + F_x[a_i^2/R_0^2, a_i^2/c_i^2, (-1)^i(\ell_i - z_i)/R_0]\, \frac{\partial a_i^2}{\partial q_j}\Big/ R_0^2 \\
& + F_y[a_i^2/R_0^2, a_i^2/c_i^2, (-1)^i(\ell_i - z_i)/R_0]\, \frac{\partial (a_i^2/c_i^2)}{\partial q_j} \\
& + F_z[a_i^2/R_0^2, a_i^2/c_i^2, (-1)^i(\ell_i - z_i)/R_0](-1)^i \left(\frac{\partial \ell_i}{\partial q_j} - \frac{\partial z_i}{\partial q_j} \right) \Big/ R_0 \\
& + F_x[a_3^2/R_0^2, a_3^2/c_3^2, (-1)^i(z_i - \ell_3)/R_0]\, \frac{\partial a_3^2}{\partial q_j}\Big/ R_0^2 \\
& + F_y[a_3^2/R_0^2, a_3^2/c_3^2, (-1)^i(z_i - \ell_3)/R_0]\, \frac{\partial (a_3^2/c_3^2)}{\partial q_j} \\
& + F_z[a_3^2/R_0^2, a_3^2/c_3^2, (-1)^i(z_i - \ell_3)/R_0](-1)^i \left(\frac{\partial z_i}{\partial q_j} - \frac{\partial \ell_3}{\partial q_j} \right) \Big/ R_0 \Bigg\} \quad .
\end{aligned}
$$

The first partial derivatives of the geometrical parameters of the quadratic surfaces of revolution with respect to the deformation coordinates have been given in appendix 6.2. The first partial derivatives of F follow immediately from the above expressions for F and are

$$F_x(x, y, z) = \begin{cases} \frac{1}{4}(-\epsilon y)^{-\frac{1}{2}} \ln\left\{z(-\epsilon y/x)^{\frac{1}{2}} + [1 - (\epsilon yz^2/x)]^{\frac{1}{2}}\right\} , & \text{regions 1, 5} \\ \frac{1}{4} z(x)^{-\frac{1}{2}} \left[1 + \frac{1}{6}(\epsilon yz^2/x) + \frac{3}{40}(\epsilon yz^2/x)^2 + \frac{5}{112}(\epsilon yz^2/x)^3 + \ldots\right] , & \text{regions 2, 4} \\ \frac{1}{4}(\epsilon y)^{-\frac{1}{2}} \arcsin\left[z(\epsilon y/x)^{\frac{1}{2}}\right] , & \text{region 3} \\ \infty , & \text{region 6} \\ \frac{1}{4}\left(1 + (-\epsilon y)^{-\frac{1}{2}} \ln\left\{\frac{z(\epsilon y/x)^{\frac{1}{2}} + [-1 + (\epsilon yz^2/x)]^{\frac{1}{2}}}{\epsilon^{\frac{1}{2}} + (-y)^{\frac{1}{2}}}\right\}\right) , & \text{region 7} , \end{cases}$$

$$F_y(x, y, z) = \begin{cases} \frac{1}{8}(2y - 1)\left(-z(x - \epsilon yz^2)^{\frac{1}{2}} + x(-\epsilon y)^{-\frac{1}{2}} \ln\left\{z(-\epsilon y/x)^{\frac{1}{2}} + [1 - (\epsilon yz^2/x)]^{\frac{1}{2}}\right\}\right)\Big/(\epsilon y) , & \text{regions 1, 5} \\ \frac{1}{4} z^3(2y - 1)\left[\frac{1}{3} + \frac{1}{10}(\epsilon yz^2/x) + \frac{3}{56}(\epsilon yz^2/x)^2 + \frac{5}{144}(\epsilon yz^2/x)^3 + \ldots\right]\Big/x^{\frac{1}{2}} , & \text{regions 2, 4} \\ \frac{1}{8}(2y - 1)\left\{-z(x - \epsilon yz^2)^{\frac{1}{2}} + x(\epsilon y)^{-\frac{1}{2}} \arcsin\left[z(\epsilon y/x)^{\frac{1}{2}}\right]\right\}\Big/(\epsilon y) , & \text{region 3} \\ \frac{1}{8} z^2(2y - 1)/(-\epsilon y)^{\frac{1}{2}} , & \text{region 6} \\ \frac{1}{8}\left[(2y - 1)\left(-z(x - \epsilon yz^2)^{\frac{1}{2}} + x(-\epsilon y)^{-\frac{1}{2}} \ln\left\{\frac{z(\epsilon y/x)^{\frac{1}{2}} + [-1 + (\epsilon yz^2/x)]^{\frac{1}{2}}}{\epsilon^{\frac{1}{2}} + (-y)^{\frac{1}{2}}}\right\}\right) - x\right]\Big/(\epsilon y) , & \text{region 7} , \end{cases}$$

$$F_z(x, y, z) = \tfrac{1}{2}(x - \epsilon y z^2)^{\frac{1}{2}} \quad , \quad \text{regions 1-7} \quad .$$

The corresponding first partial derivatives of G are given by

$$G_x(x, y) = G(x, y)/x \quad , \quad \text{regions 1-3} \quad ,$$

$$G_y(x, y) = \begin{cases} \frac{1}{8}\, x\left\{(2y - 1)(-\epsilon y)^{-\frac{1}{2}} \ln\left[(-\epsilon)^{\frac{1}{2}} + y^{\frac{1}{2}}\right] - 1\right\}\Big/(\epsilon y) \quad , & \text{region 1} \\ -\frac{1}{8}\, x\left[\left(1 + \frac{1}{6}\epsilon + \frac{3}{40}\epsilon^2 + \frac{5}{112}\epsilon^3 + \ldots\right)\Big/ y + \left(\frac{1}{3} + \frac{3}{10}\epsilon + \frac{15}{56}\epsilon^2 + \frac{35}{144}\epsilon^3 + \ldots\right)\right]\Big/ y^{\frac{1}{2}} \, , & \text{region 2} \\ \frac{1}{8}\, x\left[(2y - 1)(\epsilon y)^{-\frac{1}{2}} \arcsin\left(\epsilon^{\frac{1}{2}}\right) - 1\right]\Big/(\epsilon y) \quad , & \text{region 3} \quad . \end{cases}$$

UCRL-17958

6.3.2. Coulomb energy and forces.

The Coulomb energy of a uniformly charged axially symmetrical (but otherwise arbitrarily shaped) drop can be expressed in terms of a double integral, with the integrand containing complete elliptic integrals of the first and second kinds[1,2]. A convenient way of displaying the result is to first write the Coulomb energy as[11]

$$E_c = \frac{1}{5} \rho_e \int V(z)\, R^3(z)\, d\Omega \quad ,$$

where ρ_e is the (constant) charge density, $V(z)$ is the electrostatic potential on the surface of the drop at the point specified by z, $R(z)$ is the distance from the center of the drop to the point on the surface specified by z, and $d\Omega$ is an element of solid angle; the integration extends over all solid angles. In terms of cylindrical coordinates the combination $R^3(z)d\Omega$ is given by (after integrating over the azimuthal angle)

$$R^3(z)\, d\Omega = 2\pi\left[\rho^2 - z\left(\rho \frac{\partial \rho}{\partial z}\right)\right] dz \quad ;$$

the integration on z is from $\ell_1 - c_1$ to $\ell_2 + c_2$. For our parameterization of the shape of the drop's surface, ρ^2 is given by (4) [see also (25)], from which it follows that

$$\rho \frac{\partial \rho}{\partial z} = \begin{cases} -(a_1^2/c_1^2)\,(z - \ell_1) & , \quad \ell_1 - c_1 \le z \le z_1 \\ -(a_2^2/c_2^2)\,(z - \ell_2) & , \quad z_2 \le z \le \ell_2 + c_2 \\ -(a_3^2/c_3^2)\,(z - \ell_3) & , \quad z_1 \le z \le z_2 \quad . \end{cases} \tag{31a}$$

When the equation of the middle quadratic surface of revolution is written in the modified form (25), then

$$\rho \frac{\partial \rho}{\partial z} = \beta - (a_3^2/c_3^2)\, z \quad , \quad z_1 \le z \le z_2 \quad . \tag{31b}$$

The electrostatic potential on the surface of the drop is given by[3-5])†

$$V(z) = 2\rho_e \int_{\ell_1 - c_1}^{\ell_2 + c_2} \frac{\left\{\left[\rho\rho' + \rho'^2 + (z - z')\left(\rho' \frac{d\rho'}{dz'}\right)\right] K(k) - 2\rho\rho' D(k)\right\} dz'}{[(\rho + \rho')^2 + (z - z')^2]^{\frac{1}{2}}} , \tag{32}$$

where we use the notation $\rho' = \rho(z')$ and where

$$k^2 = \frac{4\rho\rho'}{(\rho + \rho')^2 + (z - z')^2} \quad , \tag{33}$$

$$D(k) = \frac{K(k) - E(k)}{k^2} \quad . \tag{34}$$

The functions $K(k)$ and $E(k)$ are the complete elliptic integrals of the first and second kinds, respectively.

The first partial derivatives of the Coulomb energy with respect to the generalized deformation coordinates are

---

†In appendix A.1 of ref. 2) an expression is given in spherical coordinates for the electrostatic potential on the drop's surface. However, the term $\frac{1}{2}[(\rho_i + \rho)^2 + (z_i - z)^2]$ appearing in the numerator should either be multiplied by k^2 or else replaced by $2\rho\rho_i$. Also, the limits of integration are from $-\pi$ to 0 (whereas the limits on the following integral for B_c are from 0 to π). Finally, a left parenthesis should be inserted before z_i in the denominator of the integrand for the electrostatic potential.

$$\frac{\partial E_c}{\partial q_j} = 2\pi\rho_e \int_{\ell_1 - c_1}^{\ell_2 + c_2} V(z)\ \rho\ \frac{\partial \rho}{\partial q_j}\, dz \quad ,$$

which is derived by considering the changes in Coulomb energy arising from infinitesimal displacements of the surface of the drop. The quantities $\rho \frac{\partial \rho}{\partial q_j}$ appearing in the integrand are obtained from (4) and are

$$\rho \frac{\partial \rho}{\partial q_j} = \begin{cases} \frac{1}{2} \frac{\partial a_1^2}{\partial q_j} - \frac{1}{2}(z - \ell_1)^2 \frac{\partial (a_1^2/c_1^2)}{\partial q_j} + (a_1^2/c_1^2)(z - \ell_1) \frac{\partial \ell_1}{\partial q_j} & , \quad \ell_1 - c_1 \le z \le z_1 \\ \frac{1}{2} \frac{\partial a_2^2}{\partial q_j} - \frac{1}{2}(z - \ell_2)^2 \frac{\partial (a_2^2/c_2^2)}{\partial q_j} + (a_2^2/c_2^2)(z - \ell_2) \frac{\partial \ell_2}{\partial q_j} & , \quad z_2 \le z \le \ell_2 + c_2 \\ \frac{1}{2} \frac{\partial a_3^2}{\partial q_j} - \frac{1}{2}(z - \ell_3)^2 \frac{\partial (a_3^2/c_3^2)}{\partial q_j} + (a_3^2/c_3^2)(z - \ell_3) \frac{\partial \ell_3}{\partial q_j} & , \quad z_1 \le z \le z_2 \quad . \end{cases} \tag{35a}$$

When the equation of the middle quadratic surface is written in the modified form (25), then

$$\rho \frac{\partial \rho}{\partial q_j} = \frac{1}{2} \frac{\partial \alpha}{\partial q_j} + z \frac{\partial \beta}{\partial q_j} - \frac{1}{2} z^2 \frac{\partial (a_3^2/c_3^2)}{\partial q_j} \quad , \quad z_1 \le z \le z_2 \quad . \tag{35b}$$

The first partial derivatives of the geometrical parameters of the quadratic surfaces of revolution with respect to the generalized deformation coordinates have been given in appendix 6.2. The relative Coulomb energy B_c and generalized forces $-\partial B_c/\partial q_j$ are obtained simply by dividing E_c and $-\partial E_c/\partial q_j$, respectively, by $E_c^{(0)}$.

The two-fold integrations required in the evaluation of the Coulomb energy and its derivatives were performed numerically by use of Gaussian quadrature formulas[113]). For this purpose the integration over the surface of the drop was divided into four regions, and each region was integrated separately by use of a Gaussian quadrature formula of a given order. The dividing points between the four regions were taken to be the tangency points z_1 and z_2 and the center ℓ_3 of the middle quadratic surface of revolution. (Because of the discontinuities at z_1 and z_2 in the second and higher derivatives of ρ with respect to z, it is crucial that the interval of a given quadrature formula does not extend across these points.) The order of the Gaussian formulas used depended upon the accuracy required for a particular application and varied from 8 to 32 (for each of the four regions). For the calculation of the properties of the symmetrical saddle-point shapes given in table 1 and in figs. 3-8 and 27-33 (to be presented in appendix 6.5), we used 32-point rules for $1.00 \geq x \geq 0.58$ and 16-point rules for $0.56 \geq x \geq 0.06$. For the calculation of the properties of the asymmetrical saddle-point shapes given in figs. 3-6 and for integrating the equations of motion for the dividing drops we used 8-point rules (with the relevant saddle-point properties also recalculated with 8-point rules). The error in the calculation of B_c is typically a few units in the fifth, sixth and seventh decimal places for, respectively, the 8-point, 16-point and 32-point rules.

The complete elliptic integrals K(k) and E(k) were evaluated by use of Chebyshev approximations[114]) that are accurate to within about two units in the thirteenth decimal place, which is almost the complete accuracy of the CDC-6600 computer on which the calculations were performed.

Two cautions are in order concerning the evaluation of the electrostatic potential V(z) according to eq. (32). First, when $z = z'$ the quantity k is seen from (33) to equal unity, and consequently K(k) is infinite. For this case the limiting value of ρ (not including the constant exterior factor of $2\rho_e$) should be used for the integrand of (32). Second, at each end of the

drop the value of k is seen from (33) to be zero; the limiting value of $\pi/4$ for D(0) should then be used instead of (34). [Alternatively, the problem can be eliminated by substituting (33) for the denominator of (34) and then canceling the $\rho\rho'$ factor with the corresponding coefficient of D(k) in (32).] However, since a Gaussian quadrature formula does not employ the end points the second caution can be disregarded when using such an integration formula.

6.4. INERTIA MATRIX

We discuss in this appendix the two methods that we have used for computing the inertia matrix that appears in eq. (8) for the kinetic energy. We consider first the exact method and second the approximate method of Werner and Wheeler. This is followed by numerical comparisons of several inertia matrices computed by the two methods.

6.4.1. Exact method.

The exact calculation of the inertia matrix involves solving Laplace's equation for the velocity potential and then performing appropriate surface integrations. Although the exact method is discussed in refs. [20-22]) we repeat it here because the formulas of ref. [20]) are specialized to spherical rather than cylindrical coordinates, ref. [21]) uses a different basis for expanding the velocity potential than we use, and the formulas of ref. [22]) are specialized to an expansion of the velocity potential in a series of only two symmetrical solid harmonics. [Somewhat related discussions of the irrotational motion of axially symmetrical fluids are given in refs. [115,116]).]

The total kinetic energy of the fluid flow arising from changes in the drop's boundary is

$$\mathcal{T} = \tfrac{1}{2}\rho_m \int \underset{\sim}{v}^2 \, d\tau = \tfrac{1}{2}\rho_m \int (\nabla\varphi)^2 \, d\tau \quad , \tag{36}$$

where

$$\rho_m = 3M_0/(4\pi R_0^3)$$

is the drop's (constant) mass density, $d\tau$ is an element of volume, and

$$\underset{\sim}{v} = \underset{\sim}{v}(\underset{\sim}{r},t) = \underset{\sim}{\nabla}\varphi = \underset{\sim}{\nabla}\varphi(\underset{\sim}{r},t)$$

is the velocity of fluid flow inside the drop at position $\underset{\sim}{r}$ and time t; the integration extends over the volume of the drop. That $\underset{\sim}{v}$ can be written as the gradient of the velocity potential φ follows from our assumption that the hydrodynamical flow is irrotational ($\underset{\sim}{\nabla} \times \underset{\sim}{v} = 0$). From the further assumption that the fluid is incompressible it follows from the equation of continuity that φ satisfies Laplace's equation, i.e.

$$\underset{\sim}{\nabla}\cdot\underset{\sim}{v} = \nabla^2\varphi = 0 \quad .$$

By use of this result, the vector identity

$$\underset{\sim}{\nabla}\cdot(\varphi\underset{\sim}{\nabla}\varphi) = (\underset{\sim}{\nabla}\varphi)^2 + \varphi\nabla^2\varphi \quad ,$$

and Gauss' divergence theorem, eq. (36) is transformed into the usual hydrodynamical expression

$$\mathcal{T} = \tfrac{1}{2}\rho_m \int \varphi\underset{\sim}{\nabla}\varphi\cdot d\underset{\sim}{S} \quad ,$$

where $d\underset{\sim}{S}$ is an element of surface area (directed outward); the integration extends over the surface of the drop.

We introduce the function $F(\underset{\sim}{r},t)$ so that the equation

$$F(\underset{\sim}{r},t) = \rho - P(z,t) = 0 \qquad (37)$$

defines the surface of the drop. (In this appendix ρ is used as a general cylindrical coordinate for designating an arbitrary point. Elsewhere in the text ρ denotes the distance from the symmetry axis to a point on the drop's surface and is equivalent to the symbol P of this appendix. Because we are specialized to axial symmetry, we do not indicate explicitly the dependence of $\underset{\sim}{r}$ upon the azimuthal angle.) In terms of this function the element of

surface area (after integration over the azimuthal angle) is

$$d\underset{\sim}{S} = 2\pi P \, dz \, \underset{\sim}{\nabla F} \quad ,$$

and the kinematical boundary condition on the drop's surface is[117])

$$\frac{DF}{Dt} = \underset{\sim}{\nabla F} \cdot \dot{\underset{\sim}{r}} + \frac{\partial F}{\partial t} = \underset{\sim}{\nabla F} \cdot \underset{\sim}{\nabla \varphi} + \frac{\partial F}{\partial t} = 0 \quad . \tag{38}$$

By use of these results we obtain for the kinetic energy

$$\mathcal{T} = \tfrac{1}{2}\left(\frac{3}{2}\right) \frac{M_0}{R_0^3} \int_{\ell_1 - c_1}^{\ell_2 + c_2} \varphi P \frac{\partial P}{\partial t} \, dz \quad . \tag{39}$$

We next write

$$P \frac{\partial P}{\partial t} = \sum_{i=1}^{6} P \frac{\partial P}{\partial q_i} \dot{q}_i \quad , \tag{40}$$

where $P \dfrac{\partial P}{\partial q_i}$ is given by (35).

Because the velocity potential φ is a harmonic function that must remain finite at the origin it can be expanded in a series of solid harmonics

$$B_k(\rho, z) = r^k P_k(\cos \theta) \quad , \tag{41}$$

where

$$r = (\rho^2 + z^2)^{\frac{1}{2}} \quad ,$$

$$\cos \theta = z/(\rho^2 + z^2)^{\frac{1}{2}} \quad ,$$

and P_k is the kth Legendre polynomial (not to be confused with the symbol P without a subscript). Furthermore, because the velocity $\underset{\sim}{v}$ is obtained from φ

by spatial differentiation the coefficients of the expansion must be linear functions of the generalized velocities $\dot{q}_j$, $j = 1, 2, \ldots, 6$. The form of the expansion is therefore

$$\varphi = \sum_{k=1}^{K} \sum_{j=1}^{6} b_k^j[q(t)]\, B_k(\rho,z)\, \dot{q}_j \quad , \tag{42}$$

where the unknown coefficients b_k^j are to be determined from the kinematical boundary condition (38). In general an infinite number of terms is required in this expansion to represent the velocity potential exactly, but for shapes that are not too deformed the desired numerical accuracy can be achieved by truncating the series at a moderate value of K (we use K = 32; see subsect. 6.4.3). By substituting this result and eq. (40) into (39), and interchanging the order of summations, we write the expression for the kinetic energy in the form (8), where the elements of the inertia matrix are

$$M_{ij} = \frac{3}{2}\frac{M_0}{R_0^3} \sum_{k=1}^{K} b_k^j \int_{\ell_1-c_1}^{\ell_2+c_2} P\,\frac{\partial P}{\partial q_i}\, B_k(P,z)\, dz \quad , \tag{43}$$

with $P\,\dfrac{\partial P}{\partial q_i}$ given by (35) and $B_k(P,z)$ by (41).

This is our final expression for M_{ij}, but it involves the unknown coefficients b_k^j which we now determine. Spatial differentiations of (37) and (42) give, respectively,

$$\nabla F = \underset{\sim}{e}_\rho - \frac{\partial P}{\partial z}\,\underset{\sim}{e}_z \quad , \tag{44a}$$

$$\nabla\varphi = \sum_{k=1}^{K} \sum_{j=1}^{6} b_k^j\, r^{k-1}\left[kP_k \underset{\sim}{e}_r + \frac{dP_k}{d\theta}\,\underset{\sim}{e}_\theta\right] \dot{q}_j \quad , \tag{44b}$$

where $\underset{\sim}{e}_\rho$, $\underset{\sim}{e}_z$, $\underset{\sim}{e}_r$ and $\underset{\sim}{e}_\theta$ denote unit vectors in, respectively, the ρ, z, r and θ directions. The kinematical boundary condition (38) then becomes

$$\sum_{k=1}^{K} \sum_{j=1}^{6} b_k^j R^{k-1}\left[kP_k \sin\theta + \frac{dP_k}{d\theta}\cos\theta - \frac{\partial P}{\partial z}\left(kP_k \cos\theta - \frac{dP_k}{d\theta}\sin\theta\right)\right]\dot{q}_j - \sum_{j=1}^{6} \frac{\partial P}{\partial q_j}\dot{q}_j = 0 \quad ,$$

where

$$R = (P^2 + z^2)^{\frac{1}{2}}$$

is the value of r on the surface of the drop, and

$$\cos\theta = z/(P^2 + z^2)^{\frac{1}{2}} \quad ,$$

$$\sin\theta = P/(P^2 + z^2)^{\frac{1}{2}} \quad .$$

We next multiply this equation through by P, use the relation

$$P_k^1(\cos\theta) = -\frac{dP_k(\cos\theta)}{d\theta} \quad ,$$

where P_k^m denotes an associated Legendre polynomial, and note that the equation must be satisfied for arbitrary motions of the drop's boundary. This leads to the system of six equations

$$\sum_{k=1}^{K} R^{k-1}\left[P(kP_k \sin\theta - P_k^1 \cos\theta) - P\frac{\partial P}{\partial z}(kP_k \cos\theta + P_k^1 \sin\theta)\right] b_k^j$$

$$- P\frac{\partial P}{\partial q_j} = 0 \quad , \quad j = 1, 2, \ldots, 6 \quad . \tag{45}$$

The quantity P is given by (4), $P\frac{\partial P}{\partial z}$ by (31) and $P\frac{\partial P}{\partial q_j}$ by (35).

The system of eqs. (45) for the coefficients b_k^j cannot in general be solved exactly, and, as discussed in ref. [20], various schemes exist for its approximate solution. The scheme that seems to work best in practice (and the one we have used) is to determine the coefficients in the sense of least squares from the requirement that the integrals over the drop's surface of the squares of the left-hand sides of eqs. (45) be minima. When this least-squares scheme is used, greater numerical accuracy can be achieved by not forming the usual normal equations for the coefficients b_k^j but instead by solving directly[118,119] the over-determined system (45) (evaluated at a finite number of points on the drop's surface). Once the coefficients b_k^j are determined in this way, the elements M_{ij} of the inertia matrix are obtained immediately from (43) by numerical Gaussian quadrature[113].

6.4.2. Werner-Wheeler method.

The approximate method of Werner and Wheeler[12] for the calculation of the kinetic energy is discussed in some detail in refs. [1,19]. We repeat the derivation of the formulas here because one of the key expressions of ref. [19] is incorrect.

In an exact calculation of the kinetic energy (for irrotational flow) the components $\dot{z}$ and $\dot{\rho}$ of the fluid velocity are obtained by taking partial derivatives with respect to z and ρ, respectively, of the velocity potential

$$\varphi(\rho,z;q,\dot{q}) = \sum_{i=1}^{6} \varphi_i(\rho,z;q)\dot{q}_i \quad .$$

Thus, exactly,

$$\dot{z} = \frac{\partial\varphi}{\partial z} = \sum_{i=1}^{6} \frac{\partial\varphi_i(\rho,z;q)}{\partial z}\dot{q}_i \quad , \tag{46a}$$

$$\dot{\rho} = \frac{\partial\varphi}{\partial\rho} = \sum_{i=1}^{6} \frac{\partial\varphi_i(\rho,z;q)}{\partial\rho}\dot{q}_i \quad . \tag{46b}$$

Now, the Werner-Wheeler approximation is equivalent to assuming that $\dot{z}$ is independent of ρ and that $\dot{\rho}$ depends linearly upon ρ. That is, rather than the exact relations (46), the components of the velocity are approximated by

$$\dot{z} = \sum_{i=1}^{6} A_i(z;q)\dot{q}_i \quad , \tag{47a}$$

$$\dot{\rho} = \frac{\rho}{P} \sum_{i=1}^{6} B_i(z;q)\dot{q}_i \quad , \tag{47b}$$

where $P = P(z;q)$ is the value of ρ on the surface of the drop at the position defined by z.

A relationship between the (as yet unknown) expansion coefficients A_i and B_i is obtained from the kinematical boundary condition (38). By use of this boundary condition and eqs. (37), (44a) and (47) we find that

$$\sum_{i=1}^{6} B_i\dot{q}_i - \frac{\partial P}{\partial z} \sum_{i=1}^{6} A_i\dot{q}_i - \sum_{i=1}^{6} \frac{\partial P}{\partial q_i} \dot{q}_i = 0 \quad .$$

Since this equation must hold for arbitrary motions of the drop's boundary it follows that

$$B_i = \frac{\partial P}{\partial z} A_i + \frac{\partial P}{\partial q_i} \quad , \quad i = 1, 2, \ldots, 6 \quad . \tag{48}$$

Into the exact expression for the kinetic energy

$$\mathcal{T} = \tfrac{1}{2} \rho_m \int_{\ell_1 - c_1}^{\ell_2 + c_2} \int_0^P [\dot{z}^2 + \dot{\rho}^2] \, 2\pi\rho d\rho dz$$

we substitute (47) for $\dot{z}$ and $\dot{\rho}$ and perform the integration over ρ. Upon simplification this leads to eq. (8) for the kinetic energy, with the elements of the inertia matrix given by

$$M_{ij} = \pi\rho_m \int_{\ell_1 - c_1}^{\ell_2 + c_2} P^2 [A_i A_j + \tfrac{1}{2} B_i B_j] \, dz \quad . \tag{49}$$

Expressions (48) and (49) are identical to eqs. (24) and (25) of ref. [19]), apart from obvious differences in notation.

The expansion coefficients A_i are determined from the assumption in the Werner-Wheeler approximation that the fluid in a given infinitesimal slice perpendicular to the symmetry axis remain in that slice. This is equivalent to requiring the vanishing of the total (convective) time derivative of the volume of fluid to the right (or to the left) of an arbitrary plane perpendicular to the symmetry axis. We denote by

$$V^+(z;q) = \pi \int_z^{\ell_2 + c_2} P^2(z';q) \, dz' \quad ,$$

$$V^-(z;q) = \pi \int_{\ell_1 - c_1}^{z} P^2(z';q) \, dz' \quad ,$$

the volumes of fluid to the right and left, respectively, of a plane perpendicular to the symmetry axis at the point z. It then follows that

$$\frac{D}{Dt} V^+(z;q) = \frac{\partial V^+}{\partial z} \dot{z} + \sum_{i=1}^{6} \frac{\partial V^+}{\partial q_i} \dot{q}_i$$

$$= \pi \left\{ -P^2(z;q) \, \dot{z} + \sum_{i=1}^{6} \left[\frac{\partial}{\partial q_i} \int_z^{\ell_2 + c_2} P^2(z';q) \, dz' \right] \dot{q}_i \right\} = 0 \quad ,$$

or

$$\dot{z} = \sum_{i=1}^{6} \left[\frac{1}{P^2(z;q)} \frac{\partial}{\partial q_i} \int_z^{\ell_2+c_2} P^2(z';q)\, dz' \right] \dot{q}_i \quad .$$

This gives, upon referring to (47a),

$$A_i(z;q) = \frac{1}{P^2(z;q)} \frac{\partial}{\partial q_i} \int_z^{\ell_2+c_2} P^2(z';q)\, dz' \quad . \tag{50a}$$

This equation is to be compared with the second form of eq. (26) of ref. [19], which incorrectly contains an additional term that in our notation is $\partial(\ell_2 + c_2)/\partial q_i$. Equations (A8) [and (A9)] and the first form of eq. (26) of ref. [19], from which the final result for A_i is derived, are also incorrect.

It is sometimes more convenient to calculate A_i from the alternative formula

$$A_i(z;q) = - \frac{1}{P^2(z;q)} \frac{\partial}{\partial q_i} \int_{\ell_1-c_1}^{z} P^2(z';q)\, dz' \quad , \tag{50b}$$

which is obtained by taking the total time derivative of $\bar{V}(z;q)$. A third, but not particularly useful, form for A_i can be obtained by taking one-half the sum of eqs. (50a) and (50b).

By substituting (50), (48), (35), (31) and (4) into (49), we obtain an expression for the elements of the inertia matrix by performing straightforward integrations. The resulting expression is lengthy but can be written in terms of elementary transcendental functions. It involves both the geometrical parameters of the quadratic surfaces of revolution discussed in appendix 6.1, and the derivatives of these quantities with respect to the generalized coordinates discussed in appendix 6.2. It also involves the quantities (for $j = 1, 2$)

$$\rho_j^2 = a_j^2 - (a_j^2/c_j^2)(z_j - \ell_j)^2 = a_3^2 - (a_3^2/c_3^2)(z_j - \ell_3)^2 \quad ,$$

$$H_j = \int_0^{(-1)^j(z_j-\ell_3)} \frac{dx}{a_3^2 - (a_3^2/c_3^2)\, x^2}$$

$$= \begin{cases} \frac{1}{2}\,[a_3^2(a_3^2/c_3^2)]^{-\frac{1}{2}} \ln\left\{\dfrac{a_3^2 + (-1)^j(z_j - \ell_3)[a_3^2(a_3^2/c_3^2)]^{\frac{1}{2}}}{a_3^2 - (-1)^j(z_j - \ell_3)[a_3^2(a_3^2/c_3^2)]^{\frac{1}{2}}}\right\} \quad , \quad \dfrac{(a_3^2/c_3^2)(z_j - \ell_3)^2}{a_3^2} > 0 \\ \dfrac{(-1)^j(z_j - \ell_3)}{a_3^2}\left\{1 + \frac{1}{3}\left[\dfrac{(a_3^2/c_3^2)(z_j - \ell_3)^2}{a_3^2}\right] + \frac{1}{5}\left[\dfrac{(a_3^2/c_3^2)(z_j - \ell_3)^2}{a_3^2}\right]^2 \right. \\ \qquad \left. + \frac{1}{7}\left[\dfrac{(a_3^2/c_3^2)(z_j - \ell_3)^2}{a_3^2}\right]^3 + \ldots\right\} \quad , \quad \left|\dfrac{(a_3^2/c_3^2)(z_j - \ell_3)^2}{a_3^2}\right| \ll 1 \\ [-a_3^2(a_3^2/c_3^2)]^{-\frac{1}{2}} \arctan\left\{\dfrac{(-1)^j(z_j - \ell_3)[-a_3^2(a_3^2/c_3^2)]^{\frac{1}{2}}}{a_3^2}\right\} \quad , \quad \dfrac{(a_3^2/c_3^2)(z_j - \ell_3)^2}{a_3^2} < 0 \quad , \end{cases}$$

$$L_j = \begin{cases} \frac{1}{2}(a_3^2/c_3^2)^{-1} \ln(\rho_j^2/a_3^2) \quad , & a_3^2/c_3^2 \neq 0 \\ -\frac{1}{2}\dfrac{(z_j - \ell_3)^2}{a_3^2}\left\{1 + \frac{1}{2}\left[\dfrac{(a_3^2/c_3^2)(z_j - \ell_3)^2}{a_3^2}\right] + \frac{1}{3}\left[\dfrac{(a_3^2/c_3^2)(z_j - \ell_3)^2}{a_3^2}\right]^2 \right. & \\ \qquad \left. + \frac{1}{4}\left[\dfrac{(a_3^2/c_3^2)(z_j - \ell_3)^2}{a_3^2}\right]^3 + \ldots\right\} \quad , \quad \left|\dfrac{(a_3^2/c_3^2)(z_j - \ell_3)^2}{a_3^2}\right| \ll 1 \quad , & \end{cases}$$

$$N_j = \begin{cases} \left[\frac{1}{2}(z_j - \ell_3)^2 + a_3^2 L_j\right] \Big/ (a_3^2/c_3^2) \quad , & a_3^2/c_3^2 \neq 0 \\ -\frac{1}{2}\dfrac{(z_j - \ell_3)^4}{a_3^2}\left\{\frac{1}{2} + \frac{1}{3}\left[\dfrac{(a_3^2/c_3^2)(z_j - \ell_3)^2}{a_3^2}\right] + \frac{1}{4}\left[\dfrac{(a_3^2/c_3^2)(z_j - \ell_3)^2}{a_3^2}\right]^2 \right. & \\ \qquad \left. + \frac{1}{5}\left[\dfrac{(a_3^2/c_3^2)(z_j - \ell_3)^2}{a_3^2}\right]^3 + \ldots\right\} \quad , \quad \left|\dfrac{(a_3^2/c_3^2)(z_j - \ell_3)^2}{a_3^2}\right| \ll 1 \quad , & \end{cases}$$

$$Q_j = \begin{cases} [-(-1)^j(z_j - \ell_3) + a_3^2 H_j]/(a_3^2/c_3^2) \quad , & a_3^2/c_3^2 \neq 0 \\ \dfrac{(-1)^j(z_j - \ell_3)^3}{a_3^2}\left\{\dfrac{1}{3} + \dfrac{1}{5}\left[\dfrac{(a_3^2/c_3^2)(z_j - \ell_3)^2}{a_3^2}\right] + \dfrac{1}{7}\left[\dfrac{(a_3^2/c_3^2)(z_j - \ell_3)^2}{a_3^2}\right]^2 \right. & \\ \qquad \left. + \dfrac{1}{9}\left[\dfrac{(a_3^2/c_3^2)(z_j - \ell_3)^2}{a_3^2}\right]^3 + \ldots\right\} \quad , \quad \left|\dfrac{(a_3^2/c_3^2)(z_j - \ell_3)^2}{a_3^2}\right| \ll 1 \quad , & \end{cases}$$

$$S_j = \begin{cases} -\frac{1}{3}(-1)^j(z_j - \ell_3)^3/(a_3^2/c_3^2) - a_3^2(-1)^j(z_j - \ell_3)/(a_3^2/c_3^2)^2 + (a_3^2)^2 H_j/(a_3^2/c_3^2)^2 \quad , & a_3^2/c_3^2 \neq 0 \\ \dfrac{(-1)^j(z_j - \ell_3)^5}{a_3^2}\left\{\dfrac{1}{5} + \dfrac{1}{7}\left[\dfrac{(a_3^2/c_3^2)(z_j - \ell_3)^2}{a_3^2}\right] + \dfrac{1}{9}\left[\dfrac{(a_3^2/c_3^2)(z_j - \ell_3)^2}{a_3^2}\right]^2 \right. & \\ \qquad \left. + \dfrac{1}{11}\left[\dfrac{(a_3^2/c_3^2)(z_j - \ell_3)^2}{a_3^2}\right]^3 + \ldots\right\} \quad , \quad \left|\dfrac{(a_3^2/c_3^2)(z_j - \ell_3)^2}{a_3^2}\right| \ll 1 \quad , & \end{cases}$$

$$
U_j = \begin{cases}
-\frac{1}{6}\,a_3^{\,2}(-1)^j(z_j-\ell_3)^3/(a_3^{\,2}/c_3^{\,2}) - \frac{1}{5}\,(-1)^j(z_j-\ell_3)^5/(a_3^{\,2}/c_3^{\,2}) - \frac{1}{3}\,a_3^{\,2}(-1)^j(z_j-\ell_3)^3/(a_3^{\,2}/c_3^{\,2})^2 \\
+\frac{1}{4}(-1)^j(z_j-\ell_3)(a_3^{\,2})^3\Big/\left[(a_3^{\,2}/c_3^{\,2})^2\,\rho_j^{\,2}\right] - \frac{1}{4}(a_3^{\,2})^3H_j/(a_3^{\,2}/c_3^{\,2})^2 - (a_3^{\,2})^2(-1)^j(z_j-\ell_3)/(a_3^{\,2}/c_3^{\,2})^3 \\
+(a_3^{\,2})^3H_j/(a_3^{\,2}/c_3^{\,2})^3 \quad , \quad a_3^{\,2}/c_3^{\,2} \neq 0 \\
\frac{1}{2}(-1)^j(z_j-\ell_3)^5\left\{\frac{2}{5}+\frac{3}{7}\left[\frac{(a_3^{\,2}/c_3^{\,2})(z_j-\ell_3)^2}{a_3^{\,2}}\right]+\frac{4}{9}\left[\frac{(a_3^{\,2}/c_3^{\,2})(z_j-\ell_3)^2}{a_3^{\,2}}\right]^2\right. \\
\left.+\frac{5}{11}\left[\frac{(a_3^{\,2}/c_3^{\,2})(z_j-\ell_3)^2}{a_3^{\,2}}\right]^3+\ldots\right\} + (-1)^j(z_j-\ell_3)^7(a_3^{\,2})^{-1}\left\{\frac{1}{7}+\frac{1}{9}\left[\frac{(a_3^{\,2}/c_3^{\,2})(z_j-\ell_3)^2}{a_3^{\,2}}\right]\right. \\
\left.+\frac{1}{11}\left[\frac{(a_3^{\,2}/c_3^{\,2})(z_j-\ell_3)^2}{a_3^{\,2}}\right]^2+\frac{1}{13}\left[\frac{(a_3^{\,2}/c_3^{\,2})(z_j-\ell_3)^2}{a_3^{\,2}}\right]^3+\ldots\right\} \quad , \quad \left|\frac{(a_3^{\,2}/c_3^{\,2})(z_j-\ell_3)^2}{a_3^{\,2}}\right| \ll 1 \quad .
\end{cases}
$$

We write the expression for the element M_{mn} of the inertia matrix as the sum

$$
M_{mn} = \frac{3}{4}\,M_0R_0^{-3}\sum_{i=1}^{21}\sum_{j=1}^{2}T_{ij} \quad ,
$$

where it is understood that T_{ij} refers to the (m,n) element of the inertia matrix. The individual terms have dimensions of R_0^5, so that the elements of the inertia matrix have the proper dimensions of $M_0 R_0^2$. The terms are given by (for j = 1, 2)

$$T_{1j} = \left\{ a_j^2 [c_j + (-1)^j (\ell_j - z_j)] - \frac{1}{3} (a_j^2/c_j^2)[c_j^3 + (-1)^j (\ell_j - z_j)^3] + (-1)^j (z_j - \ell_3)\rho_j^2 \right.$$

$$\left. -[1 - \tfrac{1}{4}(a_3^2/c_3^2)][(-1)^j (z_j - \ell_3) - \rho_j^2 H_j]\rho_j^2 \right\} \frac{\partial \ell_j}{\partial q_m} \frac{\partial \ell_j}{\partial q_n} \quad ,$$

$$T_{2j} = [1 - \tfrac{1}{4}(a_3^2/c_3^2)][(-1)^j (z_j - \ell_3) - \rho_j^2 H_j]\rho_j^2 \left(\frac{\partial \ell_j}{\partial q_m} \frac{\partial \ell_3}{\partial q_n} + \frac{\partial \ell_j}{\partial q_n} \frac{\partial \ell_3}{\partial q_m} \right) \quad ,$$

$$T_{3j} = \left\{ \frac{2}{3} (a_3^2/c_3^2)(-1)^j (z_j - \ell_3)^3 - [1 - \tfrac{1}{4}(a_3^2/c_3^2)][(-1)^j (z_j - \ell_3) - \rho_j^2 H_j]\rho_j^2 \right\} \frac{\partial \ell_3}{\partial q_m} \frac{\partial \ell_3}{\partial q_n} \quad ,$$

$$T_{4j} = (-1)^j [c_j + (-1)^j (\ell_j - z_j)] \left\{ \tfrac{1}{2}[c_j + (-1)^j (\ell_j - z_j)] + (-1)^j (z_j - \ell_3) - [1 - \tfrac{1}{4}(a_3^2/c_3^2)][(-1)^j (z_j - \ell_3) \right.$$

$$\left. - \rho_j^2 H_j] \right\} \left(\frac{\partial \ell_j}{\partial q_m} \frac{\partial a_j^2}{\partial q_n} + \frac{\partial \ell_j}{\partial q_n} \frac{\partial a_j^2}{\partial q_m} \right) \quad ,$$

$$T_{5j} = (-1)^j [1 - \tfrac{1}{4}(a_3^2/c_3^2)][L_j + (-1)^j (z_j - \ell_3) H_j]\rho_j^2 \left(\frac{\partial \ell_j}{\partial q_m} \frac{\partial a_3^2}{\partial q_n} + \frac{\partial \ell_j}{\partial q_n} \frac{\partial a_3^2}{\partial q_m} \right) \quad ,$$

$$T_{6j} = (-1)^j[1 - \tfrac{1}{4}(a_3^2/c_3^2)][c_j + (-1)^j(\ell_j - z_j)][(-1)^j(z_j - \ell_3) - \rho_j^2 H_j]\left(\frac{\partial \ell_3}{\partial q_m}\frac{\partial a_j^2}{\partial q_n} + \frac{\partial \ell_3}{\partial q_n}\frac{\partial a_j^2}{\partial q_m}\right) ,$$

$$T_{7j} = (-1)^j\left\{\tfrac{1}{2}(z_j - \ell_3)^2 - [1 - \tfrac{1}{4}(a_3^2/c_3^2)][L_j + (-1)^j(z_j - \ell_3)H_j]\rho_j^2\right\}\left(\frac{\partial \ell_3}{\partial q_m}\frac{\partial a_3^2}{\partial q_n} + \frac{\partial \ell_3}{\partial q_n}\frac{\partial a_3^2}{\partial q_m}\right) ,$$

$$T_{8j} = (-1)^j\left(-\tfrac{1}{4}c_j^4 - \frac{1}{3}c_j^3(-1)^j(\ell_j - z_j) - \frac{1}{12}(\ell_j - z_j)^4 + \frac{1}{3}[c_j^3 + (-1)^j(\ell_j - z_j)^3]\left\{[1 - \tfrac{1}{4}(a_3^2/c_3^2)]\right.\right.$$

$$\left.\left.\times[(-1)^j(z_j - \ell_3) - \rho_j^2 H_j] - (-1)^j(z_j - \ell_3)\right\}\right)\left[\frac{\partial \ell_j}{\partial q_m}\frac{\partial(a_j^2/c_j^2)}{\partial q_n} + \frac{\partial \ell_j}{\partial q_n}\frac{\partial(a_j^2/c_j^2)}{\partial q_m}\right] ,$$

$$T_{9j} = -\frac{1}{3}(-1)^j[1 - \tfrac{1}{4}(a_3^2/c_3^2)][N_j + (-1)^j(z_j - \ell_3)^3 H_j]\rho_j^2\left[\frac{\partial \ell_j}{\partial q_m}\frac{\partial(a_3^2/c_3^2)}{\partial q_n} + \frac{\partial \ell_j}{\partial q_n}\frac{\partial(a_3^2/c_3^2)}{\partial q_m}\right] ,$$

$$T_{10,j} = -\frac{1}{3}(-1)^j[1 - \tfrac{1}{4}(a_3^2/c_3^2)][c_j^3 + (-1)^j(\ell_j - z_j)^3][(-1)^j(z_j - \ell_3) - \rho_j^2 H_j]\left[\frac{\partial \ell_3}{\partial q_m}\frac{\partial(a_j^2/c_j^2)}{\partial q_n}\right.$$

$$\left. + \frac{\partial \ell_3}{\partial q_n}\frac{\partial(a_j^2/c_j^2)}{\partial q_m}\right] ,$$

$$T_{11,j} = \frac{1}{3}(-1)^j \left\{ -\frac{3}{4}(z_j - \ell_3)^4 + [1 - \tfrac{1}{4}(a_3^2/c_3^2)][N_j + (-1)^j(z_j - \ell_3)^3 H_j]\rho_j^2 \right\} \left[\frac{\partial \ell_3}{\partial q_m} \frac{\partial (a_3^2/c_3^2)}{\partial q_n} + \frac{\partial \ell_3}{\partial q_n} \frac{\partial (a_3^2/c_3^2)}{\partial q_m} \right] ,$$

$$T_{12,j} = [c_j + (-1)^j(\ell_j - z_j)] \left\{ \frac{1}{8} - \frac{1}{a_j^2/c_j^2} + \tfrac{1}{4} \frac{(a_j^2/c_j^2)c_j + (a_3^2/c_3^2)(-1)^j(z_j - \ell_3)}{(a_j^2/c_j^2)[c_j - (-1)^j(\ell_j - z_j)]} \right.$$

$$- \frac{2c_j[1 - \tfrac{1}{4}(a_j^2/c_j^2)]}{(a_j^2/c_j^2)[c_j + (-1)^j(\ell_j - z_j)]} \ln\left[\frac{c_j - (-1)^j(\ell_j - z_j)}{2c_j} \right] + [1 - \tfrac{1}{4}(a_3^2/c_3^2)]$$

$$\left. \times [c_j + (-1)^j(\ell_j - z_j)]H_j \right\} \frac{\partial a_j^2}{\partial q_m} \frac{\partial a_j^2}{\partial q_n} ,$$

$$T_{13,j} = [1 - \tfrac{1}{4}(a_3^2/c_3^2)][c_j + (-1)^j(\ell_j - z_j)][L_j + (-1)^j(z_j - \ell_3)H_j] \left(\frac{\partial a_j^2}{\partial q_m} \frac{\partial a_3^2}{\partial q_n} + \frac{\partial a_j^2}{\partial q_n} \frac{\partial a_3^2}{\partial q_m} \right) ,$$

$$T_{14,j} = \left\{ \frac{3}{8}(-1)^j(z_j - \ell_3) - \tfrac{1}{4}a_3^2 H_j + Q_j + [1 - \tfrac{1}{4}(a_3^2/c_3^2)][(z_j - \ell_3)^2 H_j + 2(-1)^j(z_j - \ell_3)L_j] \right\} \frac{\partial a_3^2}{\partial q_m} \frac{\partial a_3^2}{\partial q_n} ,$$

$$T_{15,j} = [c_j + (-1)^j(\ell_j - z_j)]\left\{\frac{1}{72}[-2c_j^2 + 2c_j(-1)^j(\ell_j - z_j) + (\ell_j - z_j)^2] + \frac{1}{18}[5c_j^2 + c_j(-1)^j(\ell_j - z_j)\right.$$

$$+ 2(\ell_j - z_j)^2]/(a_j^2/c_j^2) - \frac{1}{12}c_j^3/[c_j - (-1)^j(\ell_j - z_j)] - \frac{1}{12}(a_3^2/c_3^2)(-1)^j(z_j - \ell_3)$$

$$\times [c_j^3 + (-1)^j(\ell_j - z_j)^3]/\rho_j^2 + \frac{2}{3}\frac{[1 - \frac{1}{4}(a_j^2/c_j^2)]c_j^3}{(a_j^2/c_j^2)[c_j + (-1)^j(\ell_j - z_j)]}\ln\left[\frac{c_j - (-1)^j(\ell_j - z_j)}{2c_j}\right]$$

$$\left. - \frac{1}{3}[1 - \tfrac{1}{4}(a_3^2/c_3^2)][c_j^3 + (-1)^j(\ell_j - z_j)^3]H_j\right\}\left[\frac{\partial a_j^2}{\partial q_m}\frac{\partial(a_j^2/c_j^2)}{\partial q_n} + \frac{\partial a_j^2}{\partial q_n}\frac{\partial(a_j^2/c_j^2)}{\partial q_m}\right] ,$$

$$T_{16,j} = -\frac{1}{3}[1 - \tfrac{1}{4}(a_3^2/c_3^2)][c_j + (-1)^j(\ell_j - z_j)][N_j + (-1)^j(z_j - \ell_3)^3 H_j]\left[\frac{\partial a_j^2}{\partial q_m}\frac{\partial(a_3^2/c_3^2)}{\partial q_n}\right.$$

$$\left. + \frac{\partial a_j^2}{\partial q_n}\frac{\partial(a_3^2/c_3^2)}{\partial q_m}\right] ,$$

$$T_{17,j} = -\frac{1}{3}[1 - \tfrac{1}{4}(a_3^2/c_3^2)][c_j^3 + (-1)^j(\ell_j - z_j)^3][L_j + (-1)^j(z_j - \ell_3)H_j]\left[\frac{\partial a_3^2}{\partial q_m}\frac{\partial(a_j^2/c_j^2)}{\partial q_n}\right.$$

$$\left. + \frac{\partial a_3^2}{\partial q_n}\frac{\partial(a_j^2/c_j^2)}{\partial q_m}\right] ,$$

$$T_{18,j} = -\frac{1}{3}\left\{\tfrac{1}{4}(-1)^j(z_j - \ell_3)^3\left[\frac{1}{3} - (a_3^2/c_3^2)L_j\right] + [1 - \tfrac{1}{4}(a_3^2/c_3^2)](z_j - \ell_3)^4 H_j + S_j + (-1)^j(z_j - \ell_3)N_j\right.$$

$$\left. + (-1)^j(z_j - \ell_3)[(z_j - \ell_3)^2 - \tfrac{1}{4}a_3^2]L_j - \tfrac{1}{4}a_3^2 Q_j\right\}\left[\frac{\partial a_3^2}{\partial q_m}\,\frac{\partial(a_3^2/c_3^2)}{\partial q_n} + \frac{\partial a_3^2}{\partial q_n}\,\frac{\partial(a_3^2/c_3^2)}{\partial q_m}\right] \quad ,$$

$$T_{19,j} = \frac{1}{9}\left\{\frac{13}{120}\,c_j^5 - \tfrac{1}{4}c_j^3(\ell_j - z_j)^2 - \frac{1}{6}\,c_j^2(-1)^j(\ell_j - z_j)^3 + \frac{1}{40}\,(-1)^j(\ell_j - z_j)^5 - \frac{1}{15}\,[8c_j^5\right.$$

$$+ 15c_j^4(-1)^j(\ell_j - z_j) + 15c_j^3(\ell_j - z_j)^2 + 5c_j^2(-1)^j(\ell_j - z_j)^3 + 3(-1)^j(\ell_j - z_j)^5]/(a_j^2/c_j^2)$$

$$+ \tfrac{1}{4}[c_j + (-1)^j(\ell_j - z_j)]c_j^5/[c_j - (-1)^j(\ell_j - z_j)] + \tfrac{1}{4}(a_3^2/c_3^2)(-1)^j(z_j - \ell_3)$$

$$\times [c_j^3 + (-1)^j(\ell_j - z_j)^3]^2/\rho_j^2 - 2\,\frac{[1 - \tfrac{1}{4}(a_j^2/c_j^2)]c_j^5}{a_j^2/c_j^2}\,\ln\left[\frac{c_j - (-1)^j(\ell_j - z_j)}{2c_j}\right] + [1 - \tfrac{1}{4}(a_3^2/c_3^2)]$$

$$\left.\times [c_j^3 + (-1)^j(\ell_j - z_j)^3]^2 H_j\right\}\frac{\partial(a_j^2/c_j^2)}{\partial q_m}\,\frac{\partial(a_j^2/c_j^2)}{\partial q_n} \quad ,$$

$$T_{20,j} = \frac{1}{9}\left[1 - \tfrac{1}{4}(a_3^2/c_3^2)\right]\left[c_j^3 + (-1)^j(\ell_j - z_j)^3\right]\left[N_j + (-1)^j(z_j - \ell_3)^3 H_j\right]\left[\frac{\partial(a_j^2/c_j^2)}{\partial q_m}\,\frac{\partial(a_3^2/c_3^2)}{\partial q_n} + \frac{\partial(a_j^2/c_j^2)}{\partial q_n}\,\frac{\partial(a_3^2/c_3^2)}{\partial q_m}\right],$$

$$T_{21,j} = \frac{1}{9}\left\{\frac{11}{40}(-1)^j(z_j - \ell_3)^5 + (-1)^j(z_j - \ell_3)^3\left(2N_j - \tfrac{1}{2}a_3^2 L_j\right) + U_j + (-1)^j(z_j - \ell_3)\left[-\tfrac{1}{2}a_3^2(z_j - \ell_3)^4 + \tfrac{1}{4}(a_3^2/c_3^2)(z_j - \ell_3)^6\right]/\rho_j^2 + \left[1 - \tfrac{1}{4}(a_3^2/c_3^2)\right](z_j - \ell_3)^6 H_j\right\}\frac{\partial(a_3^2/c_3^2)}{\partial q_m}\,\frac{\partial(a_3^2/c_3^2)}{\partial q_n}.$$

This result for the inertia matrix is applicable only to pre-scission shapes. After scission, the inertia elements corresponding to the flow of matter between the two fragments are infinite, and a treatment of the post-scission inertia matrix would involve removing these infinities by eliminating the degree of freedom describing a transfer of matter. Also, it should be remembered that the result we give for M_{mn} is not applicable when a_3^2/c_3^2 is close to zero for an asymmetrical shape, for reasons we discussed in appendices 6.1 and 6.2.

UCRL-17958

6.4.3. Comparisons of methods.

We compare in tables 5 and 6 results computed by use of the Werner-Wheeler approximation with those computed by use of the exact method. Table 5 gives the comparison for shapes corresponding to the symmetrical saddle points for x = 0.9, 0.8, 0.7 and 0.6; the values of the coordinates σ_1, σ_2 and σ_3 defining these shapes are given in table 1. The format of table 5 is the following: The value of the fissility parameter x defining the saddle-point shape is given in the first column. Columns two through four give the elements of the inertia matrix and the squares of the frequencies corresponding to symmetrical distortions, and columns five through seven those corresponding to asymmetrical distortions. (Recall that for a symmetrical shape the elements of the inertia matrix coupling symmetrical and asymmetrical distortions are zero.) The inertia-matrix elements are given in units of $M_0R_0^2$, and the frequencies squared in units of $\Omega_0^2 = E_s^{(0)}/(M_0R_0^2)$. Two numbers are given for each quantity tabulated; the top number is calculated by use of the Werner-Wheeler method, and the bottom number by use of the exact method.

Table 6 gives the comparison for an asymmetrical shape; the coordinates defining the shape are given in the first row. This particular shape occurs on the dynamical descent for x = 0.78 after 0.5×10^{-21} sec for initial conditions of starting from the saddle point with 1 MeV of kinetic energy in the fission mode and 1 MeV in the mass-asymmetry mode (see the second shape for x = 0.78 in fig. 10). The elements of the full 6×6 inertia matrix are given, again in units of $M_0R_0^2$.

In computing the inertia matrices of tables 5 and 6 by use of the exact method, we employed terms up to and including the 32nd solid harmonic in the expansion of the velocity potential [K = 32 in eq. (42)]. In determining the coefficients b_k^j we evaluated the system (45) at a total of 128 points and then solved the resulting over-determined system directly[118,119]. Finally, a 32-point Gaussian quadrature formula was used in each of four divisions of the drop to compute the inertia-matrix elements according to eq. (43).

The inertia matrix M is a symmetrical matrix, whereas the result (43) that we use for computing the elements of M is not manifestly symmetrical. Therefore, some estimate of the numerical accuracy of the inertia matrices

Table 5

Comparisons of results computed by the Werner-Wheeler method (top numbers) and the exact method (bottom numbers) for symmetrical saddle-point shapes

x	M_{22}	M_{24}	M_{26}	M_{11}	M_{13}	M_{15}
	M_{42}	M_{44}	M_{46}	M_{31}	M_{33}	M_{35}
	M_{62}	M_{64}	M_{66}	M_{51}	M_{53}	M_{55}
	ω_2^2	ω_4^2	ω_6^2	ω_1^2	ω_3^2	ω_5^2
0.9	0.01006	-0.00743	-0.02262	0.73041	-0.33687	0.23652
	0.01003	-0.00750	-0.02258	0.73041	-0.33687	0.23652
	-0.00743	0.00838	0.01599	-0.33687	0.16058	-0.10642
	-0.00750	0.00800	0.01620	-0.33686	0.16029	-0.10653
	-0.02262	0.01599	0.05137	0.23652	-0.10642	0.07805
	-0.02258	0.01620	0.05125	0.23652	-0.10653	0.07799
	-0.1979	9.548	23.00	0.0000	2.693	19.15
	-0.1982	10.973	33.94	0.0000	2.830	24.73
0.8	0.01652	-0.01956	-0.02921	0.54541	-0.32795	0.18754
	0.01650	-0.01955	-0.02923	0.54541	-0.32795	0.18754
	-0.01956	0.03129	0.03194	-0.32795	0.21417	-0.10942
	-0.01955	0.03051	0.03201	-0.32793	0.21380	-0.10941
	-0.02921	0.03194	0.05374	0.18754	-0.10942	0.06552
	-0.02923	0.03201	0.05371	0.18753	-0.10941	0.06549
	-0.2255	5.839	17.92	0.0000	1.370	14.40
	-0.2261	6.248	22.49	0.0000	1.397	16.47

Table 5 (continued)

0.7	0.06334	-0.11636	-0.02099	0.48249	-0.43406	0.19125
	0.06326	-0.11604	-0.02105	0.48249	-0.43406	0.19125
	-0.11636	0.25433	0.02556	-0.43406	0.52810	-0.19650
	-0.11602	0.25195	0.02548	-0.43396	0.52677	-0.19597
	-0.02099	0.02556	0.01596	0.19125	-0.19650	0.08171
	-0.02104	0.02547	0.01581	0.19119	-0.19595	0.08147
	-0.1069	2.252	10.45	0.0000	0.397	7.81
	-0.1072	2.303	11.58	0.0000	0.401	8.23
0.6	0.22343	-0.30671	0.10799	0.52650	-0.60205	0.24829
	0.22168	-0.30284	0.10687	0.52650	-0.60205	0.24829
	-0.30671	0.48234	-0.17423	-0.60205	1.64620	-0.59441
	-0.30158	0.47054	-0.17117	-0.53957	1.44632	-0.52257
	0.10799	-0.17423	0.07451	0.24829	-0.59441	0.22149
	0.10688	-0.17203	0.07365	0.22520	-0.52021	0.19479
	-0.5309	0.890	6.94	0.0000	0.078	4.71
	-0.5445	0.905	7.44	0.0000	0.091	4.84

Table 6

A comparison of results computed by the Werner-Wheeler method (top numbers) and the exact method (bottom numbers) for an asymmetrical shape

σ_1	σ_2	σ_3	α_1	α_2	α_3
M_{22}	M_{24}	M_{26}	M_{21}	M_{23}	M_{25}
M_{42}	M_{44}	M_{46}	M_{41}	M_{43}	M_{45}
M_{62}	M_{64}	M_{66}	M_{61}	M_{63}	M_{65}
M_{12}	M_{14}	M_{16}	M_{11}	M_{13}	M_{15}
M_{32}	M_{34}	M_{36}	M_{31}	M_{33}	M_{35}
M_{52}	M_{54}	M_{56}	M_{51}	M_{53}	M_{55}
2.24737	-0.11721	0.66438	-0.14063	-0.25097	-0.10386
0.02933 0.02930	-0.03815 -0.03805	-0.03091 -0.03095	0.01633 0.01634	0.00075 0.00069	0.00151 0.00154
-0.03815 -0.03804	0.06524 0.06408	0.03531 0.03528	-0.03405 -0.03405	0.01518 0.01517	-0.00583 -0.00584
-0.03091 -0.03095	0.03531 0.03528	0.03718 0.03711	-0.00522 -0.00521	-0.00699 -0.00706	0.00195 0.00197
0.01633 0.01633	-0.03405 -0.03405	-0.00522 -0.00522	0.50477 0.50477	-0.35113 -0.35113	0.17006 0.17006
0.00075 0.00069	0.01518 0.01517	-0.00699 -0.00706	-0.35113 -0.35108	0.28700 0.28638	-0.11950 -0.11933
0.00151 0.00154	-0.00583 -0.00583	0.00195 0.00197	0.17006 0.17004	-0.11950 -0.11933	0.05861 0.05854

computed by use of the exact method can be obtained[†] by comparing the computed value of M_{ij} with that for M_{ji} (for $i \neq j$). It is seen that for the $x = 0.9$ and 0.8 symmetrical saddle-point shapes and the chosen asymmetrical shape the maximum discrepancies between M_{ij} and M_{ji} are about one unit in the fifth decimal place. The maximum discrepancies increase to about one unit in the fourth decimal place for the $x = 0.7$ symmetrical saddle-point shape and to several units in the second decimal place for the $x = 0.6$ shape. The use of twice the number of solid-harmonic expansion terms (up to and including 64 rather than 32) improves the symmetry of the inertia matrix for the $x = 0.6$ shape, but the inertia matrices computed with even this large number of terms in the velocity-potential expansion become grossly asymmetrical for shapes more deformed than the $x = 0.6$ saddle-point shape. For such deformed shapes the portion of the inertia matrix corresponding to asymmetrical distortions is in greater error than the portion corresponding to symmetrical distortions, a result that was also observed in ref. [20]). This is because the asymmetrical distortions involve a flow of mass through a fairly thin neck, whereas the symmetrical distortions do not. For shapes close to scission the computation of the kinetic energy by means of an expansion of the velocity potential appears hopeless.

The major purpose of this subsection is to compare the Werner-Wheeler results with the results of the exact method. It is seen that the elements of M computed by the two methods typically differ by a few units in the fifth decimal place, with the maximum difference being about a unit in the third decimal place (we disregard the $x = 0.6$ shape since the accuracy of the exact-method results is so poor). The Werner-Wheeler method is seen to yield the exact answer for the elements $M_{1j} = M_{j1}$, $j = 1, 2, \ldots, 6$, which correspond to distortions involving a shift of the drop's center of mass. (It is to be noted in this connection that the exact method is more accurate for the upper triangle of the inertia matrix than for the lower triangle.)

[†] In refs. [21,22]) the results for the inertia matrix are symmetrized prior to computing the individual elements, and this important check on the numerical accuracy of the results is consequently lost.

In examining tables 5 and 6 we observe that Kelvin's theorem[43] is satisfied—for an arbitrary displacement of the drop's surface the kinetic energy corresponding to Werner-Wheeler flow is greater than or equal to the kinetic energy corresponding to irrotational flow. This theorem can be stated in terms of the inertia-matrix elements as

$$M_{ij}^{rot} - \epsilon_{ij} \leq M_{ij}^{ir} \leq M_{ij}^{rot} + \epsilon_{ij} \quad ,$$

where

$$\epsilon_{ij} = \tfrac{1}{2}[(M_{ii}^{rot} - M_{ii}^{ir}) + (M_{jj}^{rot} - M_{jj}^{ir})] \quad .$$

The superscripts ir and rot denote, respectively, irrotational flow (exact method) and flow with a possible rotational component (Werner-Wheeler method). For the diagonal elements (i = j) this result simplifies to

$$M_{ii}^{ir} \leq M_{ii}^{rot} \quad .$$

Since by Kelvin's theorem the normal-mode inertia constants for irrotational flow are less than or equal to those for Werner-Wheeler flow, the absolute values of $\omega_i^2 = K_i/M_i$ corresponding to irrotational flow are greater than or equal to those for Werner-Wheeler flow, and this is also seen to be satisfied in table 5. It is further noted that for the four lowest modes the frequencies calculated by the two methods are in fair agreement, whereas the agreement is not so good for the 5th and 6th modes. (The frequencies have in each case been computed with the same stiffness matrix. The stiffness matrices and the inertia matrices computed by the exact method were symmetrized prior to the computation of the frequencies.)

A final comparison that can be made is between the irrotational-flow frequencies computed in the three-quadratic-surface parameterization and those computed in the parameterization in which the drop's radius vector is expanded in a series of the first 18 Legendre polynomials[20]. In about half the cases the magnitudes of the frequencies computed in the more nearly exact Legendre-polynomial parameterization are higher than those computed in the

more restricted three-quadratic-surface parameterization. At first sight this appears to violate the well-known result that the magnitudes of the normal-mode frequencies of a constrained system are greater than or equal to those of the original unconstrained system. However, it must be remembered that for this to be true the constraint must be compatible with the equilibrium configuration, which is not the case here—the (constrained) three-quadratic-surface saddle-point shapes differ slightly from the (unconstrained) Legendre-polynomial saddle-point shapes.

6.5. NORMAL-COORDINATE STIFFNESS AND INERTIA CONSTANTS AND EIGENVECTORS

We present in this appendix plots as functions of x of the normal-coordinate stiffness and inertia constants and eigenvectors. It should be re-emphasized that all these quantities have meaning only with respect to the particular parameterization of the nuclear shape in terms of three quadratic surfaces of revolution, and in addition only with respect to the particular normalization of the eigenvectors that we are using.

Figure 27 shows the stiffness constants. The n = 1 center-of-mass-shift constant is identically zero, the n = 2 fission constant is negative for all values of x (zero at x = 1), the n = 3 mass-asymmetry constant is positive for $x > x_{BG}$ and negative for $x < x_{BG}$, and the remaining constants are positive for all values of x.

The rapid variations of the stiffness constants at $x \approx 0.67$ are associated with the qualitative transition[2]) of the saddle-point shapes from cylinder-like for $x \gtrsim 0.67$ to dumbbell-like for $x \lesssim 0.67$. The maximum in the n = 4 curve at $x \approx 0.78$ arises from the transition through the cylindrical stage of the middle quadratic surface of revolution.

The normal-mode inertia constants are shown in fig. 28. The fairly rapid variations of these quantities at $x \approx 0.67$ are also associated with the transition from cylinder-like saddle-point shapes to dumbbell-like saddle-point shapes at this value of x. The maximum in the n = 2 curve at $x \approx 0.63$ is a peculiarity of the parameterization: a plot of the frequency (squared) obtained by dividing K_2 (from fig. 27) by M_2 shows a smooth variation through this value of x.

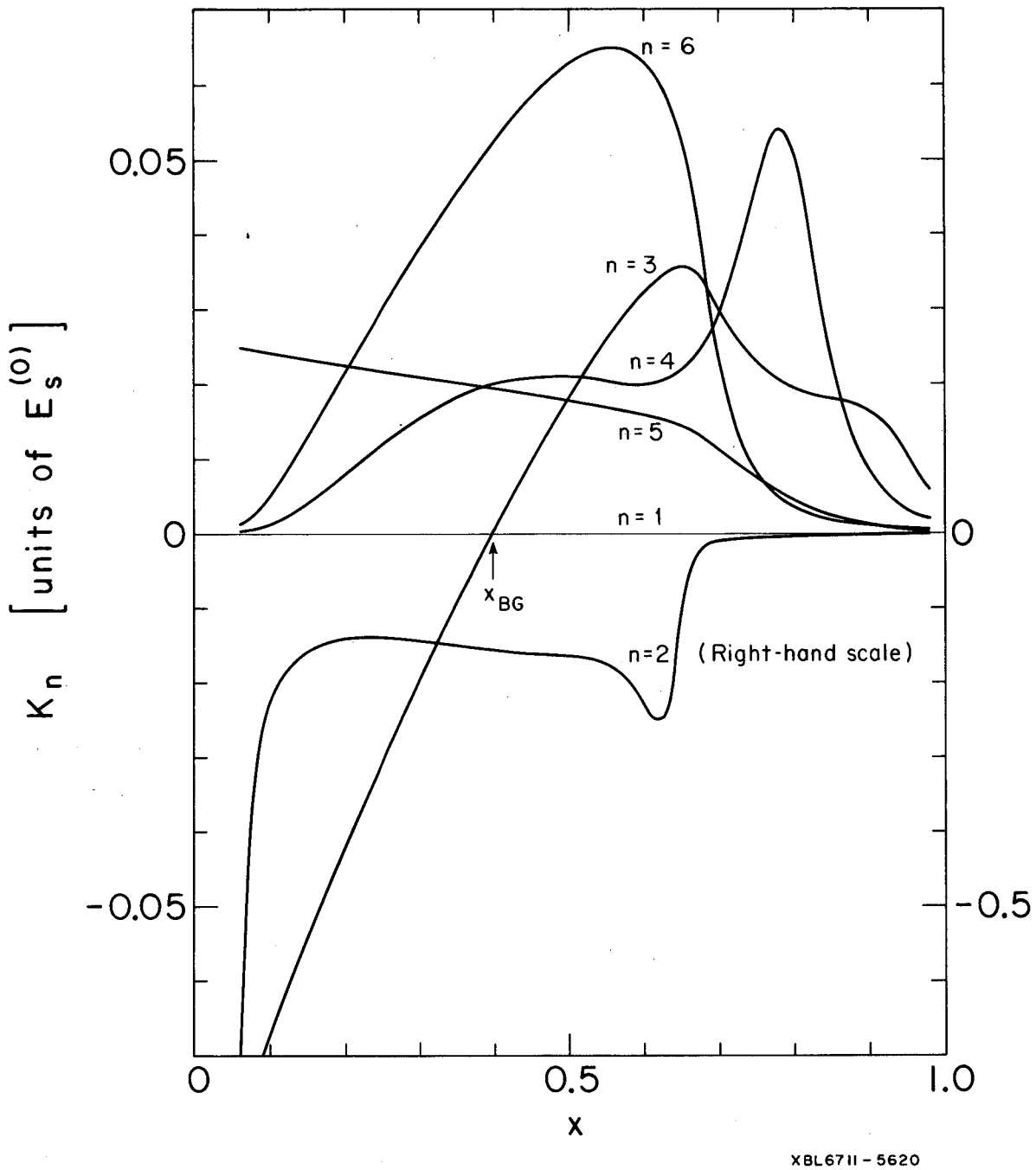

Fig. 27. The normal-coordinate stiffness constants as functions of the fissility parameter x. The Businaro-Gallone point is indicated by the arrow. Note that the n = 2 curve is plotted on a scale reduced by 10.

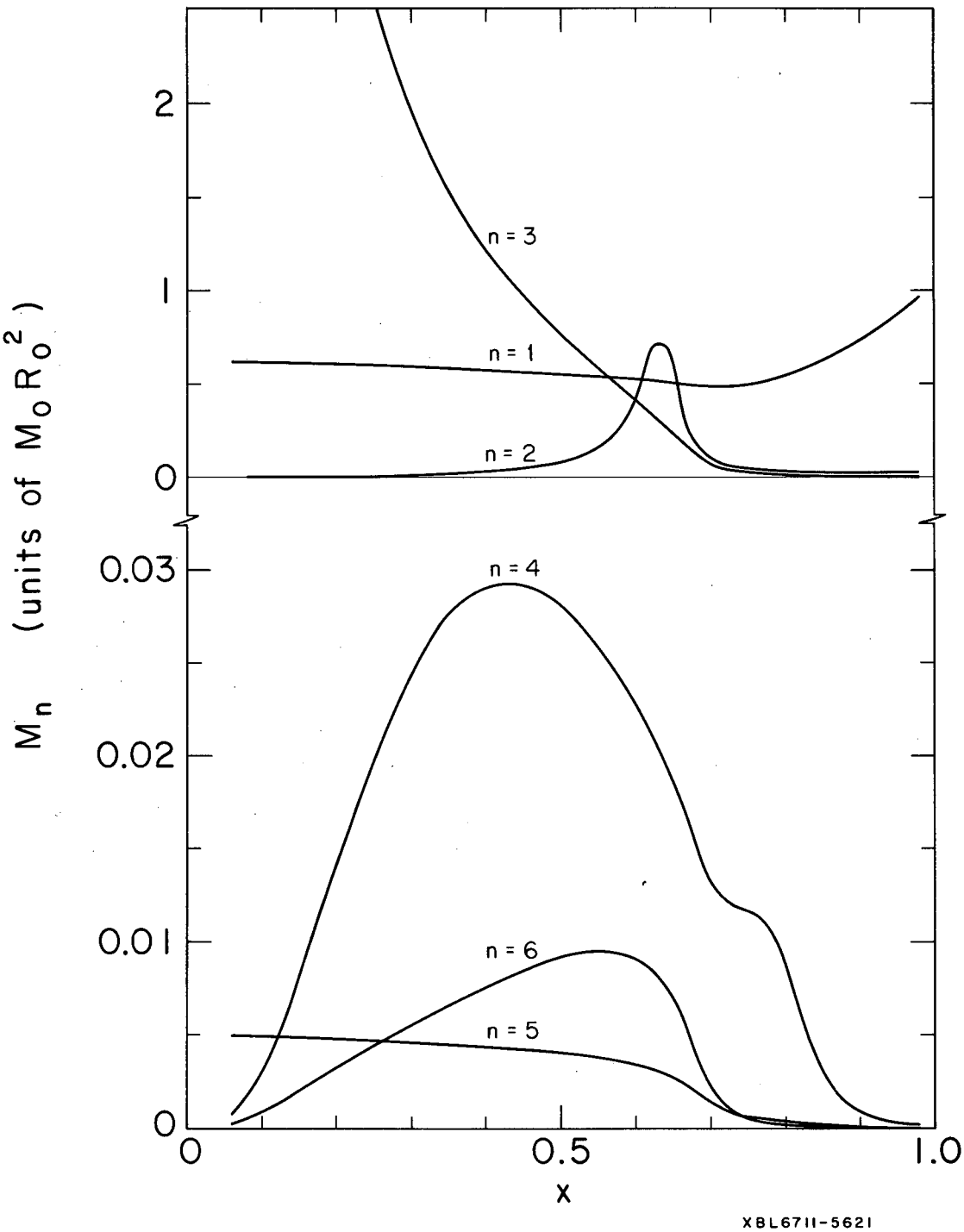

Fig. 28. The normal-coordinate inertia constants as functions of the fissility parameter x. Note that the n = 1, 2 and 3 curves are plotted on a scale reduced by 100.

Each of figs. 29-33 contains the elements of the eigenvector for a given normal mode, for n = 2-6. The n = 1 center-of-mass-shift mode is not included because for all values of x its eigenvector is simply

$$v^{(1)} = \begin{pmatrix} v_1^{(1)} \\ v_2^{(1)} \\ v_3^{(1)} \end{pmatrix} = \begin{pmatrix} 1 \\ 0 \\ 0 \end{pmatrix} .$$

We note that each of the eigenvectors shows a rapid change at $x \approx 0.67$, again corresponding to the transition in saddle-point shapes from cylinder-like to dumbbell-like.

The physical significance of the eigenvectors can be best understood by referring to eqs. (6) defining the generalized deformation coordinates to which the eigenvectors refer. For example, for the n = 2 fission mode it is seen that the motion consists primarily of an elongation of the drop for $x \gtrsim 0.67$ and a constriction of the drop's neck for $x \lesssim 0.67$. Similarly, the n = 3 mass-asymmetry motion is seen to consist primarily of changes in the transverse semiaxes and the positions of the centers of the two end spheroids for $x \lesssim 0.67$, whereas for $x \gtrsim 0.67$ changes in the relative eccentricities of the two end spheroids become increasingly important.

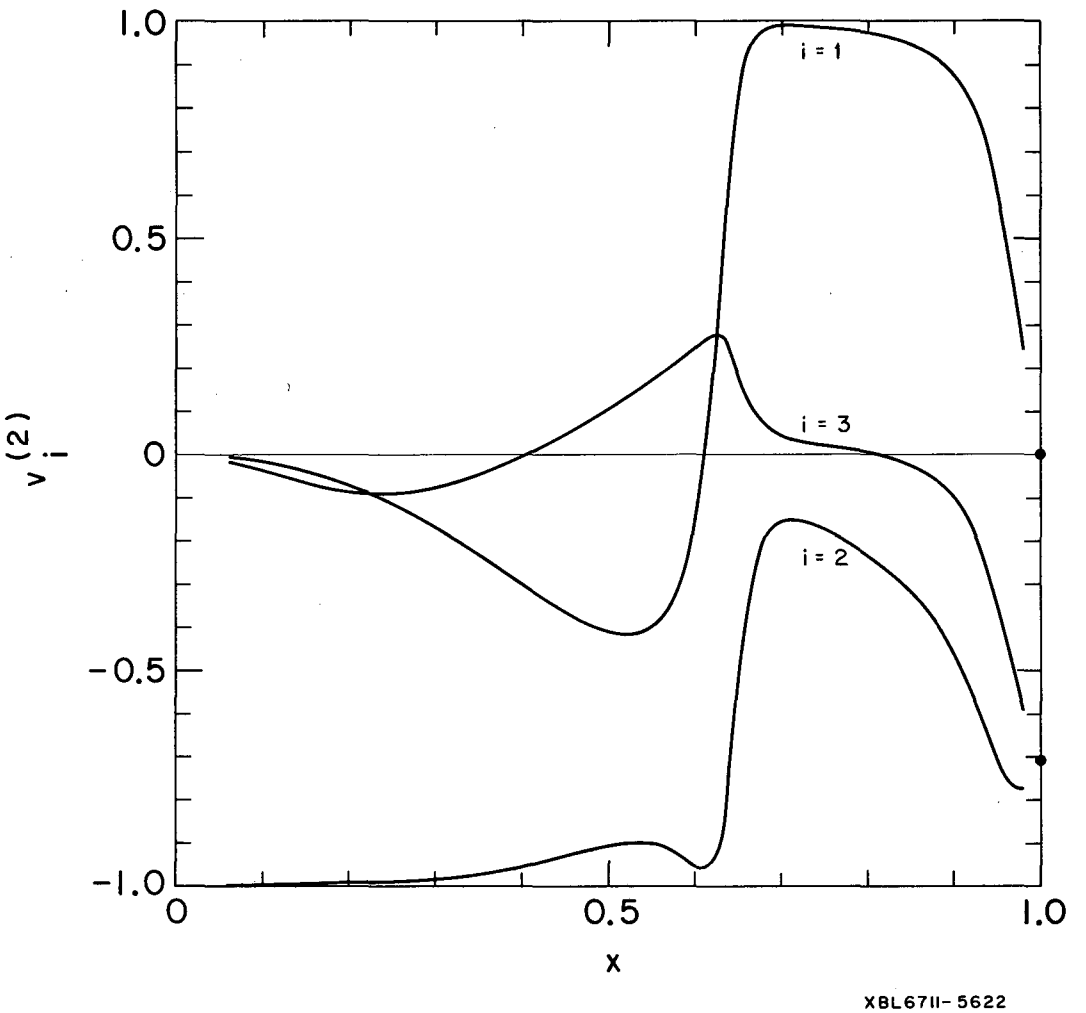

Fig. 29. The elements of the n = 2 fission eigenvector as functions of the fissility parameter x. The two solid points show the known values at x = 1 of the i = 1 curve and the i = 2 and 3 curves.

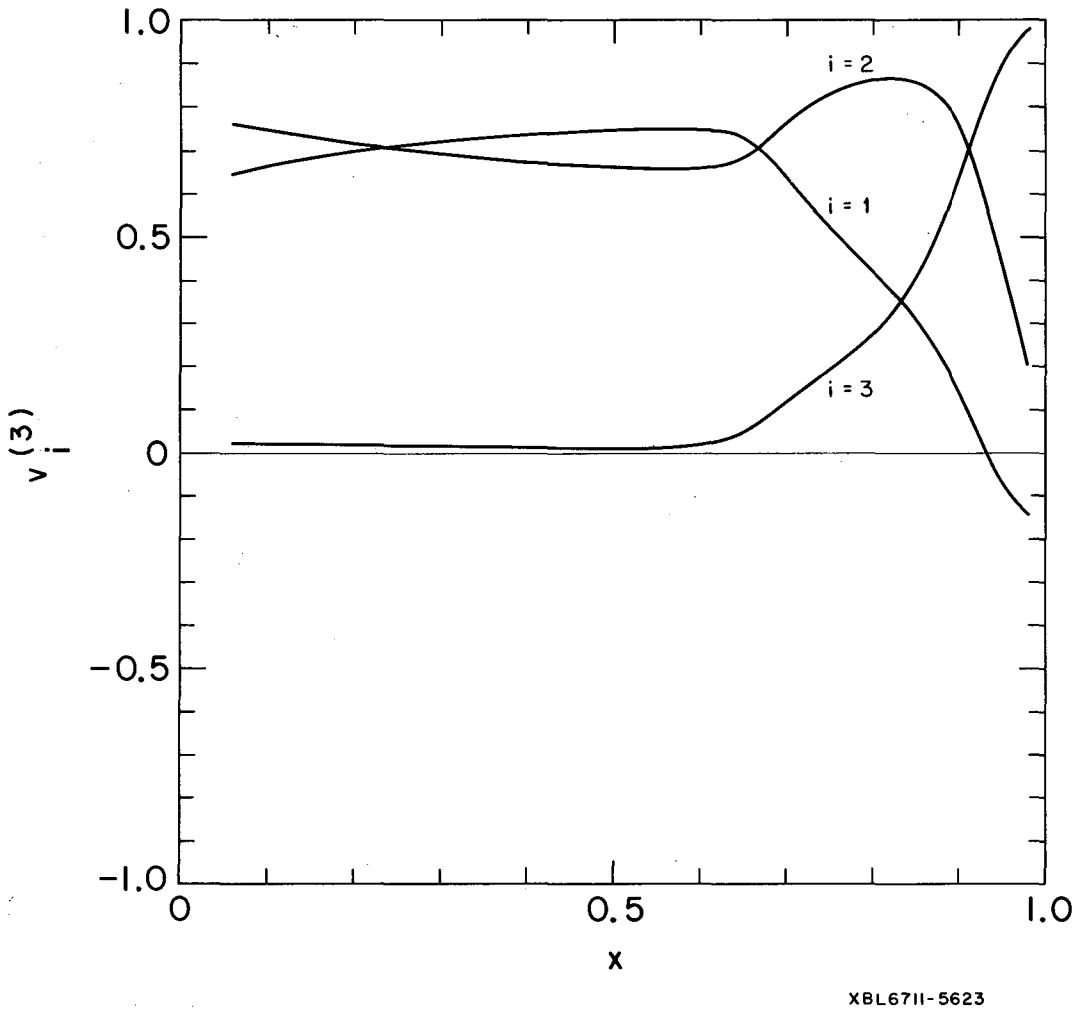

Fig. 30. The elements of the n = 3 mass-asymmetry eigenvector as functions of the fissility parameter x.

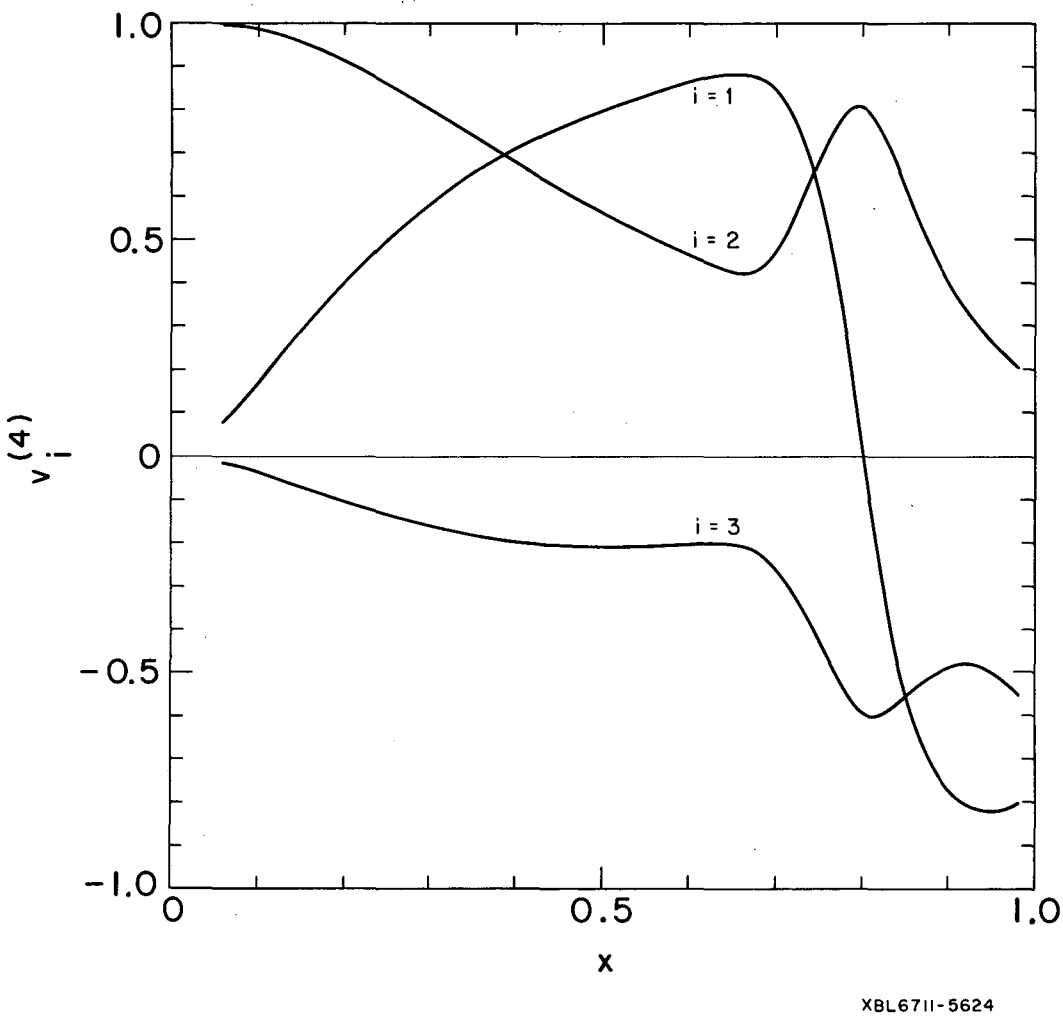

Fig. 31. The elements of the n = 4 stretching eigenvector as functions of the fissility parameter x.

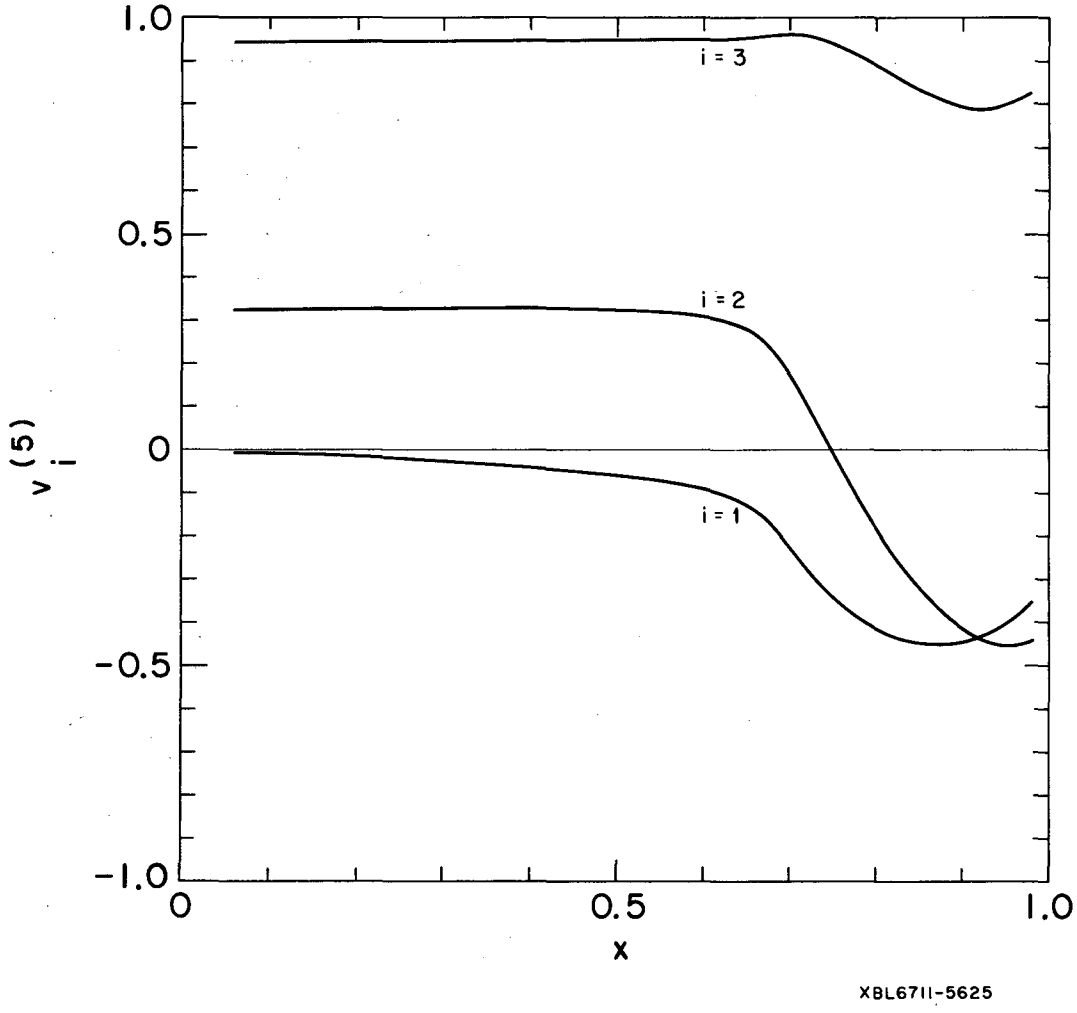

Fig. 32. The elements of the n = 5 distortion-asymmetry eigenvector as functions of the fissility parameter x.

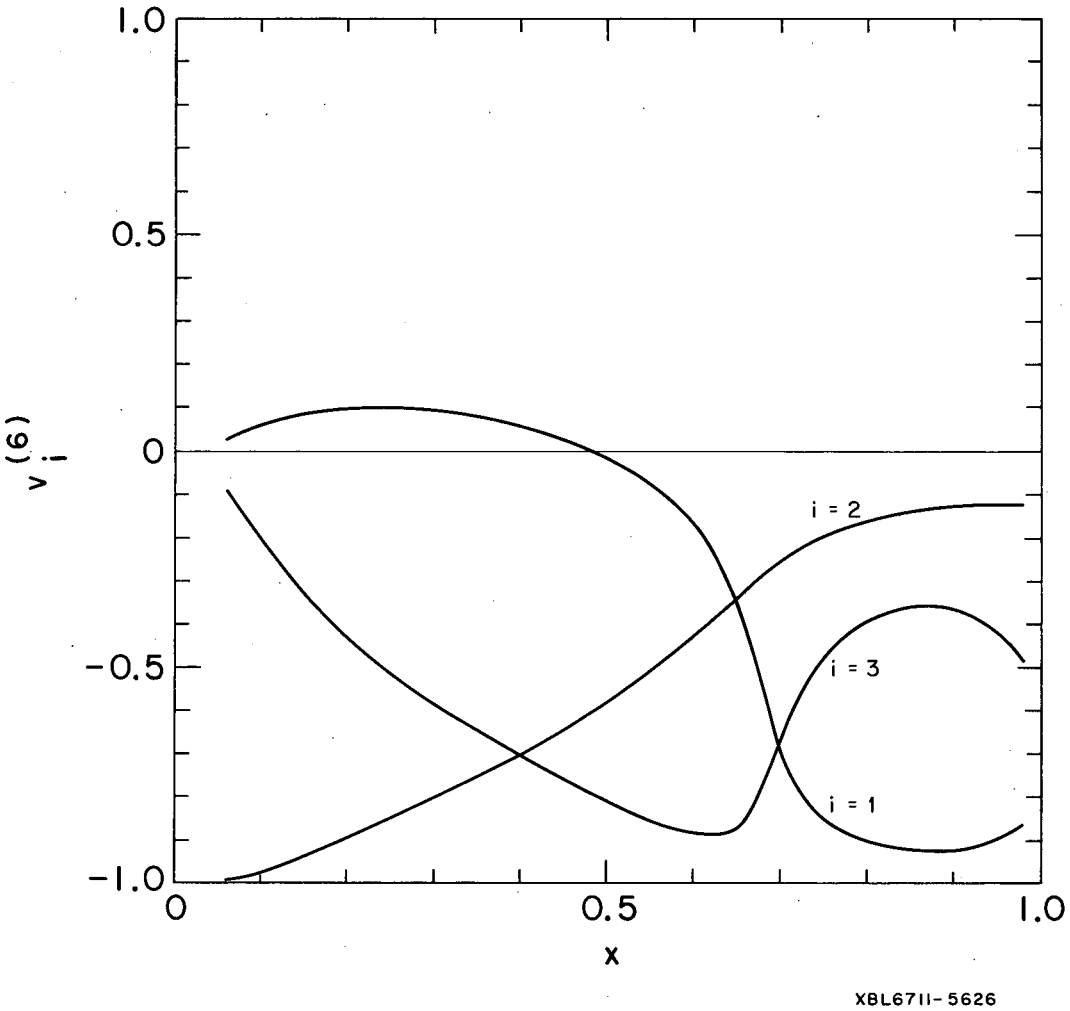

Fig. 33. The elements of the n = 6 eigenvector as functions of the fissility parameter x.

References

1) J. R. Nix and W. J. Swiatecki, Nuclear Physics 71 (1965) 1; J. R. Nix, Ph. D. Thesis, Report UCRL-11338 (April 1, 1964) unpublished
2) S. Cohen and W. J. Swiatecki, Ann. of Phys. 22 (1963) 406
3) D. L. Hill, Ph. D. Dissertation, Princeton University (April 1951) unpublished
4) D. L. Hill, in Proc. Second United Nations Int. Conf. on the Peaceful Uses of Atomic Energy, Geneva, 1958, Vol. 15 (United Nations, Geneva, 1958) p. 244
5) D. L. Hill and J. A. Wheeler, Phys. Rev. 89 (1953) 1102
6) U. L. Businaro and S. Gallone, Nuovo Cim. 1 (1955) 629
7) U. L. Businaro and S. Gallone, Nuovo Cim. 1 (1955) 1277
8) V. G. Nossoff, in Proc. Int. Conf. on the Peaceful Uses of Atomic Energy, Geneva, 1955, Vol. 2 (United Nations, New York, 1956) p. 205
9) L. Wilets, in Proc. Rehovoth Conf. on Nuclear Structure, Rehovoth, 1957 (Interscience Publishers, New York, 1958) p. 122
10) L. Wilets, Theories of Nuclear Fission (Clarendon Press, Oxford, 1964) pp. 46-47
11) S. Frankel and N. Metropolis, Phys. Rev. 72 (1947) 914
12) F. G. Werner and J. A. Wheeler, unpublished manuscript (no date)
13) D. R. Inglis, Ann. of Phys. 5 (1958) 106
14) W. D. Foland and R. D. Present, Phys. Rev. 113 (1959) 613
15) B. T. Geĭlikman, JETP (Soviet Physics) 36 (9)(1959) 168; JETP (USSR) 36 (1959) 249
16) O. Miyatake, Math. Jap. 9 (1964) 49; preprint (Sept. 1, 1967)(revised version)
17) L. Wilets, Theories of Nuclear Fission (Clarendon Press, Oxford, 1964) pp. 42-53, 71-77
18) E. K. Hyde, The Nuclear Properties of the Heavy Elements, Vol. III (Prentice-Hall, Inc., Englewood Cliffs, New Jersey, 1964) pp. 31-34
19) I. Kelson, Phys. Rev. 136 (1964) B1667
20) J. R. Nix, Ann. of Phys. 41 (1967) 52
21) R. W. Hasse, R. Ebert and G. Süssmann, Nuclear Physics A106 (1968) 117; R. W. Hasse, Diploma Work, Institute for Theoretical Physics, Frankfurt am Main (Sept. 1966) unpublished

22) J. N. P. Lawrence, Ph. D. Thesis, Report LA-3774 (Aug. 1967) unpublished

23) M. G. Urin and D. F. Zaretsky, Nuclear Physics 75 (1966) 101

24) S. G. Nilsson, J. R. Nix, A. Sobiczewski, Z. Szymański, S. Wycech, C. Gustafson and P. Möller, Report UCRL-18068 (Feb. 1968); Nuclear Physics A115 (1968) 545

25) S. G. Nilsson, A. Sobiczewski, Z. Szymański and S. Wycech, private communication

26) R. W. Hasse, preprint (April 1968) submitted to Nuclear Physics

27) R. W. Hasse, preprint (no date) submitted to Physics Letters

28) W. D. Myers and W. J. Swiatecki, Arkiv Fysik 36 (1967) 343

29) A. E. S. Green, Nuclear Physics (McGraw-Hill Book Co., New York, 1955) pp. 245, 519

30) W. D. Myers and W. J. Swiatecki, Nuclear Physics 81 (1966) 1

31) F. Dickmann, Zeits. Phys. 203 (1967) 141

32) S. Cohen, F. Plasil and W. J. Swiatecki, in Proc. Third Conf. on Reactions Between Complex Nuclei, Asilomar, Calif., 1963, ed. by A. Ghiorso, R. M. Diamond and H. E. Conzett (University of California Press, Berkeley, 1963) p. 325; unpublished manuscript (no date)

33) V. M. Strutinskiĭ, N. Ya. Lyashchenko and N. A. Popov, JETP (Soviet Physics) 16 (1963) 418; JETP (USSR) 43 (1962) 584; Nuclear Physics 46 (1963) 639

34) J. N. P. Lawrence, Phys. Rev. 139 (1965) B1227

35) U. L. Businaro and S. Gallone, Nuovo Cim. 5 (1957) 315

36) V. M. Strutinskiĭ, JETP (Soviet Physics) 18 (1964) 1305; JETP (USSR) 45 (1963) 1900

37) W. J. Swiatecki, in Physics and Chemistry of Fission, Proc. of a Symposium held in Salzburg, 1965, Vol. I (International Atomic Energy Agency, Vienna, 1965) p. 3

38) S. Cohen and W. J. Swiatecki, Ann. of Phys. 19 (1962) 67

39) V. M. Strutinskiĭ, JETP (Soviet Physics) 18 (1964) 1298; JETP (USSR) 45 (1963) 1891

40) K. Alder, A. Bohr, T. Huus, B. Mottelson and A. Winther, Revs. Mod. Phys. 28 (1956) 432

41) P. H. Stelson and F. K. McGowan, Phys. Rev. 110 (1958) 489

42) L. Moretto and W. J. Swiatecki, private communication

43) H. Lamb, Hydrodynamics, 6th ed. (Dover Publications, New York, 1945) Sec. 45, pp. 47-48

44) H. Goldstein, Classical Mechanics (Addison-Wesley Publ. Co., Reading, Mass., 1959) Chap. 10, pp. 318-346

45) P. J. Eberlein, J. Soc. Indust. Appl. Math. 10 (1962) 74

46) A. E. S. Green, Nuclear Physics (McGraw-Hill Book Co., New York, 1955) pp. 185, 250

47) E. Wigner, Trans. Faraday Soc. 34, part 1 (1938) 29

48) S. Glasstone, K. J. Laidler and H. Eyring, The Theory of Rate Processes (McGraw-Hill Book Co., New York, 1941) pp. 85-201

49) D. L. Bunker and N. C. Blais, J. Chem. Phys. 41 (1964) 2377

50) P. Pechukas and J. C. Light, J. Chem. Phys. 42 (1965) 3281

51) J. C. Light and J. Lin, J. Chem. Phys. 43 (1965) 3209

52) M. Karplus, R. N. Porter and R. D. Sharma, J. Chem. Phys. 43 (1965) 3259

53) N. Bohr and J. A. Wheeler, Phys. Rev. 56 (1939) 426

54) J. A. Wheeler, in Fast Neutron Physics, Part II, ed. by J. B. Marion and J. L. Fowler (Interscience Publishers, New York, 1963) p. 2051

55) I. Halpern, Ann. Rev. Nucl. Sci. 9 (1959) 245

56) L. D. Landau and E. M. Lifshitz, Statistical Physics, trans. by E. Peierls and R. F. Peierls (Addison-Wesley Publ. Co., Reading, Mass., 1958) pp. 86-89

57) A. Messiah, Quantum Mechanics, Vol. I, trans. by G. M. Temmer (Interscience Publishers, New York, 1961) pp. 448-451

58) E. Wigner, Phys. Rev. 40 (1932) 749

59) University of California Lawrence Radiation Laboratory Computer Center program D2 BKY ZAM (Berkeley, California)

60) University of California Lawrence Radiation Laboratory Computer Center program F4 BKY LINIT (Berkeley, California)

61) J. R. Nix, in Contributions, International Conference on Nuclear Structure, September 7-13, 1967, Tokyo, Japan (Secretariat of I. C. N. S., Institute for Nuclear Study, University of Tokyo, Japan) p. 225; Report UCRL-17540 (June 23, 1967)

62) J. R. Nix, in Proc. Third Conf. on Reactions Between Complex Nuclei, Asilomar, Calif., 1963, ed. by A. Ghiorso, R. M. Diamond and H. E. Conzett (University of California Press, Berkeley, 1963) p. 366

63) E. D. Courant and H. S. Snyder, Ann. of Phys. 3 (1958) 1
64) W. J. Swiatecki, in Proc. Second United Nations Int. Conf. on the Peaceful Uses of Atomic Energy, Geneva, 1958, Vol. 15 (United Nations, Geneva, 1958) p. 248
65) K. J. Le Couteur and D. W. Lang, Nuclear Physics 13 (1959) 32
66) D. Bodansky, Ann. Rev. Nucl. Sci. 12 (1962) 79
67) L. Wilets, Theories of Nuclear Fission (Clarendon Press, Oxford, 1964) p. 8
68) E. K. Hyde, The Nuclear Properties of the Heavy Elements, Vol. III (Prentice-Hall, Inc., Englewood Cliffs, New Jersey, 1964) p. 294
69) V. E. Viola, Jr. and T. Sikkeland, Phys. Rev. 130 (1963) 2044
70) M. Seki, preprint (no date)
71) T. Sikkeland, in Nuclear Chemistry Division Annual Report, 1965, Report UCRL-16580 (Jan. 1966) p. 105, unpublished
72) F. Plasil, D. S. Burnett, H. C. Britt and S. G. Thompson, Phys. Rev. 142 (1966) 696
73) H. C. Britt, H. E. Wegner and J. C. Gursky, Phys. Rev. 129 (1963) 2239
74) J. P. Unik and J. R. Huizenga, Phys. Rev. 134 (1964) B90
75) R. Vandenbosch and J. R. Huizenga, Phys. Rev. 127 (1962) 212
76) I. Halpern, preprint (no date)
77) Y. Boneh, Z. Fraenkel and I. Nebenzahl, Phys. Rev. 156 (1967) 1305
78) J. Terrell, Phys. Rev. 108 (1957) 783
79) J. Terrell, in Physics and Chemistry of Fission, Proc. of a Symposium held in Salzburg, 1965, Vol. II (International Atomic Energy Agency, Vienna, 1965) p. 3
80) H. W. Schmitt, J. W. T. Dabbs and P. D. Miller, in Physics and Chemistry of Fission, Proc. of a Symposium held in Salzburg, 1965, Vol. I (International Atomic Energy Agency, Vienna, 1965) p. 517
81) E. Konecny and H. W. Schmitt, preprint (no date)
82) F. Plasil and H. W. Schmitt, Bull. Am. Phys. Soc. 13 (1968) 605; private communication
83) Cyclotron Research, University of Washington, 1963 Annual Progress Report (1963) p. 15, unpublished
84) T. T. Sugihara, J. Roesmer and J. W. Meadows, Jr., Phys. Rev. 121 (1961) 1179

85) Cyclotron Research, University of Washington, 1959 Annual Progress Report (1959) p. 18, unpublished

86) A. W. Fairhall, Phys. Rev. 102 (1956) 1335; A. W. Fairhall, R. C. Jensen and E. F. Neuzil, in Proc. Second United Nations Int. Conf. on the Peaceful Uses of Atomic Energy, Geneva, 1958, Vol. 15 (United Nations, Geneva, 1958) p. 452

87) J. S. Fraser, J. C. D. Milton, H. R. Bowman and S. G. Thompson, Can. J. Phys. 41 (1963) 2080

88) H. W. Schmitt, W. E. Kiker and C. W. Williams, Phys. Rev. 137 (1965) B837; H. W. Schmitt, private communication

89) J. N. Neiler, F. J. Walter and H. W. Schmitt, Phys. Rev. 149 (1966) 894

90) H. W. Schmitt, J. H. Neiler, F. J. Walter and A. Chetham-Strode, Phys. Rev. Letters 9 (1962) 427

91) D. S. Burnett, Ph. D. Thesis, Report UCRL-11006 (Oct. 7, 1963) unpublished

92) S. L. Whetstone, Jr., Phys. Rev. 131 (1963) 1232

93) B. M. Foreman, Jr., W. M. Gibson, R. A. Glass and G. T. Seaborg, Phys. Rev. 116 (1959) 382

94) R. Vandenbosch, T. D. Thomas, S. E. Vandenbosch, R. A. Glass and G. T. Seaborg, Phys. Rev. 111 (1958) 1358

95) P. C. Stevenson, H. G. Hicks, W. E. Nervik and D. R. Nethaway, Phys. Rev. 111 (1958) 886

96) E. L. Haines and S. G. Thompson, Phys. Rev. 131 (1963) 2169

97) W. M. Gibson, Ph. D. Thesis, Report UCRL-3493 (Nov. 1956) unpublished

98) R. A. Glass, R. J. Carr, J. W. Cobble and G. T. Seaborg, Phys. Rev. 104 (1956) 434

99) E. V. Luoma, Master's Thesis, Report UCRL-3495 (Nov. 1956) unpublished

100) H. C. Britt and S. L. Whetstone, Jr., Phys. Rev. 133 (1964) B603

101) S. L. Whetstone, Jr., Phys. Rev. 133 (1964) B613

102) R. Vandenbosch, Nuclear Physics A101 (1967) 460

103) S. B. Ermagambetov, V. F. Kuznetsov and G. N. Smirenkin, Sov. J. Nucl. Phys. 5 (1967) 181; J. Nucl. Phys. (USSR) 5 (1967) 257

104) H. C. Britt, F. A. Rickey, Jr. and W. S. Hall, Report LA-DC-9562 (no date) submitted to Phys. Rev.

105) Y. Kikuchi and S. An, J. Nucl. Science Tech. 5 (1968) 86

106) J. Maly and J. R. Nix, in Contributions, International Conference on Nuclear Structure, September 7-13, 1967, Tokyo, Japan (Secretariat of I. C. N. S., Institute for Nuclear Study, University of Tokyo, Japan) p. 224; Report UCRL-17541 (June 23, 1967)

107) I. Kelson, Phys. Rev. Letters 20 (1968) 867

108) J. J. Griffin, in Proc. Second Conf. on Neutron Cross Sections and Technology, Washington, D. C., 1968, ed. by D. T. Goldman (U. S. Government Printing Office); University of Maryland, Center for Theoretical Physics, Report no. 805 (March 1968) unpublished

109) J. J. Griffin, University of Maryland, Center for Theoretical Physics, Report no. 810 (April 1968); Phys. Rev. Letters 21 (1968) 826

110) A. C. Wahl, in Physics and Chemistry of Fission, Proc. of a Symposium held in Salzburg, 1965, Vol. I (International Atomic Energy Agency, Vienna, 1965) p. 317

111) V. M. Strutinskii, Nuclear Physics A95 (1967) 420

112) P. A. Seeger and R. C. Perisho, Report LA-3751 (Sept. 11, 1967) unpublished

113) P. Davis and P. Rabinowitz, J. Res. Natl. Bur. Std. 56 (1956) 35

114) W. J. Cody, Math. Comp. 19 (1965) 105

115) R. E. Moore and L. M. Perko, J. Fluid Mech. 22 (1965) 305

116) F. N. Shklyarchuk, Technical Abstract Bulletin no. AD662246, trans. by L. Marokus, Foreign Technology Division Translation FTD-HT-66-527, Aug. 18, 1967 (Clearinghouse for Federal Scientific and Technical Information, Springfield, Va.); AN SSSR Izvestiya Mekhanika, No. 6 (1965) 123

117) H. Lamb, Hydrodynamics, 6th ed. (Dover Publications, New York, 1945) Sec. 9, pp. 6-8

118) G. Golub, Num. Mat. 7 (1965) 206

119) P. Businger and G. H. Golub, Num. Mat. 7 (1965) 269